# An Object–based analysis of Cloud Motion from Sequences of METEOSAT Satellite Data

Mr Franz Thomas Newland

Submitted for the degree of

**Doctor of Philosophy**

September 1999

*Faculty of Engineering and Applied Sciences*

*Aeronautics and Astronautics*

# ABSTRACT

UNIVERSITY OF SOUTHAMPTON

Abstract

FACULTY OF ENGINEERING AND APPLIED SCIENCES

AERONAUTICS AND ASTRONAUTICS

Doctor of Philosophy

AN OBJECT–BASED ANALYSIS OF CLOUD MOTION FROM SEQUENCES OF METEOSAT SATELLITE IMAGERY

by Franz Thomas Newland

The need for wind and atmospheric dynamics data for weather modelling and forecasting is well founded. Current texture–based techniques for tracking clouds in sequences of satellite imagery are robust at generating global *cloud motion winds*, but their use as *wind* data makes many simplifying assumptions on the causal relationships between cloud dynamics and the underlying windfield. These can be summarised under the single assumption that *clouds must act as passive tracers for the wind.* The errors thus introduced are now significant in light of the improvements made to weather models and forecasting techniques since the first introduction of satellite–derived wind information in the late 1970s. In that time, the algorithms used to track cloud in satellite imagery have not changed fundamentally. There is therefore a need to address the simplifying assumptions and to adapt the nature of the analyses applied accordingly.

A new approach to cloud motion analysis from satellite data is introduced in this thesis which tracks the motion of clouds at different scales, making it possible to identify and understand some of the different transport mechanisms present

in clouds and remove or reduce the dependence on the simplifying assumptions. Initial work in this thesis examines the suitability of different motion analysis tools for determining the motion of the cloud content in the imagery using a fuzzy system. It then proposes tracking clouds as flexible structures to analyse the motion of the clouds themselves, and using the nature of cloud edges to identify the atmospheric flow around the structures.

To produce stable structural analyses, the cloud data are initially smoothed. A novel approach using morphological operators is presented that maintains cloud edge gradients whilst maximising coherence in the smoothed data. Clouds are analysed as whole structures, providing a new measure of synoptic–scale motion. Internal dynamics of the cloud structures are analysed using medial axis transforms of the smoothed data. Tracks of medial axes provide a new measure of cloud motion at a mesoscale. The sharpness in edge gradient is used as a new measure to identify regions of atmospheric flow parallel to a cloud edge (jet flows, which cause significant underestimation in atmospheric motion under the present approach) and regions where the flow crosses the cloud boundary. The different motion characteristics displayed by the medial axis tracks and edge information provide an indication of the atmospheric flow at different scales.

In addition to generating new parameters for measuring cloud and atmospheric dynamics, the approach enables weather modellers and forecasters to identify the scale of flow captured by the currently used cloud tracers (both satellite–derived and from other sources). This would allow them to select the most suitable tracers for describing the atmospheric dynamics at the scale of their model or forecast. This technique would also be suitable for any other fluid flow analyses where coherent and stable gradients persist in the flow, and where it is useful to analyse the flow dynamics at more than one scale.

KEYWORDS Meteorology, Clouds, Cloud Motion Winds, Atmospheric Dynamics, Image Processing, Morphology, Skeletons, Shape Smoothing, Fuzzy Logic, Feature Matching.

# CONTENTS

# LIST OF FIGURES

# LIST OF TABLES

# PREFACE

This thesis provides the background, methods and results of the past four years' work on analysis of cloud motion from sequences of satellite data using novel image processing techniques. It is presented in three sections that serve very different roles. The thesis itself does not represent a chronological progression of the study undertaken. It is informative, however, to know by what route the work came together, and to this end, a brief summary of the chronological progression of the work is now provided.

Initial work concentrated on improving wind information from tracking clouds. It was realised that different types of cloud motion could be identified in movie loops of satellite data, and a mechanism for segmenting these motion types was developed. This work is detailed in Newland et al [75], and used a fuzzy system to identify the degree to which any region of cloud could be tracked using edge information, textural content and whole cloud matching. This resulted in some realisation of the multi-scale nature of cloud motion. Subsequent discussion with the Meteorological Office in Bracknell led to the more fundamental issue that different users of meteorological wind information have different interpretations of the word *wind*. The term is equally used to describe small scale eddies at spatial resolutions in the order of metres and large scale atmospheric motion over many hundreds of kilometers. In order to make some distinction between these scales, the more generic term of *atmospheric dynamics* has sometimes been used in the literature for the scale of motion captured in geostationary satellite imagery.

As a result of this early work, study then focused on identifying motion mechanisms at different scales. Historically, the atmosphere is studied at *synoptic* or large–scale (hundreds of kilometers), *meso* or medium scale (tens of kilome-

ters) and *local* scale, and therefore as a first approximation it seemed appropriate to capture the dynamics at these distinct orders of magnitude. The motion of whole weather systems is indicative of the synoptic scale dynamics, whilst the motion within a weather system as identifiable in satellite image data is better for mesoscale analysis. Local-scale information is typically too small to be identified on satellite data, but by comparing the mesoscale motion with, for example, other *point* sources of wind information (e.g. radiosonde data from weather balloons), it is possible to determine the amount of correlation between local and mesoscale motion.

Suitable parameters for tracking clouds at a synoptic and mesoscale were sought, which shifted the emphasis of the study onto cloud *objects*. This shift of emphasis to an object–based approach is detailed in Lewis et al [4]. Whole clouds, their edges and their medial axes or *skeletons* were identified as suitable parameters to capture these scales of motion. Due to the nature of clouds having vague edges, a fuzzy approach to cloud object extraction was considered. This approach and the initial work on edge and skeleton tracks are given in Newland et al [76]. The stability of these edge and skeleton tracks was limited, however, by the high local variability in the raw data. Smoothing techniques were therefore sought to remove some of the smaller–scale variation.

Having selected an object–based approach, and having identified suitable structures for tracking motion at different scales, other benefits of the approach began to emerge, in particular the potential for skeletons to provide an indication of cloud *spread*, e.g. for identifying the onset of vorticity through the various mechanisms of cyclogenesis, and the relationship between crisp cloud edges and the location of jet flows, which are notoriously difficult to capture using current techniques. It is hoped that other developments may arise with further maturity of these new parameters of cloud motion.

The thesis is laid out in three sections to enable the reader to find the pertinent information as easily as possible. Part 1 provides the background to the study, detailing the current operational approach to cloud tracking, its limitations and

some potential requirements for any improved technique. It highlights other areas of active research in this field, and identifies which problems this work addresses. An introduction to the research itself is also given, and the backgrounds to methods used are provided as necessary. Part 2 details the actual algorithms applied to the data, and identifies the desired characteristics displayed by the selected algorithms. It is split into data smoothing and object extraction, object parameterisation and parameter matching. Finally, part 3 discusses the methods and results and highlights possible future directions of research, before summarising the main conclusions of the work.

# ACKNOWLEDGEMENTS

This research has been been supported by studentship number GT4-95-283-D from the Natural Environment Research Council and a CASE award from Earth Observation Sciences (EOS), Farnborough, and many people within both organisations. Of these, I would particularly like to mention Dr. George Simpson from EOS, my CASE supervisor, who has been particularly helpful during the course of the research and my visits to EOS.

The research has been supervised at Southampton University by Dr. Martin Brown of Electronics and Computer Science and Dr. Adrian Tatnall of Aeronautics and Astronautics. Without their cajolery, questions, helpful direction and encouragement, the work would not have been possible.

My various colleagues at Southampton have similarly been invaluable, for computer advice, meaningful discussions and for providing space away from work. In particular, I would like to mention Stéphane Côté who has been a very good mentor and friend on *many* matters; Richard Moss, who has moved more boxes for Jane and me than he would care to remember; Jeremy and Hugh who both kept the office a fun place to be. Similarly, James, Isabel, and more recently Ben, Jon and Andrea who have tolerated *many* bad jokes in very good humour and have become part of my fond collective of *the office.*

I would also like to thank my current manager at IBM, Nicola Hills, who has been all that could be asked of a manager, and James Luke, who I wish well with the remainder of *his* thesis. I similarly have a number of other colleagues at IBM to thank for keeping some level of (in)sanity during the final phases of this thesis, in particular Nilou, Michael, John and Sarah, to whom I say Se'pass'go'za'ram,

Danke, Thanks and Merci... you have all been very good friends!

There have also been two sets of parents who have put up with endless requests for help in all shapes and forms, and who have listened patiently to all the struggles and frustration for the past four years without complaint. The *least* I could do in return was submit this thesis.

But mostly I need to mention Jane, without whom I'd have never started on this journey and having started, I'd have stopped at many points along it, and *with* whom, the journey has been far more vibrant and colourful than it could ever have been alone. Merci pour notre voyage en espace ensemble.

# Part I

# INTRODUCTION

# 1. INTRODUCTION

This thesis presents a novel approach to tracking cloud in sequences of geostationary meteorological satellite imagery that provides new information regarding the nature and ultimately the cause of the motion displayed by cloud. The approach considers the cloud content of the image sequences as deformable objects, and as such, interprets the image content early in the image analysis to determine the location and nature of the clouds in the imagery. This early interpretation is used to target subsequent motion analysis using the knowledge acquired. Novel shape parameters that make use of morphological image processing techniques and fuzzy logic are used to describe the cloud content such that the dynamics of the cloud can be captured at different scales.

The work uses infrared geostationary satellite imagery due to the relative ease with which the cloud content can be identified and interpreted. By contrast, visible imagery requires careful consideration of the change in shadowing effects on cloud texture as the relative solar angle changes. Water vapour imagery, which represents a deep layer mean water content, is equally less suitable than infrared as the motion mechanisms of water vapour *per se* are less well known than those of clouds, and the deep layer averaging effects reduce the usefulness of the data for analysing smaller scale phenomena. Infrared images are also freely available in the public domain at useable spatial and temporal resolutions. Geostationary satellites provide a fixed viewpoint for the data[1], avoiding the need for any complex registration of the images against one–another, giving the same viewing angle for any image region over a sequence of images and providing a higher temporal update on the data, due to the satellite's persistent view of

[1] An approximation to a fixed viewpoint, at least.

the same area of the globe. Whilst higher spatial resolution data are available for polar orbiting satellites for example, their temporal resolution for a given area on the ground is typically degraded by an order of 10–20 compared to the geostationary data over the same region. In this time the cloud over the region has typically changed and / or moved significantly.

The cloud component is first extracted from an image sequence by comparison with dynamically created template image estimates of the radiances of the underlying land and sea. Two smoothing algorithms are considered for removing noise from the enhanced cloud data: for large–scale object–matching–based motion analysis, a simple median filter can be used to remove noise at the cost of reducing precision in the data. For cloud parameterisation however, accuracy in capturing edge *strength* and maximising the *coherence* of the cloud structure are the overriding concerns, so a novel edge–preserving filter is applied. The filter is based on a *rolling ball* algorithm.

The parameters extracted from the smoothed cloud objects are designed to identify the nature of the edge of the cloud (sharply defined or dissipated) and to capture the overall structure of a cloud shape (the curvature, number of *limbs*, etc). The selected parameters used to identify these are the cloud edge gradient and the cloud *skeleton* or medial axis. In order to manage the imprecise nature of clouds as structures, ways to adapt the standard techniques for generating skeletons for crisp objects in binary images are discussed in this work. A novel technique for determining *cloud edge strength* using a fuzzy system has also been developed, to provide better identification of *crisp* and *fuzzy* edges than edge gradient can offer alone.

These parameters are then matched across the sequence of satellite images to produce sets of motion vectors. The result of this mixture of tracking methods is a much richer description of the cloud dynamics, from which it is possible to make better interpretations of the cause of the motion. In addition to identifying cloud motion resulting from the wind driving it, it is possible to determine sites of convection, locations of jet flows (where there is typically no cloud com-

ponent) and *atmospheric flows* that act on a much larger scale than most users typically interpret as *wind*. The whole process from cloud extraction through parameterisation to matching is shown in Figure 1.1.

The dynamics of each motion type can be interpreted independently. Crisp cloud edges, for example, do not have any local wind flow across them (and vice–versa for dispersed edges), therefore the motion of a crisp cloud edge is typically the result of a large scale atmospheric flow. The local wind acts (and many meteorological phenomena result from flows that are) *relative* to this large scale flow, thus a mechanism for identifying it is the first step towards identifying a number of relative–flow phenomena. Skeletal motion allows some component of a cloud's internal dynamics to be captured. Between edge and skeleton motion types, there is the potential to identify the cause of a particular cloud's development. Convective processes in clouds for example are driven by motion relative to the atmospheric flow. If the atmospheric flow can be identified from the motion of a crisp edge on the convective cell and the internal atmospheric motion is captured by the skeleton vectors, the difference between the two will show convective–type relative flows.

This highlights one of the main strengths of this new multiple motion analysis approach, namely that the combined analysis of these different types of motion offers a better understanding of each than is possible independently. This therefore offers a significant improvement over the single motion analysis currently employed operationally, which itself has no meteorological context within which to be interpreted. Unlike cloud edge and skeleton motion, which both relate directly to a meteorological concept (the cloud whose motion they describe), the current texture–based analyses track texture regions as a totally abstract concept.

The novel components of this work are therefore the consideration of cloud motion from a *cloud object* perspective and the use of multiple motion analyses to build up a more complete picture of the motion, the novel edge–preserving image filter that has been developed for this work, the adaptation and application of morphological skeleton tools for analysis of cloud shape and the fuzzy system

applied to cloud edge analysis. The potential benefits of the work for the meteorological community are new parameters describing the synoptic scale dynamics and cloud motion unassociated with the underlying windfield, better identification of suitable wind tracers and a new method for identifying possible jet flow locations for further scrutiny.

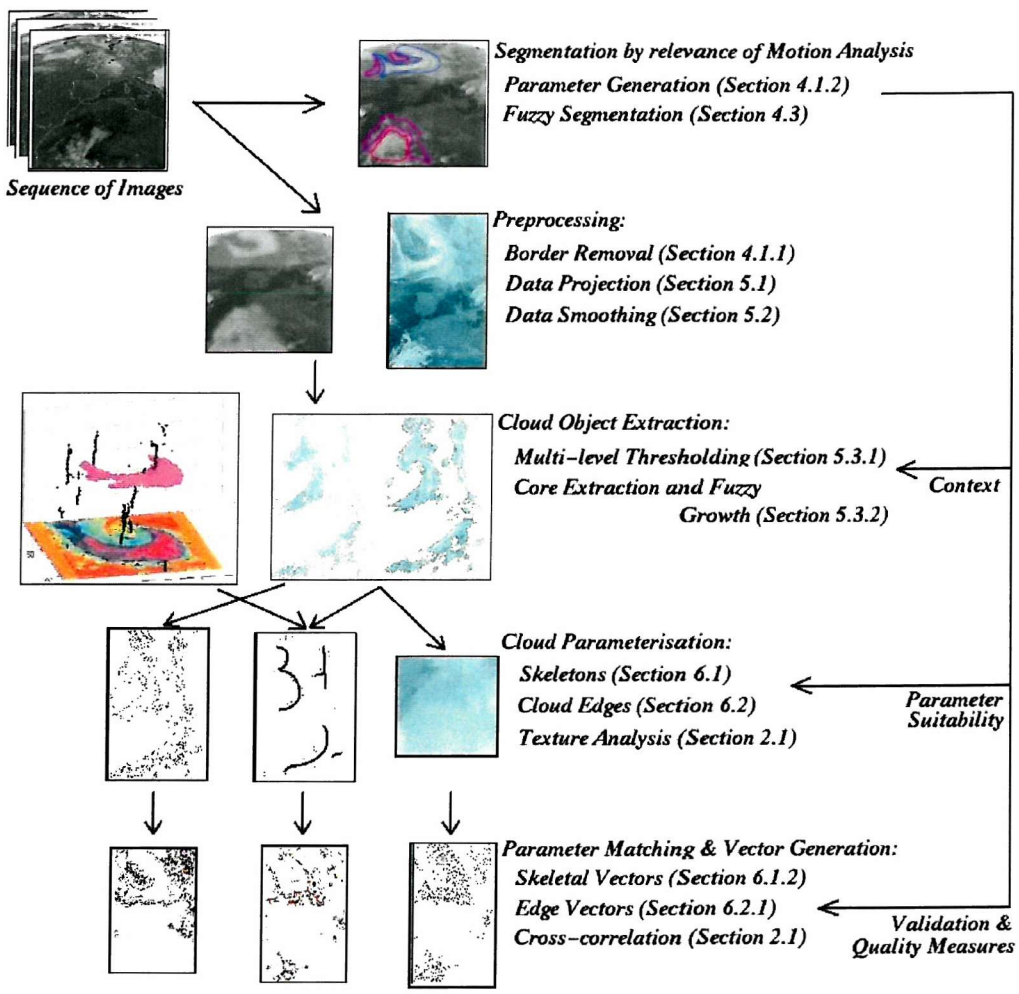


**Figure 1.1:** *Pictorial Abstract of the Proposed Approach for Cloud Motion Analysis: A sequence of satellite images is segmented based on the suitability of different motion analysis tools. The raw images are then enhanced, projected and smoothed, and the cloud objects are extracted from them. Edge, skeleton and texture window parameter extraction routines are then run. Finally, the parameter sets are matched across the sequence to generate a number of different vector fields. The original motion suitability information can be used to aid cloud extraction by providing a motion context, during parameter generation to target parameter generation algorithms at the relevant regions and during parameter matching to provide a measure of vector quality based on motion relevance.*

# 2. BACKGROUND

Satellite imagery has been an invaluable and consistent source of meteorological information since the start of the Geostationary Meteorological satellite programs in the early 1970s (Leese et al [62], Schmetz et al [87]), providing data for forecasters and weather modellers alike. The application of satellite–derived data covers such diverse areas as short–term weather forecasting for otherwise data–sparse areas of the globe or in areas of severe weather to climate modelling and earth radiation budget analyses (Baker [6]) to numerical weather model inputs (Kelly [53]) and model and forecast validation. Wind is potentially the most significant input to any weather model (Hinsman [49]), and therefore a continuous, global source of wind data is invaluable to modelling communities. Due to the unique use of visible and infrared sensors on many of the earlier platforms and subsequent refinement of these channels with satellite development, much of the meteorological study of satellite imagery has concentrated on cloud content and, using sequences of images, cloud dynamics. Trained forecasters are able to identify large– and small–scale dynamics components from analysis of such sequences, particularly with the new high spatial and temporal data resolutions available. This knowledge of cloud motion has been invaluable for generating global knowledge of the underlying wind field.

First analyses of cloud motion from satellite imagery consisted of manually matching clouds and plotting motion vectors, providing reliable motion but requiring a large amount of time. The primary use of cloud motion vectors is as an indication of the local wind (*Cloud Motion Winds* or CMWs). Hubert and Whitney [50] document the early use of cloud motion for wind field analysis, and list a number of important criteria against which cloud suitability as a tracer for the wind

can be assessed. Primarily, clouds that are advected[1] by the ambient winds act as good tracers (passive tracers), as opposed to clouds in convection[2]. There are, however, other motion mechanisms for clouds that are nonadvective. A condensed set of the guidelines provided by Hubert and Whitney for determining wind information from satellite image data is given in Table 2.1.

Cloud motion vectors have been derived using automatic techniques since the early–1970s[3] using an image texture cross–correlation approach (Leese et al [62], Smith and Phillips [93]). Numerical weather models currently use wind data derived automatically from cloud motion as a significant source of knowledge of atmospheric dynamics.

## 2.1 Automatic Derivation of Cloud Motion

Current automatic techniques for analysing cloud content make a number of simplifying assumptions both about the nature of the cloud motion and its cause. Principally, it is assumed (at least initially) that *all* cloud acts as a passive tracer for the wind field. It is also assumed that using a single measure to track the cloud (namely correlating *texture windows* of the cloud images) captures the cloud motion with both sufficient accuracy and at the scale most relevant for analysis of the wind field.

Since 1979, the standard technique for determining global winds operationally from satellite data has been a texture cross–correlation approach. This involves correlating a window of the radiance data in the first available image with an area

[1] advection: a mechanism of horizontal energy transport in the troposphere, by the wind. Any atmospheric property can be advected, but temperature and moisture advection are of most interest to meteorologists (Nese et al [74]). A frontal system is a good example of a cloud under advection.

[2] convection: a mechanism of vertical energy transport. With regard to clouds, convection is usually classified into shallow and deep, the distinction dependent on the vertical extent of the cloud undergoing convection. A stratus or layered cloud would be a good example of shallow convection, where the layer has resulted from a small upward motion of air over a large area. Cumulonimbus or storm clouds are the most extreme example of deep convection.

[3] Fujita [37] performed basic analyses of cloud motion from the U.S. Applications Technology Satellites (ATS) as early as the mid–sixties, but operational computation started in the 1970s.

1. Cyclones, fronts, jet streams and squall lines can be found from spirals, large bands, abrupt cloud edges and lines or zones of bright cloudiness.

2. The stages of cyclone development can be determined from the character of the cloud (see also Browning's discussion of leaf to comma to vortex transitions [14]). High clouds in well–developed tropical cyclones move slowly and both cyclonically and anti–cyclonically, whereas low and middle clouds move rapidly in a cyclonic direction.

3. Interaction between air masses and underlying surfaces can be determined by looking, for example, for cloud types of cold advection over warmer water or warm advection over colder water. Clouds influenced by coastlines and by ocean temperatures are low-level clouds.

4. Bright clouds with sharp edges usually are cumuliform and are easily tracked.

5. Thin clouds with diffuse edges tend to be cirriform and are less easily tracked than cumuliform and middle clouds. Clouds associated with jetstreams are often cirriform. Large masses of bright multilayered cloud associated with jetstreams will often obscure the thin gray cirrus of jetstream level.

6. Motions which appear to move through a pattern of cloud, alternately suppressing and enhancing brightness, often conflict with motion of the individual cloud elements in the same layer and are probably due to gravity waves. The orientation of such waves and their direction of motion bear no fixed relation to the ambient wind.

7. Clouds that appear to penetrate vertical shear layers should be tracked by the upshear edge rather than the center of mass. For example, in areas of active convection the cloud area grows rapidly because of anvil growth. The origin of the anvil (the brightest area at the rear of the growth region) moves with the middle– and low–level wind. The leading edge of the anvil, while advancing with the high–level wind, may be moving more slowly than the wind because of evaporation.

***Table 2.1:*** *Guidelines for satellite image analysis. Collated from Hubert and Whitney [50]*

of the second image and selecting the maximum cross–correlation between the two image windows as the best match and correspondingly the best local estimate of cloud motion (Figure 2.1). The assumption that clouds act as passive tracers for the underlying windfield is then used to derive a global windfield estimate, at least in the cloud-covered regions of the imagery. This has been a reliable and successful approach to wind estimation both for the modelling and forecasting communities for the past two decades. With no corrections, this approach can

achieve accuracies of around 8–10 m/s RMS error averaged across all windspeeds when compared to the standard source of wind information[4].

A more detailed description of the current operational techniques applied by NASA and NOAA to Geostationary Operational Environment Satellite 7 (GOES-7) Infrared data, and EUMETSAT's Meteorological Product Extraction Facility (MPEF) to METEOSAT Infrared data processing is now given[5].

Images are analysed in their raw (i.e. orthographic) projection, and the resultant motion vectors are converted to a constant distance projection to determine their magnitude and direction relative to an observer on the ground below the cloud [88]. The image data are initially segmented into 32*32 pixel segments. The region over which data are generated extends to the 55 degree arc about the subsatellite point, although more recently, Purdom [81] has shown that the new high-temporal-density data available with GOES-9 enable accurate texture correlation well beyond this. Around 1/2 to 2/3 of segments have identifiable cloud tracers for subsequent use [87][6]. Image filtering is applied to enhance the highest layer of cloud. Only the highest layer of cloud in any segment is tracked operationally. By setting all low-cloud clusters to a threshold greyscale and stretching the histogram of mixed low- and high-cloud clusters away from the high cloud radiometric range, the high cloud regions stand out from their background, thus making the tracking correlation algorithms much more effective. Clusters are assigned a particular pressure level based on their IR brightness temperature and forecast temperature profiles. The assignment of height to a CMW vector is critical to its usefulness, since the change in wind field with respect to height can be significant, the most obvious example of this being shown by the jetstream.

Three successive IR images are used to determine a displacement vector: A given segment at time t forms the target area to be correlated with segments at times (t - 30) minutes and (t + 30) minutes (Figure 2.1). The search starts at the cloud displacement suggested by a wind forecast. The correlation with the (t

[4] Inertial radiosondes attached to weather balloons (Gray et al [43]).
[5] For a complete description of the approach applied by EUMETSAT, see Schmetz et al. [87]
[6] Wade et al [107] suggest an optimal clustering approach for multispectral vector extraction.

- 30) and (t + 30) segments uses a search centred on the predicted location. Within the search windows, every 6th correlation is performed, with a full search being performed around the peak correlation coefficient. The correlation peak is parabolically interpolated to the sub-pixel level. The (t + 30) correlation is performed for each 3*3 matching template over a 19*19 grid centred at the symmetry point of the (t - 30) correlation.

The two displacements have to agree with one–another to within a specified magnitude and are curvature constrained. The corresponding cloud motion vector is suppressed if it is smaller than $5ms^{-1}$. Considering that there is a $1.5 - 2ms^{-1}$ error from image registration, this is an acceptable lower threshold. Once displacement vectors are calculated from correlation centres, the velocity vectors are computed. A final manual quality check is performed, before the data are disseminated to the NWP modelling communities and other users.

Globally, around 20,000 wind vectors are disseminated daily across the three main image channels offered by the main meteorological satellite operators[7]. The transmitted data are assumed valid for between 12 and 30 hours after generation.

## 2.2 Variations by operator

A comparison of texture tracking techniques applied operationally and used experimentally, and comparisons with some of the sources of ground truth, is given in Wang et al[109]. The main variations in the analyses performed by the different meteorological satellite operators are now listed for completion[8]. Hinsman [49]

[7] Note also that NOAA has been disseminating a high-density wind product since March 1998, which alone can produce around 50,000 vectors per day for the GOES-8 and 9 satellites. This has received mixed reviews from user communities, however, and its adoption at the time of writing was still being fine-tuned. The discussion of wind generation approaches is therefore limited to the low-density approach adopted by MPEF and GMS, and that used by NOAA prior to the advent of the high-density product. In addition, EUMETSAT are now disseminating high-resolution water-vapour winds as of the end of 1998

[8] INSAT winds, and winds generated by agencies other than satellite operators (e.g. Australia and China in the case of GMS-5 data) have not been included in this review: INSAT winds have been blacklisted by many modelling communities awaiting a more stable product (and INSAT imagery is not widely available), and the discussion provided is only intended

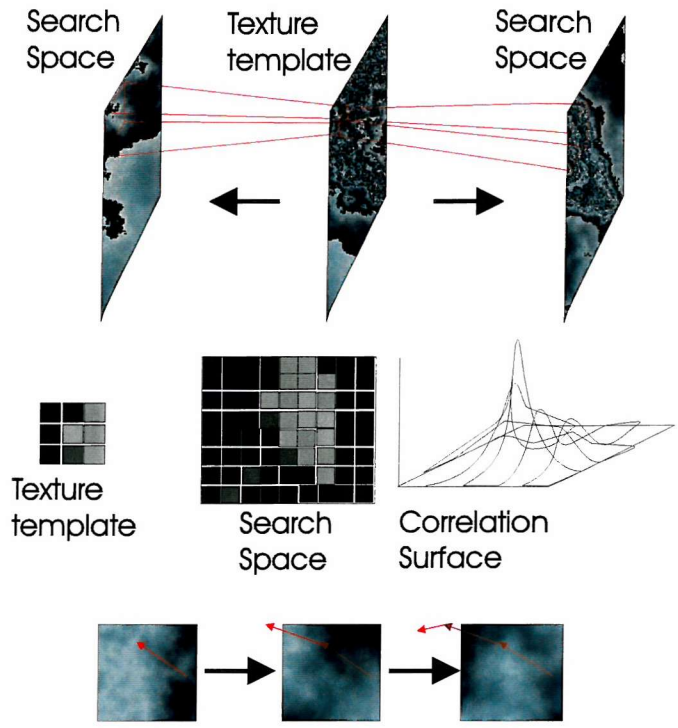


***Figure 2.1:*** *2–D cross–correlation applied to cloud texture tracking. A texture template is cross–correlated with a window of texture from the images before and after the template's timestep. The peak of the correlation surface (the maximum cross-correlation) is taken as the best match between the template and the window, and a vector is drawn between the matching points.*

expressed the desire of the World Meteorological Office for a standardised approach to cloud motion wind analysis: he reported that error analyses of the current satellite operators' techniques show sufficient deviations that some cloud track winds are routinely discarded. The differences between the satellite platforms currently in use limits the ability for a single tracking technique to be achieved in practice, particularly in light of the differences between the satellite sensor platforms.

to give an overview of the techniques in operation. Whilst there *are* differences between the texture tracking techniques applied by the non-operator agencies and those described here, the *main* technological advances and differences have been covered in the discussion of the satellite operators listed.

### 2.2.1 Japan Meteorological Agency

[9] The generic approach highlighted above assigns cloud motion vectors to the cloud top height. In the case of low level cumulus cloud, the motion is generated from winds driving the base of the cloud. In the operational Japanese Geostationary Meteorological Satellite (GMS) data analysis scheme, low-level winds[10] are assigned a fixed altitude of 850hPa. There are also two additional screening steps during target selection, namely removal of targets that may be subject to sun glint or those that may contain cumulonimbus. If the solar zenith angle is greater than 85° (or 60° in the case of low–level targets), the target is excluded from subsequent analysis as there is a high possibility of sunglint affecting it. The difference in brightness temperature between the infrared and water–vapour channels is calculated and the average difference over 2*2 pixel squares is used to low–pass threshold cumulonimbus data (a small temperature difference between the two channels signifies cumulonimbus). If more than 10 pixels are *contaminated* with cumulonimbus then the grid square is not used.

The quality checks applied fall into two categories, namely automatic assessment of both the quality of the correlation surface and the degree of agreement between vectors across an image triplet, and an objective quality control. The objective check ensures both horizontal and vertical consistency across neighbouring vectors, and ensures agreement with NWP model data. It is important to note that these are quality checks, and are used to remove poor data only. They are not used during vector generation to improve vectors. Hamill and Nehrkorn [99] describe an approach where horizontal consistency can be used during vector generation to select correlation surface maxima that provide locally consistent vectors. Collocated radiosonde data are, in a similar vein, not used for quality control, only for post-dissemination assessments of vector accuracy.

[9] As described in Tokuno [101]
[10] For cloud tops below 700hPa.

### 2.2.2 EUMETSAT

The EUMETSAT model takes into account the fact that low cloud is driven by wind at its base by way of a variable height correction for low cloud vectors. Quality control is mainly automatic, using similar tests to the JMA. The output of each quality test is continuous in the interval 0 to 1 from which a final quality measure is generated by means of a weighted average. A threshold for the final quality measure is used to pass some vectors, fail others and mark the remainder for manual assessment. During manual quality control, in addition to assessing the vectors marked for manual sorting, rejected winds can be reinstated and accepted winds deleted. It is worth noting that the use of continuous outputs from the quality tests makes them suitable for combining using a fuzzy system, e.g. to prototype new quality measures or determine the most appropriate weights for each quality measure.

Gärtner [39] discusses the moves towards full automation of CMW generation by EUMETSAT, by making the consistency checks (spatial and temporal agreement of vectors) more rigorous, and by combining winds generated from all channels into a single winds product, thereby ensuring cross-spectral consistency also. The new Satellite Applications Facility at EUMETSAT also aims to provide greater levels of vector interpretation for METEOSAT Second Generation (MSG) data, in terms of identifying zones of interest such as the onset of convection and shear structures, although no proposed approaches for this have yet been identified.

### 2.2.3 NOAA / NESDIS

An additional significant source of error from the NOAA GOES platforms results from their use of a 3-axis stabilised satellite, rather than the spin-stabilisation of both GMS and METEOSAT. 3-axis stabilised platforms are subject to differential heating, resulting in degraded image navigation, i.e. poorer co-registration of images. An automatic image registration stage is applied to GOES data using landmark identification and matching. Cloud-free landmarks are able to be

cross-correlated to a very high degree due to the prior knowledge of the landmark shape and the spatial agreement necessary between all landmark correlations. Brown [12] gives a thorough review of image registration techniques. The registration error is still significant in Southern Hemisphere GOES–9 data, however, where there are few cloud-free landmarks available for registration. Instrument-induced errors are not discussed any further in this thesis, but Diekmann [30] provides a useful overview of the typical geometric and radiometric errors and their treatment for METEOSAT satellites.

Quality control has been fully automated in the NOAA / NESDIS product since 1994 (Menzel et al [69]). Since late–1997, a new *high density* wind product has been generated operationally (Gray [43]), with about ten times as many vectors as the standard approach. GOES–8 and –9 have also been collecting a number of special imaging sequences at down to 30–second time resolution, mainly of hurricane data, from which high temporal resolution cloud motion vectors have been generated, aimed at improving wind information from hurricane regions where the standard 30–minute temporal resolution is too crude for the cross–correlation technique (Purdom [81]).

## 2.3 Need for Improvement

In light of improvements to numerical weather models, new sources of wind data and new forecasting tools, the satellite wind community held its first independent meeting in 1991 to identify and address the changing needs and uses for satellite wind data (EUMETSAT [33]). Some of the needs for improvement highlighted by the community (EUMETSAT [33] [34] [35]) are given in Table 2.2.

Butterworth [19] gives a similar review of the UK Meteorological Office's recommendations for changes to satellite winds. Much recent work has been targeted at improving height assignment of cloud motion winds, with significant improvements having been achieved for semitransparent and subpixel cloud using the difference between infrared and either water vapour or $CO_2$ absorption channel

1. Improved height assignment for cloud tracers (the major problem, especially near jetstreams).
2. Reductions in RMS error of the vectors produced, to the WMO target of 1-2m/s.
3. The need to address the assumption of cloud as a passive tracer for the wind: Cloud motion vectors are not always representative of the windfield.
4. Better and different validation techniques.
5. Better and different quality indicators.
6. Changes to current data collection schemes to include *rapid scans.*
7. More information about the meteorology local to tracers, to help identify their cause or at least their usefulness.
8. Some discussion as to whether model data should be used as a first guess for improving cross–correlations.
9. Better use of satellite winds by the user communities.
10. The need to develop other uses of cloud dynamics, many of which have already been identified.

***Table 2.2:*** *Some of the requirements for change in satellite wind data as highlighted by the Satellite Wind Community in its past three workshops (EUMETSAT [33] [34] [35])*

data. In addition, a growing number of studies have used spatially and temporally collocated geostationary and polar orbiting satellite image pairs to improve cloud height assignment using stereographic matching techniques. The difficulty in collocating the different sources of image temporally and registering them to the same projection is significant, however. More success has been achieved using the overlapping regions of neighbouring geostationary satellites, whose projections are more easily co–registered due to the fixed view of the satellites, and whose data collection cycles are temporally collocated.

Many of the remaining issues of concern relate to the lack of meteorology in the current approach. Without some understanding of cloud dynamics incorporated into the vector extraction technique, the suitability of any tracer for any specific task cannot be assessed automatically. Unless the cause of cloud motion can be

identified at least in part, no appropriate validation can be performed. If the generated vectors are not compared to motion data of the same scale or do not track the same meteorological phenomena then the comparison is at best difficult and at worst not valid. The main source of ground truth is rawinsonde data from weather balloons, which are generated from the change in horizontal position of the balloon during its ascent, as reported by onboard inertial guidance or ground-based tracking. This is effectively a point measurement of the windfield through the atmosphere, and is indicative of the local winds about the balloon's ascending track only. In steady conditions, the data can be accepted as good estimates for the windfield over a large area, but atmospheric turbulence can vary significantly, both vertically and horizontally. Without any means of measuring this on the radiosondes, the usefulness of these point measurements for assessing the accuracy of much larger mean flow measurements must be limited.

Other sources of ground truth data include ASDAR[11] and ACARS[12] aircraft reports of winds, ground-based stereographic cameras and model data.

ASDAR and ACARS are a useful source of wind information, but have two significant limitations: wind data are only available along aircraft tracks, and aircraft do not tend to fly through cloud for extended periods of time. Tracking clouds from satellite images over land is complicated by the variability in the background appearance and temperature, and satellite motion vectors over land are therefore taken as less reliable, when they are used at all. Since the majority of flight time through cloud is on ascent and descent from and to an airport, the usefulness of ASDAR / ACARS for verifying cloud track is limited. Morone [71] provides a review of aircraft wind data and details the error sources and degree of spatial and temporal data averaging from the technique.

Stereographic ground-based cameras provide local estimates of cloud motion. Comparisons between these motion estimates and satellite data are potentially simpler than for other validation sources in that both provide indications of *cloud*

[11] Aircraft to Satellite Data Relay

[12] ARINC [Aeronautical Radio, Incorporated] Communications Addressing and Reporting System, which transmits data directly from aircraft to ground stations

*motion* rather than *wind.* The main limitations are the amount of coverage possible with stereographic cameras, typically over land, and the necessary assumption that the top and bottom of the cloud is showing the same type of motion, which is not the case for many cloud dynamics.

Using predicted winds from numerical models to validate cloud motion winds is controversial and causes concern due to the fact that the validated CMWs are then fed to the model as inputs. This coupling between input and output data would normally be unacceptable, but due to the lack of sources of ground truth and the complexity of the atmospheric models, this is accepted practice. Models reject data that are significantly different from their predictions in any instance, however the differences between models both of different scales and run by different communities globally can be significant. Any quality control of vectors using one model prediction only may therefore bias other models using the same vectors towards the same solution.

More serious, however, is the use of model data in *generating* cloud motion vectors, as per the NOAA / NESDIS *autoeditor*(Schmetz [86]). The centre of the cross-correlation template matching windows are selected based on model-predicted wind vectors. Whilst this is a weak link between model input and output, this approach could bias the correlation match incorrectly where the model is incorrect. Since inputs are most critically needed when and where the model is in error, this has potentially serious consequences.

At the first International Winds Workshop, Schmetz [85] reported that the numerical modelling community had improved their models since the introduction of CMWs to a stage where the impact of satellite wind data was not very significant, i.e. the forecast winds from the models showed little or no improvement when supplied with the cloud motion winds. Forecasters similarly rely far less on satellite derived wind observations due to their tendency to have clusters of errors, incorrectly assign heights and underestimate fast moving airmasses (Butterworth [19]). Kelly [53] has more recently shown the influence of each of the different sources of wind information on the ECMWF model forecast, and has

produced a mixed picture of the benefits of cloud motion winds in the presence of other satellite and/or radiosonde data. Different quality indicators, independent of validation sources, are still however needed to assist in good vector selection.

It is worth discussing briefly the nature of the measurements of wind listed above for completion. The rawinsonde and ASDAR / ACARS data are a measure of windspeed. The aircraft measurement is collected at the operating speed of the aircraft, and is fairly immune to small-scale variations over hundreds of metres. The rate of climb / descent of the aircraft is slow relative to the wind measurement, therefore the data can be taken as a mean single-layer estimate of wind for every point at which a measurement is taken. Rawinsonde data depend on the weather balloon acting as a passive tracer for the wind. The balloon's buoyancy causes a strong vertical ascent, but the horizontal momentum of the atmosphere at any level is able to be recorded by the degree of horizontal displacement through the ascent. This involves averaging horizontal displacement over some vertical extent, but this is of a much smaller scale than the equivalent aircraft data. Ground-based stereographic cameras and Satellite-based cloud motion winds [13] track clouds. The conditions necessary for clouds to be good tracers for wind have already been given (Table 2.1), but the motion of clouds is of interest independently of the wind information it contains: cloud dynamics have produced some significant impacts to hurricane forecasts and tropical weather analyses (Velden [105] [106]), for example. Finally, model data provide a magnitude and direction for the dynamics of the atmosphere at every grid point.

Clearly grouping all of these motion types under the heading *wind* is not constructive, especially now that the issue of passivity for cloud tracers needs to be addressed for further improvement of cloud motion wind data. Mahrt and

[13] The use of the term Cloud Motion Wind is restricted to visible and infrared channels, where the structure being tracked is able to be interpreted as a cloud. The newer Water Vapour channel vectors are called Water Vapour Motion Winds, to signify their significant differences, essentially acting as deep layer mean motions. More recently, the term Atmospheric Motion Wind (AMW) has cropped up in the literature. The author believes that this still confuses the scale of motion detected, and the concept of atmospheric motion at synoptic scales should avoid use of the term wind, which is most commonly used for local and mesoscale phenomena, and should be restricted to this use for clarity. This debate does not address the other types of motion captured by these metrics (such as cloud motion not driven by the wind) that should be described separately again.

Sun [68] have considered the problems of scale–dependence of motion data for modelling and comparing models of different spatial resolutions. For example, in a region where average flows are weak at a large scale, there may be significant turbulence disguised within the averaging at a mesoscale that reduces the usefulness of the large scale analysis for local areas and vice–versa. Stohl et al [95] propose a method for overcoming this to some extent by interpolating low–horizontal–resolution vertical wind profiles using a high–resolution horizontal wind profile at a single level as a seed to provide high resolution profiles at any height. This does not address the issue of combining different *descriptions* of wind motion, however, such as imprecise knowledge of the development of a weather system and an array of anemometers providing small–scale details of wind motion. Ray [83] presents a spatial and temporal definition of various meteorological phenomena ranging from macro scales (of the order of tens of thousands of kilometres and months) to micro scales (of the order of metres and seconds), including wind phenomena.

## 2.4 Active Research

A variety of changes and new techniques have been and are being explored to overcome the problems of the current approaches to cloud and atmospheric motion analysis from satellite image sequences. A review of this current research is given briefly, by field.

### 2.4.1 Water-Vapour Winds

Water vapour structures were first tracked over sequences of images using WV images from the Temperature / Humidity Infrared Radiometer aboard NIMBUS-5(Kastner et al [52]). Due to the complexity of water vapour motion, the development and operational acceptance of a WV wind product has been a piecewise process. Initial studies considered the cloud–like components of the imagery, and high–level motion analyses. Mid–level motion was first discussed by Eigenwillig and Fischer [32], where small–scale structures in cloud-free zones were success-

fully tracked. Laurent [60][61] considers the specific properties of water–vapour data and the requirements for preprocessing. The results of the first study led to the use of the standard cross-correlation approach to cloud motion analysis being applied to water-vapour motion too, as detailed in Laurent. Height assignment techniques for water-vapour structure tracking are described in Büche et al [16]. The main advantage of tracking water–vapour structures over the visible and infrared counterparts is that they exist in cloud–free regions. The main difficulty of water vapour motion interpretation relates to the fact that water vapour structures are typically far deeper than clouds, and therefore their motion represents a very deep mean layer motion.

### 2.4.2 New Sensors

Interest in high resolution visible data has increased, despite the difficulties concerning changes in cloud representation with solar zenith angle, and the daytime-limited collection period for visible data: The use of high resolution METEOSAT imagery has provided significant improvement in the yield of low-level information from satellite winds (Ottenbacher et al [78]).

An important improvement to reduce errors locally without changing current wind analysis techniques is to change the satellite radiance data collection schemes to include *rapid scans* at 15 minute temporal resolution or better over areas of meteorological significance. This is particularly useful in light of the new platforms and sensors that are now able to offer temporal resolutions at significantly better than 15 minute resolution (indeed up to 30 *second* resolution for limited area scans), at up to 1km spatial resolution. Stable methods able to handle this resolution of analysis will be needed to process the quantity of data expected in the next few years. Swadley [97] discusses a non-correlation-based approach to analysis of GOES rapid-scan data, using template matching numbers, or the sequential similarity detection algorithm, where the absolute difference in greyscale between pixel values in a template and possible matches within a search area give good performance for 1km data. An ability to generate variable resolution

vector fields may also be of interest, for example to analyse severe weather more densely than the background weather pattern. Another major concern with the new sensors, however, is management of the data collection to optimise the use of rapid scans, particularly to meet the needs of many different end users.

### 2.4.3 Height assignment

An area of concern regarding height assignment of cloud tracers which has received much attention is that of semitransparent or sub–pixel cloud. Typically in the case of sub–pixel contamination of a low cloud from a thin higher–level cloud input, the underlying cluster is assigned too high a pressure altitude. Conversely semitransparent cloud is typically assigned too low an altitude. This has been addressed to some degree by the $CO_2$ slicing technique (Susko and Herman [96]), which also helps identify regions of strong vertical shear. In the case of METEOSAT data, the difference between infrared and water vapour data is used to identify where cloud may be semitransparent or subpixel, as opposed to IR and $CO_2$ data. This is also similar to the JMA application of the difference in brightness temperature for identifying cumulonimbus.

On a slightly different issue, Kishtawal et al [57] apply complex empirical orthogonal functions (EOFs) to determine vertical wind profiles from cloud motion vectors by analysing the vectors over dense radiosonde station areas. The use of the EOFs gives reasonable performance where two or more levels of cloud motion wind vector are available in a small area. Clearly an improvement in height assignment of cloud motion vectors would improve this performance further.

### 2.4.4 Smoother cross-correlation

Correlation-relaxation approaches provide smooth vector fields typically by applying spatial or temporal constraints on correlation peak selection, resulting in the most appropriate correlation peak being selected, rather than the maximum.

A good introduction to relaxation labelling techniques can be found in Hummel and Zucker [51]. Wu et al [112] introduce a correlation relaxation approach for analysing sea surface velocity vectors. In Wu [111], a fast relaxation algorithm applied to cloud motion is demonstrated. Côté [24] describes a new approach to correlation relaxation using a Hopfield neural network to select the optimal correlation surface peak to give locally smooth vectors.

### 2.4.5 4D Variational Assimilation

The newest techniques in numerical weather modelling involve direct assimilation of satellite radiance imagery without any data preprocessing, allowing the models to infer information as necessary, including dynamics information, from the raw data. The data assimilation techniques can still make use of satellite winds however. In fact, according to Kelly et al [54] both more frequent production cycles for satellite winds and greater knowledge of the nature of the motion measurement (i.e. whether it is a deep layer mean motion or a shallow layer cloud wind) would be particularly useful to the new approach. At their simplest, the variational assimilation techniques are optimal filters of weather data. Courtier [25] and Lorenc [67] give a thorough introduction to the theory behind atmospheric data assimilation, with the equations for 3– and 4–dimensional variational assimilation (3–D and 4–D VAR) being provided by Courtier. Thépault [100] provides details of the operational 4D–VAR scheme as implemented at ECMWF, and comparisons are drawn with the full extended Kalman filter. He argues that the 4D–VAR approach achieves similar results to the Kalman approach but at significantly less computational cost. He also justifies the use of linear approximation, as perturbations at model resolution evolve approximately linearly over the 24 hours of the temporal assimilation. Andrews [2] provides similar detail for the UKMO implementation.

Whilst it has been recognised by the modelling communities that satellite winds still provide a useful separate input from the direct radiances, models are beginning to address some of the more fundamental questions of cloud motion descrip-

tion. It is increasingly necessary both to define the meteorology associated with any particular cloud dynamic and to determine that component of cloud motion independently of other motion components. In addition, radiance assimilation has led to predicted radiance data. To determine the success of this to capture the cloud dynamics at all the scales of meteorological analysis, some mechanism to determine the dynamics at these different scales is required, both for validation and as a potential new data source in itself.

### 2.4.6 Cloud Tracks

Work by Szantaï and Desbois [98], and Raffaelli and Seze [82] has considered the use of tracking clouds over longer time periods than the current image triplets to produce more stable tracks of cloud motion. The current approach is subject to greater error, but allows small-scale or turbulent flows to be captured. By identifying the trends over longer series, different components of the cloud dynamics can be identified, however. Related to this is the determination of relative motions, particularly storm-relative motion. For example, Kerr and Darkow [56] have captured and removed the major motion component from thunderstorm motion analyses, and have seen some pattern in tornado development locations within the storm as a result. It is generally known that deformation zones, one of the main mechanisms of cloud development, occur from flow relative to the mean flow (Bader et al [5]).

# 3. PROPOSED CLOUD MOTION ANALYSIS

This thesis considers a number of the concerns of the cloud motion wind community given in Table 2.2. The principal topic of inquiry relates to the issue of the suitability of cloud as a tracer for the wind. Rather than focussing on cloud motion analysis with the sole aim of determining the underlying *windfield*, the approach aims to describe the cloud motion *itself* as richly as possible, even the components that are unrelated to the underlying wind. From this start point, there is the possibility of determining the cause of any different motion behaviour present, i.e. once a rich description of the cloud motion has been obtained, it is easier to determine which if any of the components of that motion are due to the underlying windfield.

New quality measures for wind data arise directly from this work, with an analysis of the causality of cloud motion providing a *suitability* measure for using any vector as descriptive of any particular type of dynamic, whether that be wind, weather system motion or some other description of motion. In addition, by providing a number of new measures of the motion of a cloud, the issue of data validation is re-exposed. In itself, this is not of benefit, but by discriminating between the different types of motion displayed by cloud, it is hoped that the unsuitability of using point measurements of wind data for validating cloud motion winds in many instances will be highlighted. Clearly there is a need for a greater number of independent validation tools, to validate each component of the cloud motion identified. By suggesting spatial and temporal scales over which the motion types act, and where possible identifying the meteorological cause of the motion types, validation sources suitable for the scale and meteorology can be developed.

Whilst not proposing to offer any specific benefits for those charged with identifying suitable uses for *rapid scans* and novel data collecting schedules, it may be possible to determine automatically which types of cloud motion have significantly different dynamics components at different temporal scales, i.e. which would benefit from greater temporal resolution, purely from a multi-scale analysis point of view.

Any analysis of RMS error for the new motion vectors generated would require careful scrutiny: In light of the previous discussion regarding validation sources, it is not obvious what measure of error would be suitable. The potential for identifying suitable and accurate vector representations of wind data from this rich cloud motion analysis should result in a reduction in vector error, but such work is beyond the scope of this thesis.

This thesis is therefore limited to introducing this cloud-centric analysis of motion in satellite imagery, and the mechanism by which the new measures of cloud motion are obtained. The approach presented is justified with examples and comparisons to other techniques where appropriate. Quantitative performance analyses are generated for specific components of the approach. In addition, the thesis introduces fundamentally new descriptors of cloud and parameters of cloud motion, the benefits of which are discussed qualitatively. On more widespread adoption of the fundamental concept of *rich cloud motion description*, it is possible that other techniques and methods will be identified as equally suitable for each step of the analysis presented.

## 3.1 Motion-based Segmentation

The initial premise of this thesis is that fundamentally different *types* of information regarding the motion of cloud in satellite image sequences can be obtained from more than one set of motion analysis tools. The initial research in this thesis considers the issue of segmenting the image data based on the suitability of certain motion analysis tools to track any given region of image content.

A top–down approach for processing the cloud imagery has been selected. Sonka et al [94] describe top–down and bottom–up image understanding control strategies in more detail. The main principle of top–down or *model–based* image processing, however, is that it is *goal–driven*, imposing certain criteria on lower–level processing. *Intelligent* computer vision systems are not restricted to top–down analyses, and indeed there are good arguments for both approaches under different circumstances. Where a technique is applied to a variety of unknown or widely differing problem spaces, bottom–up analyses allow hypotheses to be built up from knowledge acquired directly from the raw data. Where the problem is more fixed or known, as is the case here, using the available prior knowledge helps remove spurious information and directs processing towards suitable values [7].

It is interesting to note that research into the mechanisms of *human* vision has still to show conclusively whether our visual system uses a top–down or bottom–up approach (or something in–between, such as the feedback or heterarchical approaches described in Banks [8]). Marr captures the contradiction by theorising that human vision serves primarily to derive shape information, suggesting that the edge, brightness, colour and texture etc. collected enroute are driven by this high–level goal [42], yet the image filters he describes for the initial visual field transform require little or no call on high–level knowledge [44]. Much active research in the field of human vision follows the top–down analysis approach, however, as it is widely believed that the *visual buffer*[1] is left mainly unprocessed until such time as information is required, when the data are processed according to the task required (e.g. Kosslyn [58]). Whilst human vision systems should not unduly affect the choice of approach for computer–based automatic image processing, there is much active work on models of human vision processing that provide inspiration for new computer algorithms.

Using form to derive motion information and vice-versa are both problems that have a number of applications and coupling context / shape and motion information is an area of active research. Weiss and Adelson [110] provide an introduction to the types of problem with this coupling, and provide a framework within which

[1] The raw signal collected from the retina

the two can be analysed simultaneously. In order to identify the different types of motion in satellite image sequences, an automatic technique for segmenting the image sequence by motion type has been developed. Two classes of algorithm are of interest for this specific problem, namely *fuzzy segmentation* where regions of imagery can be assigned a degree of association based on the degree to which they display similar characteristics, and *model based motion segmentation* where the motion displayed is matched to model motion types and successful matches are used to segment the data. *Multiresolution motion analyses* provide a useful starting point for this discussion also.

Dimitrova and Golshani [31] discuss the concept of a multiresolution hierarchy for describing video content in *spatial* terms ranging from the pixel data through objects and features to semantic descriptions of the image content, and in *temporal* terms from pixel matching through to a semantic motion description. Given some video data, a description of the motion in the data is built up across this known hierarchy of analysis types. Any query is then mapped onto the most suitable level of the hierarchy. For cloud motion analysis it is suggested that there is a similar hierarchy relating to different types and scales of motion displayed by cloud, from small local–scale phenomena to synoptic–scale atmospheric motion. The nature of this hierarchy is not as clear, however. Dimitrova and Golshani have effectively solved the reverse of the current problem: their system is used to allow the known hierarchy of motion in video data to be mapped to a query whose position in the hierarchy is unknown. For the cloud analysis problem, the scale of the motion of interest *is* known (the query will typically request knowledge about synoptic or mesoscale or local scale motion), but the nature of the hierarchy of motion types in the data is not. Blostein and Ahuja [10] provide a useful discussion of multiscale analysis for single image region detection, where regions are segmented based on their textural *uniformity*. Uniformity is determined relative to neighbouring regions or *neighbourhoods* to the identified regions. The multiresolution aspect of the analysis is driven by the fact that small uniform regions require comparison with correspondingly small neighbourhoods with the analogous relationship for large uniform regions. In determining the suitability of a motion analysis tool for tracking cloud, it is necessary to consider

the spatial and temporal scales over which such an analysis is suitable. Indeed the choice of parameters for discriminating between the suitability of the different motion analysis tools is based on spatial and temporal variability in the data.

Multiresolution analyses are not suited to the analysis of cloud motion in two fundamental ways, however. The analysis tool applied to cloud motion tracking is different at each resolution, so, for example, where Blostein and Ahuja use the same measure of uniformity over different sized neighbourhoods (see also Nam et al [73], for example), in the case of cloud motion tracking a textural analysis may be suitable for small scale tracking, but structure tracking is more suited to lower–resolution analyses. Also the types of motion analysis to be applied to the cloud data do not differ solely by resolution. For example, tracking small cloud objects as structures and tracking texture windows are of approximately similar scale, as are tracking the edges and medial axes of clouds, but each of these techniques gives a fundamentally different viewpoint on the cloud motion, providing different information.

The application of fuzzy logic for segmenting *video* data is a new area for research and is novel in the field of satellite image analysis. Fuzzy logic has, however, been applied successfully to static image segmentation problems. Udupa and Samarasekera discuss the fuzzy connectedness of image elements to define *fuzzy objects*, a discussion which is revisited when considering extracting cloud objects. Ghosh [41] similarly uses fuzzy sets on the output of a self organising map for extracting objects from imagery. In addition, there have been a number of applications of fuzzy systems for segmenting satellite data for describing land use (an inherently vague concept), e.g. Lewis et al [65], [63].

Model based motion segmentation is an active area of interest primarily for movie data analysis, where models of camera motion (pan, zoom etc.) are known. Torr [102] uses three motion models[2] to segment features in a movie sequence where the specific motion of the camera and the objects in the imagery is unknown. Torr identifies limitations of vector clustering after image analysis and highlights

[2] The correspondence between points in any two images conform to a fundamental matrix, affine fundamental matrix or projectivity

many more limitations specific to moving source and target problems.

In the case of cloud motion from geostationary satellite image sequences, the viewing point is taken as fixed. This provides a much simpler starting condition on which to base any motion analysis, as the motion of interest is confined to the cloud data itself. In addition, whilst the suitability of the three different motion analysis techniques to track different types of content in the image is not explicitly known[3], the nature of the motion analysis techniques themselves and the criteria that affect their performance *are* known. The motion models therefore consist of some representation of the abstract concept of the *suitability* of each motion analysis techniques to track the phenomena under analysis.

Three complementary types of motion analysis tool were considered in this initial research, all aimed at identifying the wind component of cloud motion. At this stage of research, the accepted definition of *wind* was its widest possible definition, i.e. any atmospheric motion phenomenon from global scale to local eddy. Object extraction and tracking applied to small open- or closed-cell cumulus (i.e. small cellular cloud or *cloud hole* structures) gives details of the flow typically at small to medium scales that is *content–dependent* (it requires knowledge of the cloud content in the imagery to determine the location of small cloud cells and cloud holes). Cloud edge tracking is most suitable for large cloud masses that do not persist in a given region for a significant length of time (e.g. fronts that translate across an image over a sequence), and uses extended content-dependent features defined over a much larger scale than the other parameters. Texture-based tracking, which provides knowledge of the flow in an image *without* using any *understanding* of the scene under analysis, typically at small scales, is clearly suited to regions where a strong texture gradient or variation is visible in the imagery, but can also be used generically over cloud, where edge and object analyses are inappropriate. It is uniquely suited, therefore, to regions where cloud *does* persist in a given region for an extended amount of time. Many other motion analysis tools could have been selected for analysis, but these three capture

[3] The selection of the three techniques was made using a binary decision on their suitability, i.e. each is able to identify cloud motion to some useful extent, but the variation in that degree of usefulness over the spatial and temporal extent of the image sequence is unknown

different scales of motion and different dependencies on data interpretation, and therefore provide an indication of how motion analysis algorithm suitability can be used to segment image sequence data. Figure 3.1 illustrates the characteristics of the three types of motion considered, and Figure 3.2 shows these in real imagery.

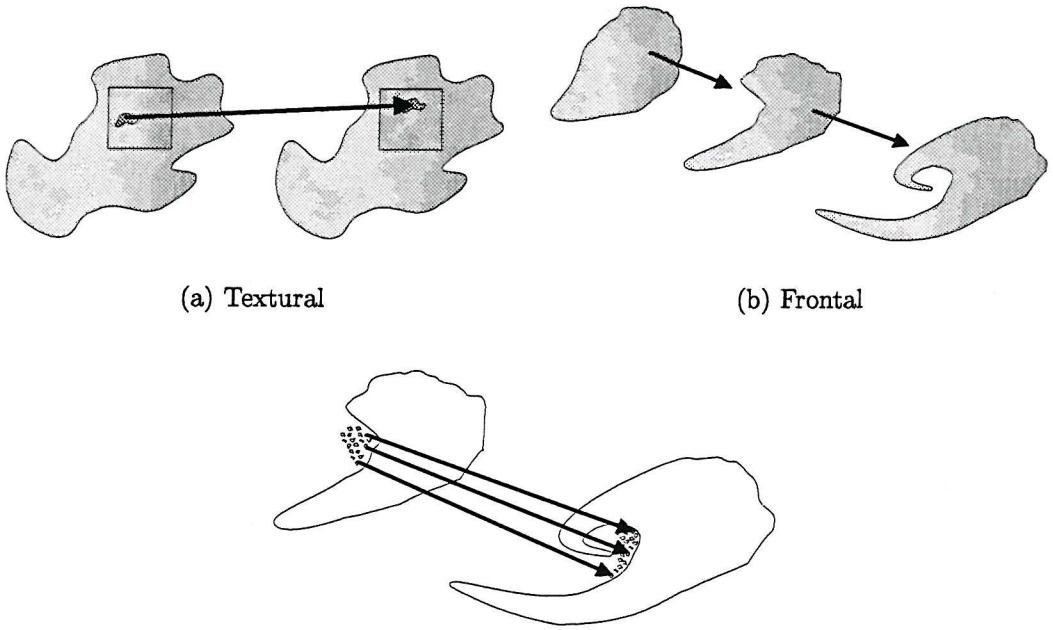

(a) Textural (b) Frontal

(c) Small Objects

***Figure 3.1:*** *Sketch of motion types for segmentation (a) Texture tracking, where for example the cloud sheet does not move significantly between timesteps, but the cloud tops within the sheet are buffetted by the wind, (b) Frontal tracking where the cloud moves significantly between timesteps and often changes shape and (c) Small Object tracking, where individual small cloud structures can be identified and matched.*

For small object analysis, the strength of greyscale variation is an indication of this suitability. In the case of texture–based motion analysis, the strength of greyscale variation is important, but also the time–persistence of a high mean greyscale (the presence of cloud). For frontal motion, a low time–persistence of a cloud region is desired. Whilst these indicators of suitability do not capture the complete requirements for successful application of any of the motion analyses identified, they are indicative of the types of indicator that could be used for any set of motion analysis tools.

Due to the nature of the segmentation desired, a fuzzy output is almost essential as any particular region of the imagery may be suitable for analysis by any of the motion analysis tools under consideration. The suitability of applying any tool to any given region of the imagery will similarly be a continuous rather than discrete function. As motion is analysed at different scales by the different motion algorithms, it is in fact likely that two or all three of the tools will be suitable for analysing a given region of the image, though at their respective scales. The motion types are clearly mixed, and there is no relevance in making the suitability functions sum to unity, as there will be regions of the imagery where none of the analyses are suitable and regions where more than one is ideally suited. A fuzzy system with non-normalised outputs has been developed to determine the suitability of these three motion analysis tools for generating sensible cloud motion information.

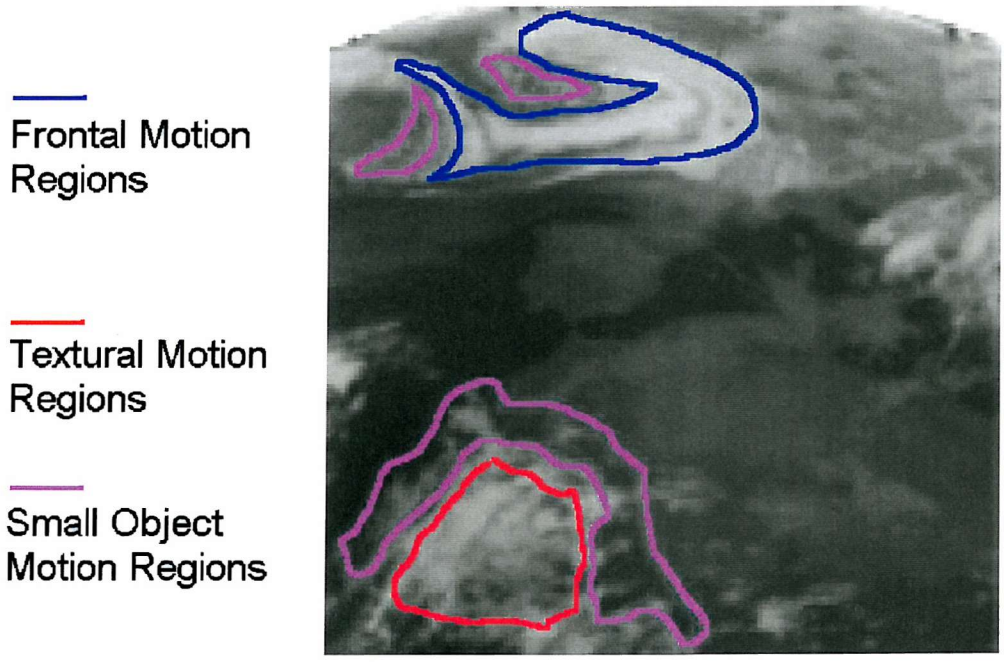


***Figure 3.2:*** *A sketch of a possible flowfield segmentation based on motion analysis tool applicability for METEOSAT IR data (the particular satellite image shown is from February 18th 1996 at 0030h).*

The three tools selected are not the only possible ones for analysing the motion of cloud, but are valid choices: texture analysis is uniquely used at present for cloud motion analysis operationally, therefore has been selected by the operational community as a suitable tool. Frontal analysis, or the analysis of large moving

cloud bodies, is useful for studying significant weather phenomena and the onset of vorticity / the formation of depressions. Their motion can be categorised as that of a non–rigid body, and has a clearly identifiable *whole body* component in addition to any smaller–scale internal components of interest. Small object tracking again is useful for significant weather phenomena, although on a smaller scale (e.g. storm cells), and tracking the feature can be directly related to the meteorology in the region since the feature being tracked is a meteorological one (as compared with the abstract concept of tracking *texture regions*). Future work in this field should, however, consider new parameterisations, e.g. in particular for better description of frontal motion analysis. The skeletons generated later in this study would provide one source of this information, and some work by Gamage and Blumen [38] also suggests the potential for wavelet and fourier techniques for such analyses. The concept of clustering or segmenting data based on their suitability for analysis using specific motion analysis tools is new, however, and the aim of this research is to prove the concept of such a segmentation. The selected tools and indicators will be shown to have proved this concept later in this thesis.

The questions raised by the concept of multiple motion analyses, identifying their suitability in any particular instance and the mechanism for combining them generate a number of more immediate questions relating to the nature of cloud motion at different scales. In particular, a careful examination of the term *wind* is necessary once multi–scale analyses are embarked upon, and as a result of this early study the term is redefined for the remainder of the research into the scale–specific terms *atmospheric dynamics* for global and synoptic–scale phenomena and the generic *wind* for local–scale motion. Whilst still unsatisfactory in many regards, this initial recognition of the differences between atmospheric motion phenomena at different scales is important. Ray [83] provides a very good definition of spatial and temporal scales of many meteorological phenomena including some wind–related phenomena.

In addition, the complexity of cloud motion itself as shown in satellite image sequences can be recognised as a direct consequence of this initial work. Subsequent

discussion therefore focuses on mechanisms to capture this complexity in as much detail as possible, and give some analysis of its causes from the perspective of the different scales of atmospheric motion phenomena identified.

## 3.2 Cloud extraction

Identification of cloudy pixels and cloud objects is performed early in the processing chain due to the potential gain from imposing such image knowledge. The cloudy pixels contain all the information necessary to identify cloud motion, and separating them from underlying data potentially reduces both computational cost and errors from background noise by allowing analyses to be targeted at the regions of motion (Banks [8] p234). In order to identify and track cloud pixels and objects, prior knowledge of clouds can be used. This knowledge most easily relates to large–scale information (likely dynamics of cloud structures, for example) or image content (synoptic–scale cloud features).

In order analyse the motion of the cloud component, it is first *enhanced.* A number of techniques are given in the literature for identifying cloud in satellite imagery, ranging in complexity from simple thresholding techniques to radiance modelling (e.g. Pankiewicz [79], Boekaerts [11] (the operational scheme applied by EUMETSAT to METEOSAT data), Kelly [55]). Figure 3.3 shows the difficulties with simple thresholding schemes for identifying the cloud content in an image. A fast approximate identification of cloud regions can be obtained by comparing the raw image data with a radiance template image of the underlying land and sea, however, and this is sufficient for the purposes of an initial image filter. A method for producing such a template using a simple persistence model of the radiance of the land and sea over a few days prior to the image under analysis is introduced later in the thesis.

Some smoothing of this initially filtered data is necessary to optimise the parameterisation of the cloud in a manner suitable for tracking its motion, both at differ-

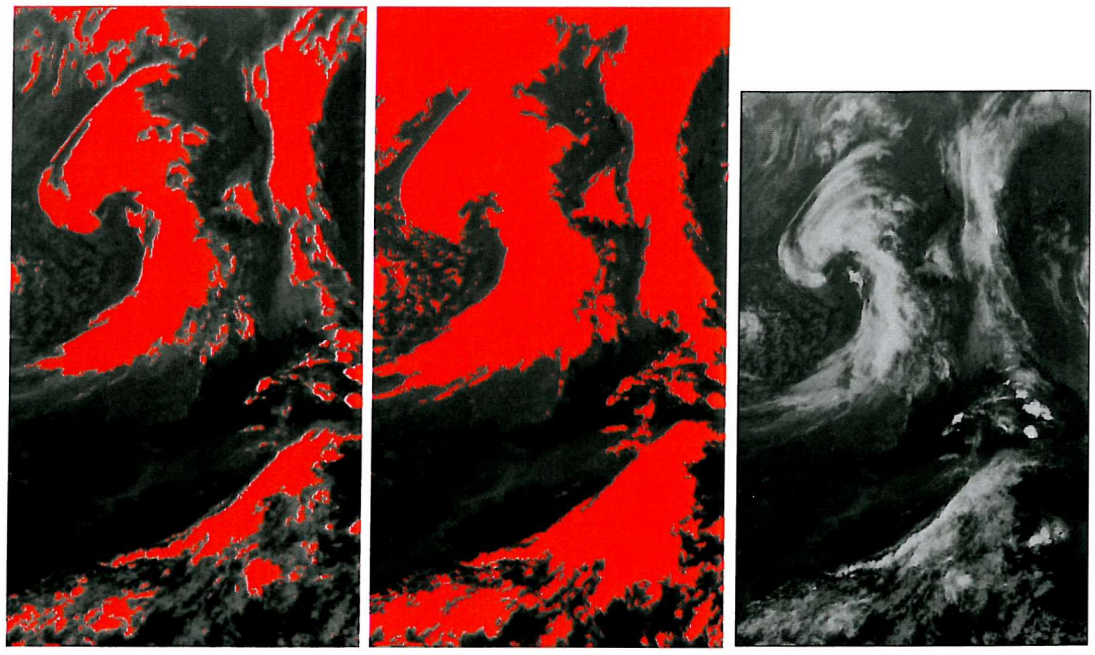

(a) High threshold (b) Low threshold (c) Raw Image

***Figure 3.3:*** *Difficulty of single–layer thresholding for cloud extraction. Figure (a) shows the extracted cloud objects for a high single–level greyscale threshold. The threshold has acceptably captured the majority of cloud in the upper half of the image, but has missed alot of cloud in the lower half. Figure (b) shows a lower greyscale threshold, which has captured more of the cloud in the lower half of the image, but results in non–cloud having been captured in the upper half of the image. Figure (c) shows the raw projected data for comparison. The imagery is METEOSAT D2 (infrared) from August 27, 1997.*

ent scales and using different tracking mechanisms[4]. Clearly the appropriateness of any given smoothing technique is driven by the selected parameterisations of the cloud, beyond a certain level of smoothing appropriate for most parameterisations of the data and for removing any noise in the data. Discussion of these smoothing filters is therefore left until after the selection of parameterisations.

In order to parameterise the image cloud content[5], it is first necessary to identify and extract the clouds themselves. The methods for extracting clouds should take into consideration the type of parameters to be used in analysing the cloud. In particular, any smoothing or characterisation of the raw data performed in object extraction should not be detrimental to the accuracy and performance of the subsequent parameterisations, and indeed may be used to improve them.

As has previously been discussed in the context of motion–based image segmentation, there has already been a large amount of research into image segmentation techniques. Reed and Hans du Buf [84] provide a good overview of texture segmentation techniques and differences between region– and boundary–driven segmentations[6]. Cloud analyses are often based on pixel–classifications of image data into cloud type. Dewitte et al [28] provide a particularly interesting example of this using greyscale morphology and various clustering and probabilistic techniques to classify cloud data, which are combined using a fuzzy logic approach. Other cluster analysis approaches to satellite data classification include Seddon and Hunt [89] and Burrough [17]. Adaptations of image thresholding techniques have been applied successfully to object extraction. In particular, Feher and Zabusky [36] introduce a *local filtering* technique that allows coherent vortex structures to be extracted from computational fluid dynamics flow analyses.

The most difficult aspect of image segmentation related to cloud extraction is the ability to capture the imprecise edge of the cloud and the ability to identify the vertical structure of the cloud to some extent. To generate any parametric

[4] e.g. texture tracking and vector feature tracking

[5] i.e. content–dependent parameters such as cloud shape or size, as distinct from parameters that do not require any prior interpretation of the imagery such as texture

[6] Principally, looking for homogeneous regions then finding their boundaries, vs. looking for the boundaries directly

representation of the degree to which the edge of the cloud is dissipated, it is necessary both to capture as much of the cloud edge as possible and to determine the degree to which the edge is associated with the cloud core, where possible[7]. Algorithms suitable for such analyses include snakes, clustering techniques and multi–level thresholding.

Hashimoto et al [48] describe a sampled active contour model approach to segmenting images, where sample points along a contour line are moved by attractive and repulsive forces towards the lowest energy state for each contour point. For cloud analysis, the difference between weak and strong cloud edges is significant, and the nature of a dissipated edge would require different active contour management to a crisp edge for successful cloud extraction.

Nichol and Fiebig [77] apply a multi–level thresholding approach to image segmentation using a technique known as the *binary object forest*, where connected regions are identified as objects and the change in objects with change of greyscale at which the slice is taken vertically generates a connected tree of binary objects. Nichol and Fiebig use the concept of a binary tree to analyse the motion in image sequences by comparing the differences in the binary trees over time. Motion is identified by areas of the image where the tree structure has changed. This is particularly suitable for analysis of rigid body motion from a static camera, where the rigid body moves a long distance between frames, but the background does not change significantly. It is worth noting, however, that the binary object forest provides a useful mechanism to describe the vertical variation of clouds, as will be discussed later[8].

Seddon and Hunt [89] use an unsupervised clustering approach for cloud segmentation and highlight the need for good segmentation for cloud tracking problems. Zhang and Postaire [113] propose an interesting addition to standard clustering algorithms: to enhance the boundaries between clusters, they use morphological erosion and dilation operators to enhance the modes and enlarge the valleys be-

[7] A dissipated edge region is *weakly* associated with the cloud core, showing less association across the region with distance from the core, and a crisp edge is *strongly* associated with it.

[8] In particular with reference to the work of Peak and Tag [80]

tween clusters in abstract data analysis problems. This *concept* has been adopted in this work for prefiltering the cloud data. Meyer and Beucher [70] provide a review of the direct application of mathematical morphology for image segmentation, using the *watershed line.* Such morphological segmentations are commonly applied to geographical data, from which the approach has acquired its name. Burrough and Frank [18] provide an excellent reference to geographical object identification and handling, and many of the issues they discuss, related to vague boundaries for geographical objects, are directly applicable to cloud objects too. A number of approaches considered in Burrough and Frank for imprecise geographical objects use fuzzy logic and fuzzy system analyses to handle the inherent vagueness.

Two approaches have been selected for this thesis, namely the use of a cloud core extraction and fuzzy growth algorithm and a technique that analyses slices through smoothed cloud data from the top down. This second approach doesn't identify clouds as structures, but provides vertical profiles of the cloud structure. Peak and Tag [80] use a very similar approach to satellite image segmentation for cloud feature interpretation.

## 3.3 Cloud Parameterisation

Cloud motion has been attributed with semi–rigid body motion characteristics by human analysts to a much greater extent than other fluid motions: clouds are identified as *objects*, the motion of collections of clouds are described as *weather system dynamics* and even highly dynamic subcomponents of clouds, such as storm cells, are identified and tracked as individual structures. Identifying an appropriate representation to capture the semi-rigid motion characteristics for each of these motion types is the domain of *parameterisation.*

The principal difference between each of these semi-rigid representations is the *precision* with which they describe the cloud. Synoptic scale meteorology studies atmospheric flows over thousands of kilometers, represented in cloud motion by

the displacement of large cloud sheets. To determine such flows from the motion of individual clouds requires stable centres for each cloudmass and a reduced level of precision when describing the motion of those centres. This motion is *extrinsic*, i.e. it relates to the interaction *between* large cloud systems or between a system and other global effects. Mesoscale meteorology in contrast concentrates on phenomena that extend over hundreds of kilometers, such as cloud systems displaying cyclogenesis[9], and fronts. To analyse this scale of motion, time series of shape and elongation information are necessary for each of the cloud structures. This motion is *intrinsic* to the cloud in that it identifies the change *within* a specific cloud object over time. It is important to distinguish mesoscale and local scale phenomena, however. Mesoscale motion considers the development of a whole cloud structure, where local scale motion captures change in a small portion of the structure, at the order of a few pixels (tens of kilometers). Mesoscale analyses must therefore be able to minimise the influence of truly local-scale effects, whilst capturing the effects that grow large enough to affect the whole structure. A related problem that is not tackled with current operational motion analyses is that of motion underestimation near jet flows (e.g. the jetstream). Here, the wind moves significantly faster than the surrounding regions and any cloud in the vicinity is cut by the fast flow.

Lewis et al [64] use shape characteristics such as area, edge eccentricity and elongation to describe cloud shape for classifying the cloud. Chin et al [22] use time series analysis (Autoregressive moving average) of morphological parameters of clouds to determine properties such as cloud directionality, clustering and cloud coverage, as well as to predict the trend of these parameters. Skeletons or *medial axis transforms* are another standard technique for describing shape. They provide a line representation of the shape under consideration, the lines forming the skeleton of that shape (e.g. Meyer [91], Arcelli and di Baja [3], Lam et al [59] (the comprehensive survey of thinning methodologies), di Baja and Thiel [29] and Ge and Fitzpatrick [40]).

Analysis of the development of skeletons provides knowledge about likely develop-

[9] In essence, the onset of a depression

ment of large–scale systems: whether they are likely to develop, or to collapse on themselves. Skeletons may also offer the potential to identify the onset of cyclogenesis: clouds in developing depressions typically undergo one of seven standard shape changes, most typically from a leaf shape to a comma to a vortex (Bader et al [5]). The skeleton of these three shapes is distinct, and the transition between states should be identifiable. This may require some analysis of skeletal curvature to identify regions of increasing general curvature. In addition, fuzzy skeletons can identify the degree of onset by the degree and direction of spread of the skeleton through its transition. The development of a vortex from various starting cloud configurations is described in Browning [14] and Bader et al [5].

It can be argued that human operators are very good at discriminating the different motion characteristics, and that an automatic system that is modelled on a biological vision system may offer an optimal mechanism for identifying these different characteristics. Many types of animal eye receptor cell axon respond to spatial boundaries by an increase in pulse frequency on the lighter edge and an inhibition of pulses on the darker edge, the pulse frequency therefore performing a type of fourier transform of the visual input stimulus (e.g. Bruce and Green [15] or Carterette and Friedman [20]). This in effect allows light gradient variations both spatially and temporally to be analysed. The variation in light (greyscale) gradient is of particular significance to the edge motion analysis problem. A crisp edge to a cloud, where the gradient in greyscale is very steep, may signify a wind flow parallel to the edge of the cloud, and thus crisp edges are good for identifying jet flow locations. Similarly, dispersed edges with weak gradients must have some component of wind flow across them, causing the dispersion effect. Cloud edges and edge *strengths* (the gradient of the edge) provide lines suitable for tracking cloud as structures. Crispness can be used as an indicator of the suitability of edge motion for use as wind motion, and similarly crisp edge motion can be used for describing *weather system* dynamics.

Due to the nature of cloud structures and the imprecision in defining an *edge* to a cloud, a fuzzy system has been chosen to sign a degree of *edgeness* to the cloudy pixels surrounding the core region of a cloud. The greyscale gradient for

smoothed cloud data could be used directly as a measure of the association to the cloud core. There are other factors, however, in identifying the degree of association of a pixel to a cloud core. For example, the similarity in brightness and the absolute greyscale of the pixel under scrutiny are all possible alternatives. Combining these in a fuzzy system provides a measure of the degree to which the pixels near the edge of the cloud are associated with the cloud core. A dissipated edge region is loosely coupled to the core, whereas all cloudy pixels right up to a crisp edge would be expected to have a high degree of association with the core cloudy pixels.

## 3.4 Data Smoothing

The primary measure of structural stability for objects used in this study is *coherence*[10], as apparent from multiple greyscale thresholds of the objects. Two smoothing algorithms are used to remove noise: a simple median filter removes noise at the cost of reducing precision. For coherence and edge gradient preservation, a novel filter based on the rolling ball algorithm has been developed. Wang [108] describes a morphological–based filter for removal of small local minima that uses some similar concepts. In contrast, Gupta and Knopf [46] describe image enhancement algorithms for handling image imprecision by mapping the raw pixel data onto an array of singletons on which the neighbourhood relationships can be analysed using a fuzzy system, prior to remapping the adapted singletons back into a pixel array.

Cloud shape is arbitrary, therefore the skeleton of a cloud must capture the significant structure (body and limbs) at the selected resolution under analysis. It must similarly be stable to variation in cloud shape / content at smaller scales and be robust enough to be trackable over time. The preprocessing performed in object extraction assists in creating clean skeletons, and is seen as a necessary component of skeleton generation, with particular regard to removing spurious

[10] See Figure 5.5 for a description of coherence

'holes' in binary object representations (e.g. Arcelli [3]).

Although considerable work has been done in the field of grey–scale morphology, the use of grey–scales in infrared satellite imagery primarily conveys height information[11]. As such, 3–D morphological operations are more appropriate than grey–scale algorithms. Fuzzy mathematical morphology allows the vagueness intrinsic in cloud structures to be captured and analysed, the primary difference between this and grey–scale morphology being the fuzzification both of algorithm and object. Fuzzy cloud objects have previously been described, but the fuzzification of morphological algorithms is a new and subtle step (Sinha and Dougherty [92]). It provides an approach for determining the degree of membership of each standard morphological operator. The approach taken by Sinha and Dougherty is that of finding a degree of subsethood. Chou et al [23] use morphological filtering (dilation / erosion) to remove small–scale variations in Landsat data.

## 3.5 Motion Analysis

Motion analyses can be split crudely into *optical flow* and related techniques and *feature matching*. Optical flow approaches use a change–constrained algorithm that considers a patch of image radiances as they are displaced a distance $(\delta x, \delta y)$ in time $\delta t$, where it is assumed that the radiance patch does not change over the timestep. Feature or parameter matching techniques, in contrast, use metadata derived from the raw radiances and match the *metadata* over time. Vega–Riveros and Jabbour [104] and Aggarwal and Nandhakumar [1] compare these two fundamentally different approaches to motion analysis and highlight the advantages and disadvantages of each.

The constraint of consistency on the radiance patch under analysis over time in

[11] Transforms between radiance grey–scale, temperature and height are possible via temperature–pressure profiles from sources such as sounder measurements or numerical weather models

optical flow techniques typically limits its application to nonrotating rigid bodies or imagery that is updated at a high temporal rate relative to the visible motion and as a consequence is not ideally suited to cloud analyses. Parameter matching requires suitable parameters, as previously described. A third class of algorithm consists of approaches that combine segmentation and tracking. These are numerous, for example active contour analyses are commonly applied across image sequences. Leymarie and Levine [66] provide a thorough introduction to using active contours for segmenting and tracking objects, and discuss their limitations too. Delagnes et al [26] discuss their application on complex backgrounds, such as would be encountered for cloud tracking in IR imagery.

To match the parameters selected in this thesis, distance measures and other topological metrics can be used. The vector joining successive skeleton points is determined using a nearest neighbour approach, where a circle centred at the *starting* point or the point under consideration on the skeleton in the first frame of the sequence is grown until it touches the skeleton in the next time frame (Figure 3.4). The vector joining the circle centre to the touch–point then defines the match. Where the circle from the starting point touches more than one next position, the mean direction is selected for the touching vector. Cloud edges are analysed similarly, only edges are matched based both on proximity to each other and relative membership to the associated cloud core, so that crisp edges are matched identically to skeletons, but dispersed edges are matched at each level of dispersion.

This approach has a number of potential risks and causes of error (see also Figure 6.4), but its performance on sparse skeletons and edges is sufficient to provide accurate matches in a majority of cases, and shows the potential of the selected parameters for describing the motion of clouds. Since this aspect of the research has been performed to allow the benefits of the rich parameterisation of the cloud to be highlighted, this initial level of line matching algorithm suffices. A discussion of the sources of error and simple enhancements to address these is given in Section 6.2.

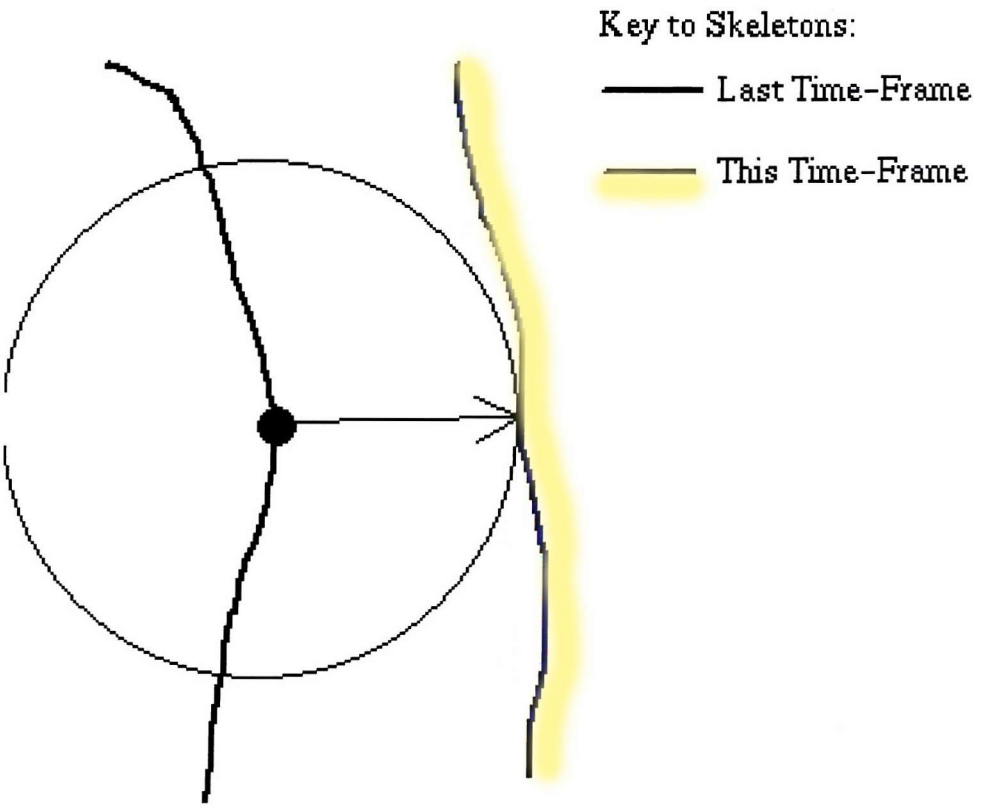


***Figure 3.4:*** *A simple nearest neighbour approach to skeleton matching. A circle centred on a point on the skeleton from the last time frame is grown until it touches the skeleton in the current time frame. The line joining the circle centre to the point on the circumference is the match vector. See also Figure 6.4 and Section 6.1.2 for a discussion of the limitations of this approach and methods to overcome them.*

By using the different parameters described, more of the cloud dynamics are captured than any single parameterisation can offer. This allows the motion to be described at different scales and is the starting point for analysing motion causality.

# Part II

# METHODS

# 4. FUZZY MOTION SEGMENTATION

A number of simplifying assumptions have been made in segmenting a moving scene according to the appropriateness of the motion analysis tools applied. Texture tracking, small cloud tracking and frontal analysis are assumed to capture, or at least be indicative of, the main motion types present in the satellite image sequences. Texture tracking algorithms have been assumed most appropriate within cloud regions. Whilst the greyscale gradients are strongest at cloud edges and strong gradients improve correlation, cloud edge motion is not indicative of the wind flow in a cloud[1]. Small objects have been associated with regions of high textural variation, and this has been taken as the only indicator of suitability for small object tracking techniques. The appropriateness of frontal system motion analysis has been determined by identifying cloud regions which do not persist in one place over a prolonged period of time. Figure 3.2 provides an indication of the types of region the segmentation should identify.

The image data used in this study have been obtained from Nottingham University's METEOSAT data archive[2]. Current images are available in Graphics Interchange Format (GIF), whereas archived data are stored in Joint Photographic Experts Group (JPEG) format at a lossy level of compression. In order to collocate imagery with other data sources, archived data have been used widely in this work. Appendix B details the differences between the image formats and gives examples of the degradation. The Nottingham data which are publicly disseminated by EUMETSAT as their standard WEFAX format are also contrasted

[1] At this stage, the distinction between the different scales of cloud motion is not being made, therefore the requirement for tracking the *wind component* of the cloud motion is less restrictive here than in subsequent chapters. It is used here to mean local scale phenomena *and* weather system motion.

[2] http://www.nottingham.ac.uk/meteosat

against raw image data available intermittently from Dundee University's Remote Sensing Resource Centre[3]. National borders and latitude–longitude marks are pre–superimposed on the Nottingham data. These have been removed using a border mask template to identify the location of border pixels and mean filtering across the border neighbours.

The underlying factor that remains in the approach is the necessity for different motion analyses to be applicable in overlapping areas. For example, cloud in a frontal system gives a good indication of the frontal dynamics in the region. Local winds in the neighbourhood of fronts are typically prone to significant variation, however, therefore strong textural markings related to convective structures on the leading edge of the front may act as good wind tracers. The edge of the front will therefore be a rich source of information for two distinct types of dynamic, and as such will require both motion analyses to be applied. As a consequence, a fuzzy motion region segmentation algorithm has been developed and applied to sequences of satellite data.

## 4.1 Data Preparation

Due to the nature and source of the imagery, it is first necessary to remove the country border and marker data added by EUMETSAT prior to dissemination. Having removed the borders and markers, suitable parameterisations are used to discriminate between the types of motion identified in the imagery, before passing the parameters to a fuzzy system that determines the degree of suitability of each analysis.

### 4.1.1 National Border Removal

In the case of METEOSAT, the data from the satellite are first received by EUMETSAT in Darmstadt where national country borders and position crosses

[3] http://www.sat.dundee.ac.uk/pdus.html

are added prior to retransmission to the satellite for dissemination. Public data archives store this disseminated data, requiring the borders etc. to be removed prior to analysis.

A template of the location of the borders and markers was produced manually from a METEOSAT D2 infrared image whose border regions were distinct. The thickness of the border region was made one pixel wider than the identified border[4] to account for any border misregistration or border template alignment variation up to a magnitude of one pixel in any direction. This increases the number of pixels in the edge region, but ensures that any possible pixels contaminated with border or marker greyscales are suitably identified (Figure 4.1(b)).

The pixels in the border and marker region are replaced with the median value of the immediate neighbours to the edge (Figure 4.1(d)). Whilst these pixels do not contain valid data for analysis, larger–scale analyses that are unaffected by pixel–scale errors are possible as a result of such smoothing. The smoothing algorithm applied is given in Equation 4.1.

$$S(x,y) = X_m(x,y,\delta), \text{ the median of } X(x,y,\delta) \tag{4.1}$$

*where*

$S(x,y)$ = smoothed border pixel value

$X(x,y,\delta)$ = The set of non–border pixel values at a distance $\delta$ from $(x,y)$

$\delta$ = the minimum value for which $X(x,y,\delta) \neq \emptyset$

The algorithm was coded in C++ and the border template accuracy and median filtering was validated against a number of different METEOSAT images by checking for missed or inappropriately replaced border pixels. The compu-

[4] In an 8–connected sense, 8–connected referring to the fact that all eight neighbours of an identified marker point were similarly marked as marker points. This contrasts, for example, to 4–connected regimes where only the pixels above / below and left / right of the pixel under concern are analysed, or weighted schemes where the diagonally–connected pixels are marked for *partial* smoothing only.

tational cost of this algorithm was found to be negligible[5] for METEOSAT D2 images when run on a machine with a 150MHz processor with 64Mb of RAM running Windows NT 4.0.

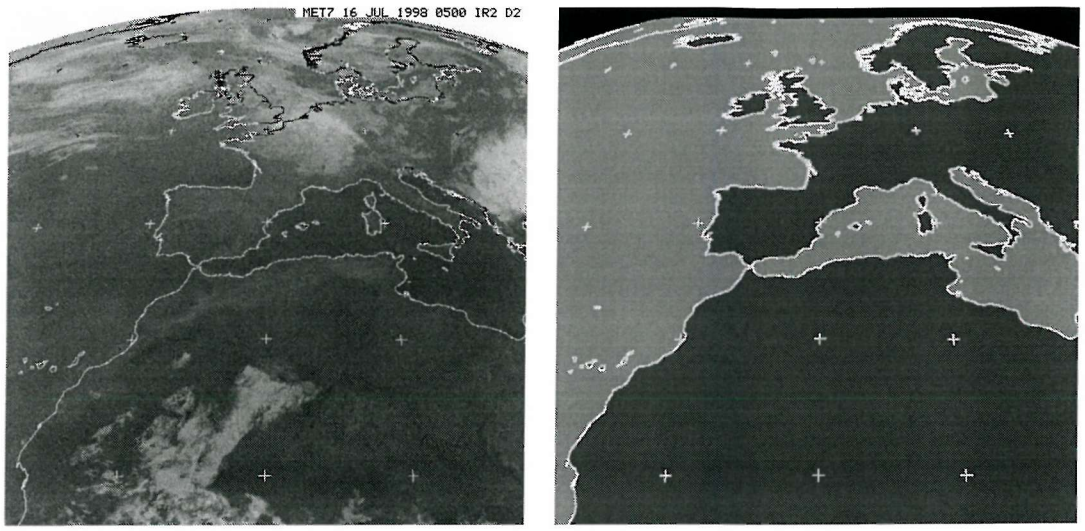


(a) Raw Data (b) Border Template

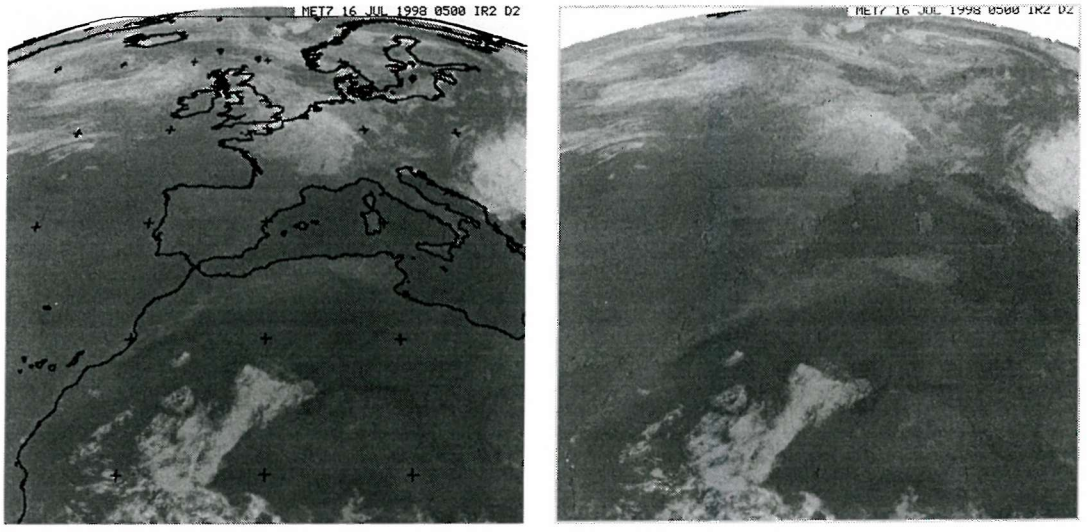


(c) Border Removed (d) Border Smoothed

***Figure 4.1:*** *(a) Raw Image Data, (b) The border template image for METEOSAT D2 imagery, (c) The border region is marked in black prior to (d) smoothing. The image shown is a METEOSAT D2 IR image from 0500 on July 16th 1998.*

[5] i.e. less than 5 seconds

### 4.1.2 Parameter Generation

Three parameters were chosen to differentiate between the regions suitable for a frontal motion analysis technique, those suitable for textural analysis and those containing small objects. To identify the degree of texture in a region, a spatial grey level difference vector was used. This indicates the degree of homogeneity in greyscale across a region of pixels. In the case of small cloud objects, this texture measure shows a lack of homogeneity, and within an extended cloud sheet there is a high level of homogeneity. To determine the time–persistence of cloud in a region, a *temporal* grey level difference measure was used, which rather than comparing the greyscale of a pixel with its spatial neighbours, compares its value over time. A thresholded measure of greyscale itself was also used for easy identification of cloud core regions and more ambiguous cloud edges, low cloud and thin cloud. The parameters used to generate this initial motion type assignment were as follows:

**Thresholded Raw Image Data**: The image was high–level thresholded using a context–dependent (underlying land / sea) threshold mask (see Figure 4.1(b)). A threshold of 135 was found to be appropriate for most conditions over land. Land temperature changes by a much greater degree over time than sea, and since the complexity of the land data is much greater than sea data, a relatively high threshold was selected to ensure that all the content classified as cloud over land was correctly identified[6]. The sea is a significantly more stable background against which to identify cloud, and as a result, a context–dependent threshold over the sea was used to try to extract as much of the cloud content as possible. The threshold is offset from the sea mean greyscale by an amount equal to the difference between the land mean greyscale and the fixed land threshold. Due to the large expanse of typically exposed land over North Africa, the land mean was mostly lower than the sea mean: this resulted in a higher pass threshold for cloud over the sea. At the hottest point in the day, the land mean is at its most different relative to the sea mean, but also the sea surface is slightly

[6] Although consequently some cloud may be missed.

warmer than, for example, in the middle of the night. The greyscales of the high–pass thresholded data are not subsequently stretched to enhance the cloud data any further. It is important to note however that only a crude measure of the location of cloud was required in this initial work, and significantly better cloud extraction tools using background suppression and cloud enhancement are presented in Chapter 5. The radiance data are on a greyscale of 0 to 255:

$$Threshold = \begin{cases} 135 & \text{over land} \\ 135 - (\textit{land pixel mean} - \textit{sea pixel mean}) & \text{over sea} \end{cases} \tag{4.2}$$

**Temporal Grey-Level Difference**: The pixels immediately surrounding the pixel under analysis over the twelve hours prior to the current frame are analysed, providing a measure of the degree of *temporal homogeneity* in greyscale in the region of the pixel. The probability distribution of the difference in greyscale over a timestep, $f_{\delta\theta}(k)$, is generated for the 20*20 pixel window around the pixel under analysis over the twelve hour time period, giving a measure of the likelihood that the pixel greyscales in that region will have changed over time. Clearly the length of the time frame over which the temporal homogeneity of greyscale is measured influences the result of the analysis. The intention of this parameter is to differentiate between the motion of weather systems and convective cloud sheets, therefore the time frame must be sufficient for significant motion of a weather system within the spatial frame of view. In twelve hours, most weather systems are able to travel a significant portion of the frame of a D2 METEOSAT image.

$$TGLD = \frac{\sum_{t=-24}^{-1} \sum_{i=-10}^{9} \sum_{j=-10}^{9} \sum_{k=0}^{255} k f_{\delta(x,y),\theta}(k)}{24 * 400 * 256} \tag{4.3}$$

where

$(i, j)$ are pixel co-ordinates relative to the pixel concerned

$k$ is the greyscale

$t$ is the timestep in hours

$f_{\delta(x,y),\theta}(k)$ is the probability distribution of $\Delta GS(\delta t)$

at spatial separation $\delta(x, y) = 0$

i.e. the probability distribution of the change in greyscale over time ONLY

$\Delta GS(\delta t)$ is the difference in greyscales across 1 timestep

**Spatial Grey-Level Difference**: This is a standard measure of spatial greyscale homogeneity

$$SGLD = \frac{\sum_{i=-10}^{9} \sum_{j=-10}^{9} \sum_{k=0}^{255} k F_{\delta\theta}(k)}{400 * 256} \tag{4.4}$$

where all parameters are defined as per the time grey level difference except

$F_{\delta\theta}(k)$ is the probability distribution of $\Delta GS(\delta t)$ at spatial separation $\delta = 1$ and angular separations of $\theta = 0°$, $45°$, $90°$ and $135°$

As can be seen from comparison between Figures 4.2 and 3.2, the chosen parameters are able to discriminate between the three desired region types and the background. The thresholded image is a crude measure for removing land and sea pixels from an image selection. The time grey–level difference parameter shows clearly the time persistence of the lower region of cloud, compared to the moving frontal cloud. The spatial grey–level difference parameter enhances the regions of strong texture, which are indicative of areas containing many small clouds in close formation.

The parameter generation routines were written in C++ and run on a computer

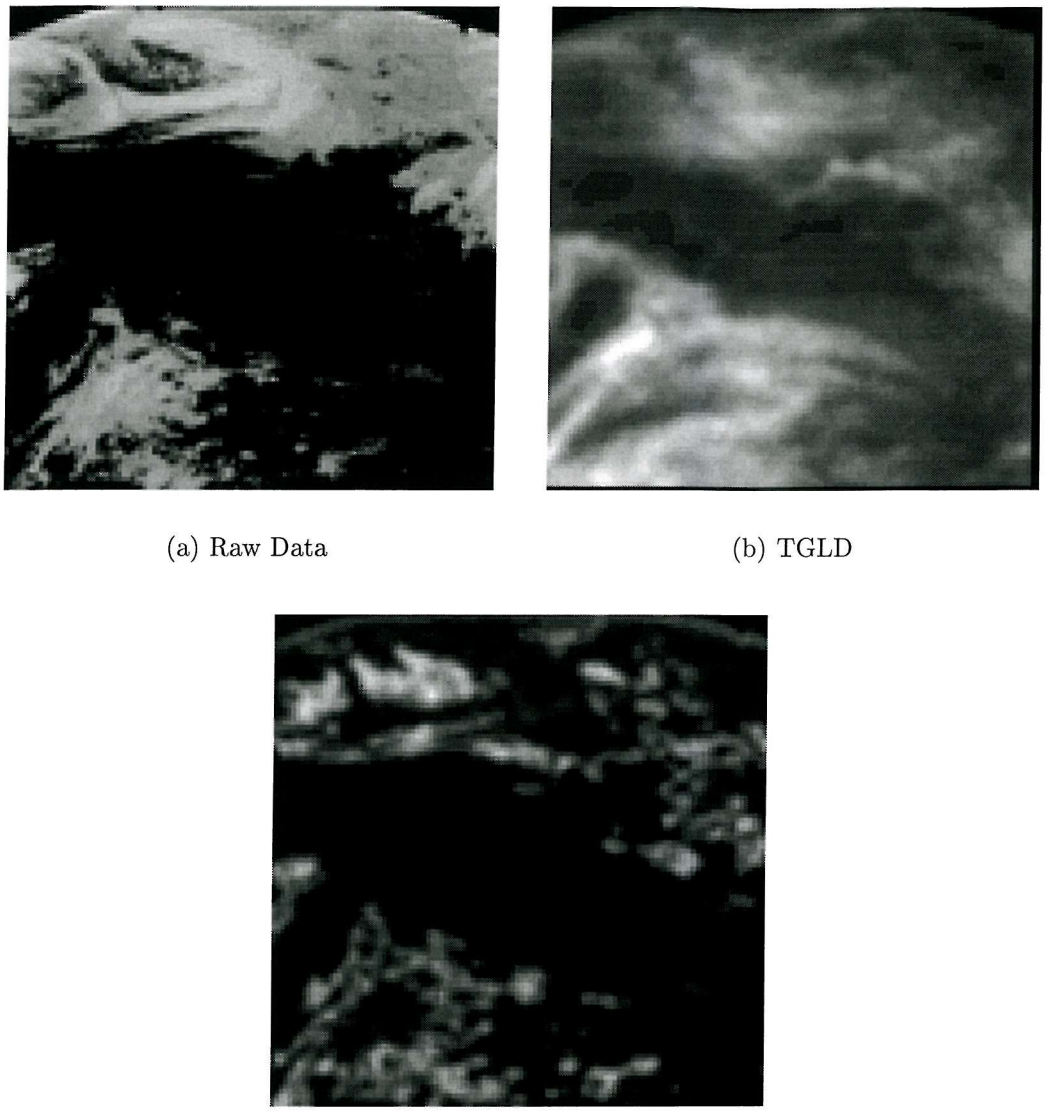

(a) Raw Data

(b) TGLD

(c) SGLD

***Figure 4.2:*** *(a)Thresholded Raw Image Data, (b)Time Grey-level Difference and (c)Spatial Grey-level Difference parameter sets.*

with a 75MHz processor and 60Mb of RAM. The Time Grey–level Difference parameter took of the order of one hour to generate for the sequence of twenty–four $800 * 800$ pixel METEOSAT D2 images. Newer processors and more memory would enable this computational cost to be reduced to a level where the parameters could be generated well within thirty minutes, which would be required operationally to make use of the full thirty minute temporal resolution of the data.

## 4.2 Fuzzy Systems for Motion–Type Segmentation

The fuzzy systems for associating pixel regions with object motion types consist of sets of if–then rules relating the input parameters to degrees of membership of the motion types. Each rule has a *confidence* which defines its significance compared to other rules relating to the same output. The output of such a system consists of degrees of appropriateness of the chosen output labels to the data applied. Four fuzzy systems were used, one for each flow type (frontal, textural, small object and *background*). The algorithm used in the fuzzy systems in this thesis is given in Table 4.1[7]. In all cases a product operator was used for the T–norm, a maximum operator for the S–norm and a sum operator for the aggregation. The output memberships were taken as the centroid membership value(s) of the resulting consequent(s).

To illustrate the function of the system, the generation of frontal motion membership for pixel regions will now be analysed more closely. The frontal motion identification system used the time grey-level difference parameter and threshold parameter. Three labels were defined for each of the system inputs and two for the outputs, as shown in figure 4.3.

Having assigned any given data point to one or two labels for each parameter, the rules relating to those labels were activated, and the association to output membership was made. The output was generated from a combination of the active rules, based on the degree of membership of the input labels in those rules and the associated rule confidences. The rules for the fuzzy system for frontal analysis is given in Table 4.2 as an example. The basis function greyscale transition points and rule confidences were deduced empirically as optimal from repeated testing.

[7] For a more detailed discussion of fuzzy systems, T–norms, S–norms and other fuzzy system operators, see Chi et al [21]

1. For all inputs, work out which rules are active based on mapping inputs to rule antecedents (the IF clauses). To do this, for each input $x$, determine whether in any of the fuzzy sets $A$ in the universe of discourse $X$ there is a non–zero membership function $\mu_A(x)$ in the ordered pair $A = (x, \mu_A(x))$ indicating $x$ has some degree of $A$–ness. The memberships of each rule antecedent are the resulting values of $\mu_{A,B,...}(x)$.

2. If there are multiple antecedents in an active rule, apply the appropriate fuzzy logic operator to combine antecedent membership functions into a *degree of support* for the rule. For AND functions (IF $A$ AND $B$...), typically combine the memberships of each antecedent using a minimum or product operator, the *T–norm*. For OR functions (IF $A$ OR $B$...), combine memberships using a maximum or probabilistic OR operator, the *S–norm* or *T–conorm*. If for example fuzzy sets $A$ and $B$ are active in a rule, the combined rule antecedents would be:
$\mu_{A \cap B}(x) = T(\mu_A(x), \mu_B(x)) = \mu_A(x) \otimes \mu_B(x)$ or
$\mu_{A \cup B}(x) = S(\mu_A(x), \mu_B(x)) = \mu_A(x) \oplus \mu_B(x)$

3. Use the degree of support for the rule antecedents to truncate the rule consequents (The THEN statements). If the combined rule antecedent support for example is 0.4 then the support function on the output space for the consequent(s) in the active rule is (are) truncated at a value of 0.4.

4. Combine rules for each consequent using the selected aggregation method (the maximum or sum of truncated outputs) and rule confidences.

5. Select the output class from the aggregated output for each consequent using the selected defuzzification method (calculate the centroid, bisector or other moment of the aggregated truncated support functions).

***Table 4.1:*** *Algorithm for a fuzzy system*

## 4.3 System Output

Figure 4.4 shows the identified motion type applicability for the data, as generated by the fuzzy systems. The lighter pixels depict greater relevance of that motion type to the region.

The system has identified the weather system in the upper half of the image as suitable for frontal analysis, although its performance is potentially the least successful of the four outputs. The area of cloud identified as suitable for frontal analysis within the extended cloud sheet over Africa, however, was a fast moving core that had clearly defined boundaries that would have been suitable for

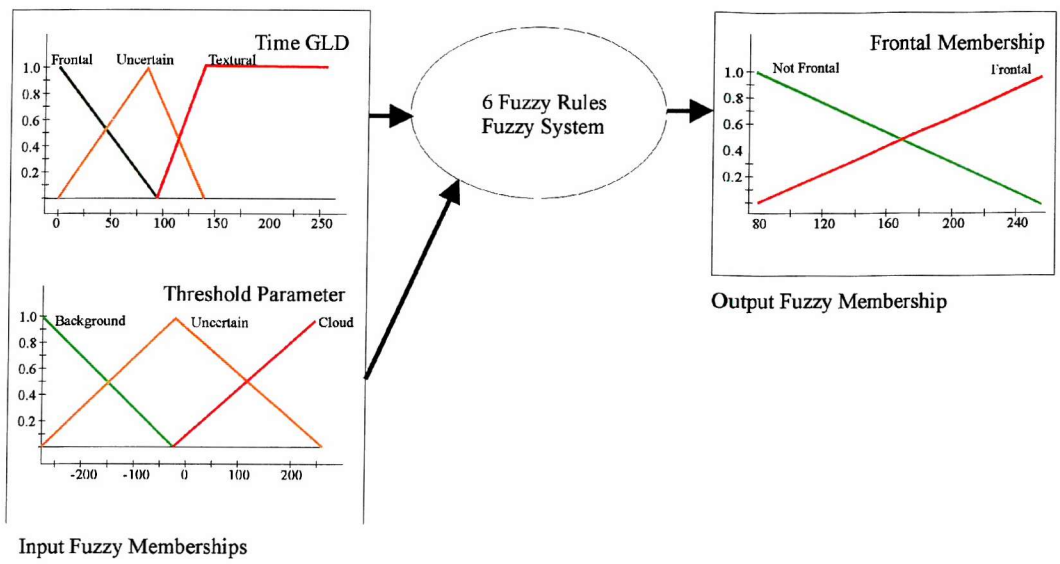


***Figure 4.3:*** *Frontal feature identification fuzzy system. To identify frontal features, the Time Grey–level Difference (TGLD) and Cloud Threshold parameters are used. Regions with a low TGLD and high greyscale in the thresholded image are typical of frontal cloud.*

| *IF* | *THEN* | *Conf.* |
|---|---|---|
| Threshold Parameter is Background | Frontal Output Parameter is Not Frontal | 100 |
| Threshold Parameter is Cloud AND Time GLD is Frontal | Frontal Output Parameter is Frontal | 100 |
| Threshold Parameter is Cloud AND Time GLD is Textural | Frontal Output Parameter is Frontal | 10 |
| Threshold Parameter is Cloud AND Time GLD is Textural | Frontal Output Parameter is Not Frontal | 90 |
| Threshold Parameter is Likely Cloud AND Time GLD is Uncertain | Frontal Output Parameter is Frontal | 55 |
| Threshold Parameter is Likely Cloud AND Time GLD is Uncertain | Frontal Output Parameter is Not Frontal | 45 |

***Table 4.2:*** *Fuzzy rule bases for motion–type image segmentation. The first and second column make the if–then statement pair, with the third column giving the confidence in the particular rule.*

tracking separately from the remainder of the cloud sheet.

The areas flagged as suitable for textural analysis were potentially *most* successfully identified. The region of frontal weather system in the upper half of the image that has been flagged for textural analysis started as the leading edge of the system and ended as the trailing edge at the end of the sequence of data

analysed. As a result, there was a persistent portion of cloud over this region for the duration of the analysis.

The small object regions correlate quite successfully with the edges of the extended cloud sheet and with the open and closed cell cumulus around the weather system. The background data parameterisation was biased too high against cloud regions, however, due to the thresholds selected. Section 5.3.2 discusses an improved approach to cloud region identification that ameliorates this effect.

## 4.4 Discussion on Fuzzy Motion Segmentation Approach

These results have significantly demonstrated the potential for a fuzzy system with suitable input parameters to identify the degree of suitability of different motion analysis techniques for analysing cloud motion. The issue of suitability of timescale for analyses has been highlighted by the use of the time persistence measure for identifying frontal motion. Unless large enough timescales are used, time persistence of cloud is unsuitable for identifying frontal motion as over short timescales any large body of cloud will mostly persist in the same location. Texture–based analyses in contrast require small timesteps for optimal texture matching: the textural make–up of a region must not have changed too significantly over a timestep in order for a motion analysis to be successful.

Other issues of suitability relate to a greater or lesser extent to questions of *scale* of motion, and the degree to which any motion at a particular scale can be generalised across other scales. On considering the mechanisms for comparing the results of a frontal analysis, textural analysis and small object matching for analysing winds on a global scale, it was realised that the issue of scale and the nature of cloud dynamics raise fundamental questions about the nature of wind *itself*. Cloud in a front is a passive tracer for the weather system's dynamics, and cloud peaks driven by a local system–relative wind are similarly passive tracers

for a local–scale wind component: in both of these instances, the passivity of the cloud is not, to greater or lesser extent, in dispute. The motion captured by the cloud motion, however, is of a fundamentally different scale in the two instances, moving the problem domain from one of identifying where cloud acts as a passive wind tracer to one of identifying the type of wind motion captured by the cloud. As a consequence, this research now focuses on capturing the cloud motion at different scales. This will then provide a starting point for future work to resolve the complex question of causality of the motion.

The fuzzy systems used in this chapter were developed using MATLAB's neuro-fuzzy toolbox[8]. To determine the degrees of suitability of the three motion types from the three input parameter images took of the order of five minutes on a computer with a 150MHz processor and 64Mb of RAM running Windows NT. The whole processing cycle from raw images through parameterisation to fuzzy system output would therefore be possible within a potential operational constraint of thirty minutes with a faster processor and more memory. Identifying the suitability of different motion analyses in different regions of an image could be performed in parallel with the motion analyses, and used as a filter on the resulting motion vectors. If the processing described were to be a *precursor* to applying the motion analyses, however, different algorithms and parameters may need to be considered.

The results from this chapter were presented at the Third International Winds Workshop, as detailed in Newland et al[75].

[8] http://www.mathworks.com

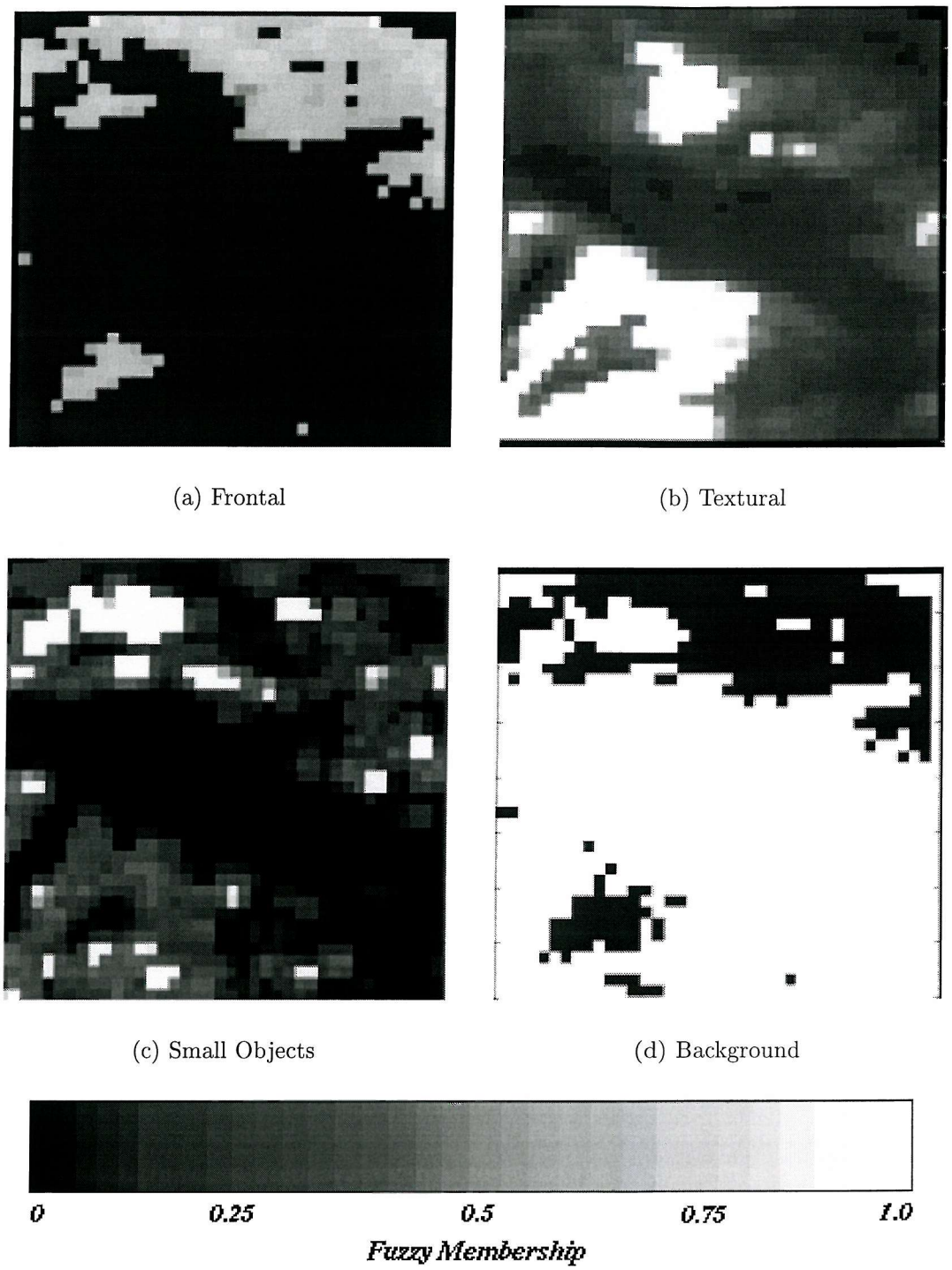


(a) Frontal

(b) Textural

(c) Small Objects

(d) Background

**Figure 4.4:** *Fuzzy Region Memberships for the image: (a) Frontal, (b) Textural, (c) Small Objects and (d) Background. Bright regions indicate high memberships of the particular motion type.*

# 5. CLOUD OBJECTS

Two approaches are used to extract the cloud component of satellite images in this thesis. One focuses on analysing the vague nature of the edge of the cloud by identifying the *core* regions of all the clouds in the image then *growing* them to include the dispersed edges of cloud. The added edge regions are assigned a degree of association with the core[1], resulting in an extracted cloud shape with areas of various degrees of association to a central cloud core. The second approach slices smoothed cloud data vertically at a number of heights to identify some of the characteristics of the vertical profile of the cloud.

To analyse the satellite data successfully, it is first necessary to prepare it suitably for analysis. As previously, the overlaid national border and position markers are first removed. In order to analyse cloud structures that can extend over a considerable portion of the raw imagery, it is also necessary to project the data onto a constant distance grid, to minimise the effects of viewing location and hence distortion across the data.

The difficulties of identifying cloud over complex land and sea backgrounds are addressed to some extent by suppressing the underlying data using prior knowledge of its characteristics and stretching the remaining greyscale data to enhance the cloud component. This enhancement of the cloud component is particularly useful for analysing thin cloud and cloud edges, where the distinction between the radiance of the cloud and the underlying land or sea is at its weakest.

There is some noise in the raw data, partly from artefacts of the compression strategy applied in the data archive used for this study (see Appendix B). There

[1] Their *fuzzy membership*.

is also a large amount of pixel–scale variability that makes analysis of larger–scale phenomena more difficult. As a result, some smoothing filters are applied to the cloud–enhanced data to improve the data characteristics for subsequent feature extraction and tracking. Two schemes for smoothing have been applied, each with different applications, namely median filtering and a derivative of the rolling ball algorithm related to fuzzy morphological filtering.

Having cleaned up, projected and smoothed the data, it is ready for the object–scale cloud extraction algorithms to be applied.

## 5.1 Data Preparation

The national border and marker data are initially removed from all images as detailed in Section 4.1.1. The images are then projected from raw orthographic view to a constant distance projection, where distances measured anywhere in the image are to the same scale. The final phase of data preparation involves suppressing the underlying land and sea data, to aid analysis of the cloud content.

### 5.1.1 Background Template Generation

To help identify the cloud content in images, an estimate for the underlying land and sea radiances has been generated. Identifying any deviation between this *background radiance template* and the corresponding current image provides a first pass at identifying cloudy pixels. A simple persistence model for the background radiance has been used from the non–cloudy pixels over the six days prior to the data under analysis: the maximum radiance (minimum greyscale) per pixel across the previous data for a given time of day is used as an approximation for the clear sky radiance. This method has limitations where cloud has persisted in a given location at a specific time for the previous six days, but is broadly stable since such areas are rarely densely saturated. A high–pass greyscale threshold is applied, however, to remove the majority of remaining cloudy pixels from the

template images. A median filter is used to fill in any thresholded pixels, applied as per the border and marker filter discussed previously.

An example of the resulting background radiance template is given in Figure 5.1.

### 5.1.2 Constant Distance Projection

The raw data (minus borders and markers) and background radiance templates are then projected onto a constant distance grid, so that every pixel covers the same spatial area on the ground (see Figures 5.2 and 5.3).

This differs from the current practice at the ECMWF and EUMETSAT, where the data projection is postponed until motion analysis has been completed, at which time the vectors generated from the raw imagery are projected onto a constant distance space for ground–relative magnitude and direction. The small spatial scale over which current cloud motion analyses are performed requires this: radiance data projection necessitates padding pixels away from the sub-satellite point, adding unacceptable levels of noise to these small–scale analyses. In addition, distortion is not such a problem with small–scale analysis: Whilst distortion is a factor of distance from the sub-satellite point globally, it affects local–scale features less. Indeed, a small texture window in unprojected image data is able to be tracked even at a considerable angle from the sub–satellite point (e.g. Purdom [81]) where distortion is considerable, since the amount of distortion does not change significantly over the distance covered by cloud in the image sample interval of 30 minutes.

When analysing larger structures such as weather systems, the significance of the distortion is greater and must be addressed. The use of a constant distance projection early in the analysis process overcomes this problem, and is a necessary starting point for cloud structure analysis. To make relative judgements of shape change and relative motion along the extent of a cloud, the shape must be at the same scale across its extent. The error introduced by data projection is therefore less significant than the potential error from ignoring distortion. Larger–scale

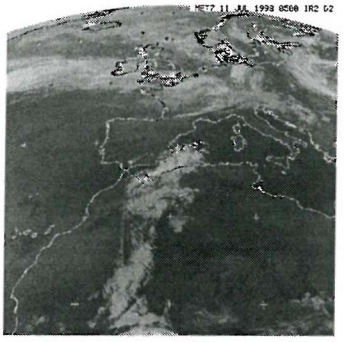

(a) 11th July 1998 0500GMT

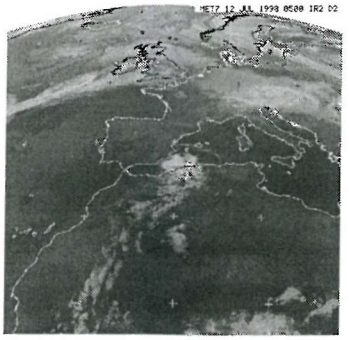

(b) 12th July 1998 0500GMT

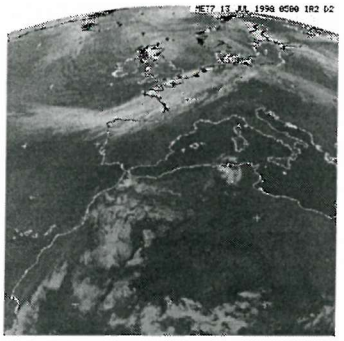

(c) 13th July 1998 0500GMT

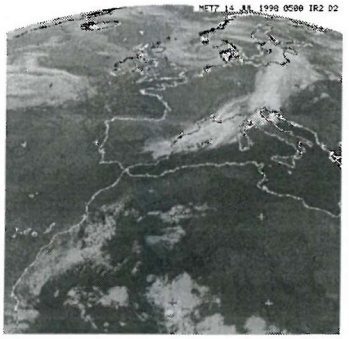

(d) 14th July 1998 0500GMT

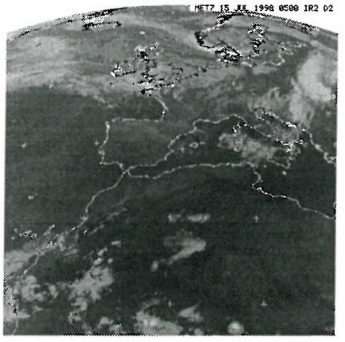

(e) 15th July 1998 0500GMT

(f) Generated template

***Figure 5.1:*** *(a)-(e) METEOSAT D2 (infrared) imagery from 0500 GMT over the period 11th–15th July 1998 and (f) the corresponding background template consisting of a maximum–radiance (minimum greyscale) pixel composite from these five images. Some noise remains in the background template over the Atlantic from long–term cloud persistence in the region.*

analyses are also less sensitive to pixel–scale errors introduced by padding data for projection, since they tend to average out across the extent of the structure. Pixel enlargement is handled using the same median smoothing filter over new data pixels that are required for the projection as has been used previously for border removal and background template smoothing.

Initially, the latitude and longitude of every pixel in the original image is determined using the geometry of the satellite relative to the earth, which is taken as an oblate spheroid for the projection, as per Equations 5.1, 5.2 and Figure 5.2.

$$Latitude(x,y) = \begin{cases} \Upsilon_{LAT} * \frac{180}{\pi}, & \frac{1}{cos(x^2)} \leq \frac{y_k^2}{y_k^2-1} \\ 180, & \text{otherwise} \end{cases} \quad (5.1)$$

$$Longitude(x,y) = \begin{cases} \Upsilon_{LON} * \frac{180}{\pi}, & \frac{1}{cos(x^2)} \leq \frac{y_k^2}{y_k^2-1} \\ 180, & \text{otherwise} \end{cases} \quad (5.2)$$

*where*

$(x,y)$ are the image co–ordinates $= \frac{\pi}{180} xr\delta x, \frac{\pi}{180} yr\delta y$ respectively

$\Upsilon_{LAT} = tan^{-1}(\frac{R_P}{R_E} tan\theta)$

$\Upsilon_{LON} = tan^{-1}(\frac{X_T}{Z_T})$

$\delta x, \delta y$ = angle subtended at satellite by 1 pixel

$R_E$ = Equatorial radius of the earth = $6378km$

$R_P$ = Polar radius of the earth = $\frac{R_E}{1+\alpha}$

$\alpha$ = Earth oblateness = $\frac{1}{297}$

$\theta = sin^{-1}(\frac{Y_t}{R_P})$

$X_T = -S_N tan(x)$

$Y_T = \frac{S_N tan(y)}{cos(x)}$

$Z_T = R_S - S_N$

$S_N = \frac{R_S - R_E\sqrt{y_k^2 - \frac{y_k^2-1}{cos(x^2)}}}{\frac{1}{cos(x^2)}}$

$R_S = R_E$ + altitude of satellite (=42164km for Geostationary orbit)

$y_k = \frac{R_S}{R_E}$

Having determined the equivalent latitude and longitude of all the pixels in the unprojected image, the data of interest are projected onto a new grid (Equation 5.3). Pixels from the original image are placed in the new grid where appropriate. Since each pixel is in effect projected to a different shape, the pixel placing often leaves a number of holes in the projected data, especially at high

latitudes. These are filled in using the usual median filter as applied in border removal etc. (Equation 4.1). Figure 5.3 shows the effect of projection on a portion of an image, and the result of smoothing.

$$I_{proj}(x,y) = I_{raw}(i,j) \forall (x,y) \text{ s.t. } x_{min} \leq x \leq x_{max}, y_{min} \leq y \leq y_{max} \quad (5.3)$$

*where*

$(i,j)$ = unprojected image co–ordinates

$(x,y)$ = projected image co–ordinates

$$x_{min} = \frac{2\pi R_2 LON_{min}}{360 * RES}$$

$$y_{min} = \frac{2\pi R_2 LON_{max}}{360 * RES}$$

$$x_{max} = \frac{2\pi R_E LAT_{min}}{360 * RES}$$

$$y_{max} = \frac{2\pi R_E LAT_{max}}{360 * RES}$$

$$x = \frac{2\pi R_3 LON(i,j)}{360 * RES}$$

$$y = \frac{2\pi R_E LAT(i,j)}{360 * RES}$$

$$R_2 = R_E cos(LAT_{min})$$

$$R_3 = R_E cos(LAT(i,j))$$

The algorithms for projecting the imagery were written in C++ and were initially validated by projecting many different subsections of raw data that included latitude–longitude markers. The latitude–longitude marker positions and separations were then checked to ensure they were the correct distance apart in both axes.

### 5.1.3 Cloud Data Enhancement

To reduce the impact of the complex and changing underlying radiance of the land and sea, the underlying data is suppressed in the sequence under investigation

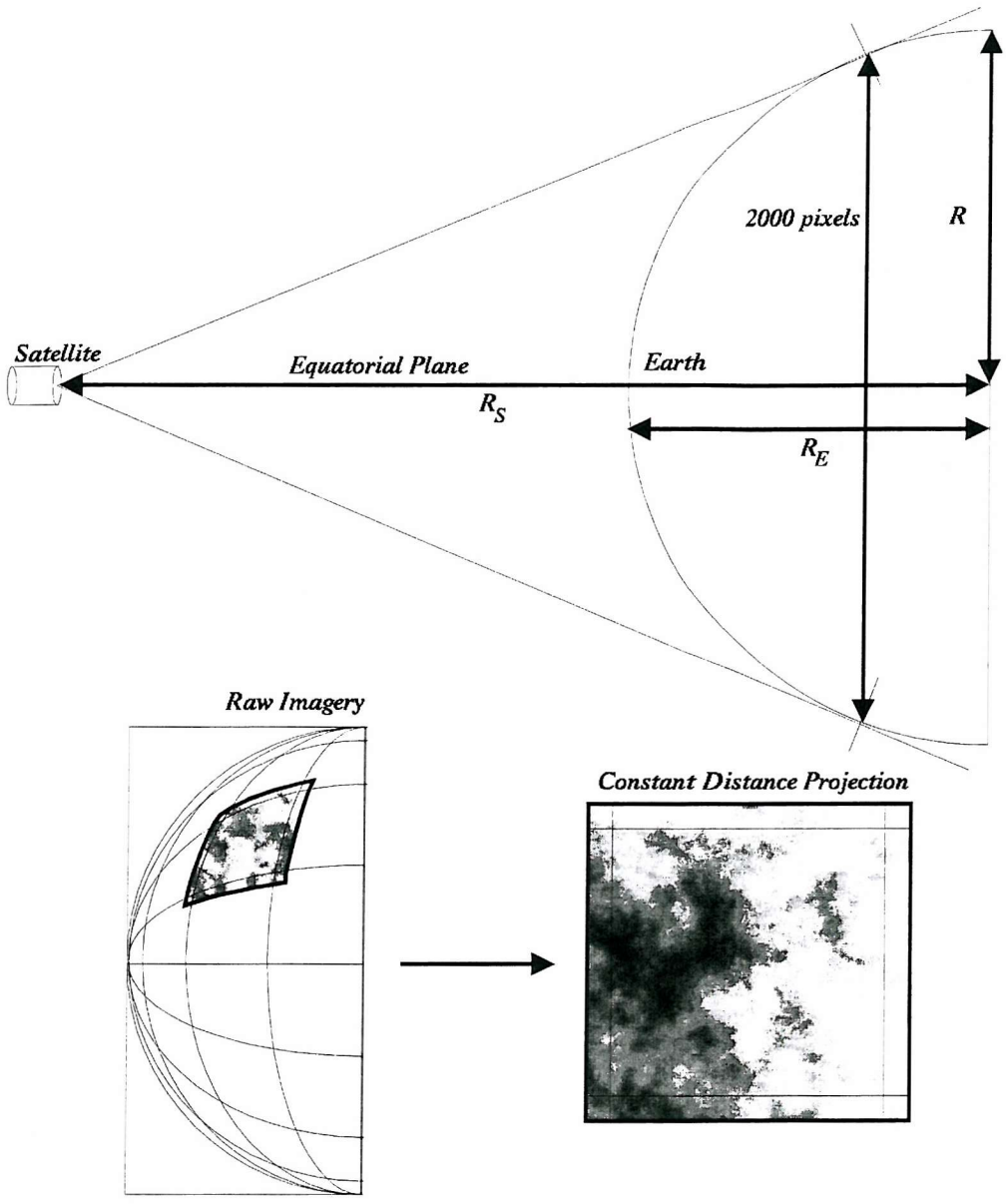


***Figure 5.2:*** *Projection of satellite data from raw to constant–distance representation. The distances shown are referred to in Equations 5.1 and 5.2*

using the background templates to identify regions of cloud and non-cloud. Pixel greyscale values in the background template are subtracted from pixel values in the image under analysis. Where the resulting pixel value is less than 10, or if the pixel value in the image under analysis is less than a greyscale of 80[2] then the output pixel is suppressed to zero. Pixels brighter than the background by more than 10 greyscales and in the greyscale range 80–208 are stretched across the

[2] An empirical minimum greyscale for a pixel to be considered as cloudy

greyscale range of 0–255, and pixels of a greyscale higher than 208 are saturated at 255 on the new scale (Equation 5.4).

$$I_{sup}(x,y) = \begin{cases} 0, & I(x,y) - B(x,y) < 10 \\ & \text{or } I(x,y) - GS_{Thresh} < 0 \\ 2(I(x,y) - GS_{Thresh}), & I(x,y) - B(x,y) \geq 10 \\ & \text{and } 0 \leq 2(I(x,y) - GS_{Thresh}) \leq 255 \\ 255, & \text{otherwise} \end{cases} \tag{5.4}$$

*where*

$I_{sup}(x,y)$ = image data with suppressed background

$I(x,y)$ = unsuppressed image data

$B(x,y)$ = background template data

$GS_{Thresh}$ = Lower greyscale threshold for cloud data = 80

Whilst this does not remove the entirety of the land / sea components, it is easier to identify the cloud content in the resulting imagery, as is demonstrated in Figure 5.4.

The national border removal, data projection and cloud enhancement code was all written in C++. The computational overhead of all three steps was found to be negligible[3] on a computer with a 150MHz processor and 64Mb of RAM running Windows NT 4.0. The cost of generating background image templates was equally negligible, but this would not necessarily form part of an operational cycle for cloud analysis, as the templates could be generated up to 24 hours prior to use.

[3] i.e. less than 1 minute

## 5.2 Cloud Data Smoothing

To analyse cloud structures at synoptic and mesoscale, some smoothing is required to remove the variation at smaller scales. Any smoothing degrades the information content of data, however. For clouds, the gradient of the edge is of particular importance, as is explained further in Section 6.2, thus any filtering must be able to maintain or enhance object edge gradients. In addition, the structure is analysed using its *medial axis* or *skeleton* (Section 6.1), and therefore filtering must not unduly change the medial axis except where the nature of the medial axis algorithm is unduly affected by artefacts in the data. The principal example of this is *holes* in a cloud sheet which may result from individual noisy pixels in the cloud having been thresholded out of the cloud structure. In practice, the requirement this imposes on a smoothing algorithm is that of increasing the *coherence* of a cloud shape. Figure 5.5 shows the difference between a coherent and a fragmented object. The choice of image filter is therefore tied to some tight constraints, which are listed again for completion in table 5.1.

| *Area of Concern* | *Issues of Concern* |
|---|---|
| Remove local variability | Where there is no global component of variation |
| Variable precision in cloud structure | Must be able to extract different parameters for object analysis at different levels of precision by running the filter with different conditions or iteratively for different lengths of iteration. |
| Generate coherent structures | As depicted by multi-level thresholds of the structure. In particular, it is necessary to remove any 'holes' from thresholded slices where inappropriate. |
| Maintain Edge Gradients | And smooth where possible. Edges must remain as sharp at a global scale, whilst removing any local–scale gradient information. |

***Table 5.1:*** *Constraints for cloud smoothing filter*

Two approaches have been applied to filtering the image data, namely median and fuzzy morphological filtering. These are assessed using two data plot types: Edge

plots are a 3–dimensional representation of the cloud data, where the vertical axis is greyscale[4]. These show the effect of filtering on edge gradient. In order to analyse the characteristics of the cloud edge, it is necessary to preserve the edge gradient during smoothing as far as possible. Coherence plots show a high–pass threshold of the filtered data at a greyscale of 170[5], providing a single slice indication of the effectiveness of the filter for increasing the coherence of the cloud object. Coherence is of key importance for skeleton generation.

[4] Figures 5.8 and 5.18
[5] Figures 5.7 and 5.17

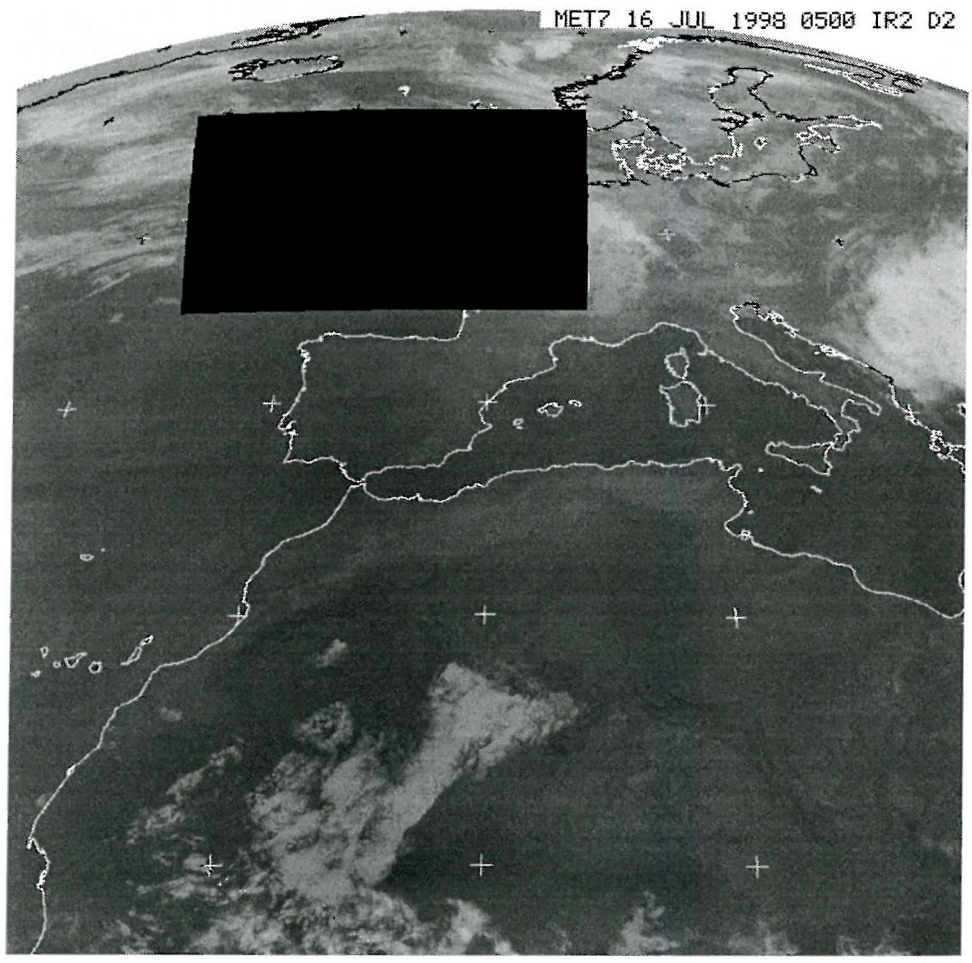


(a) Raw Data

(b) Projected Data Pre Smoothing

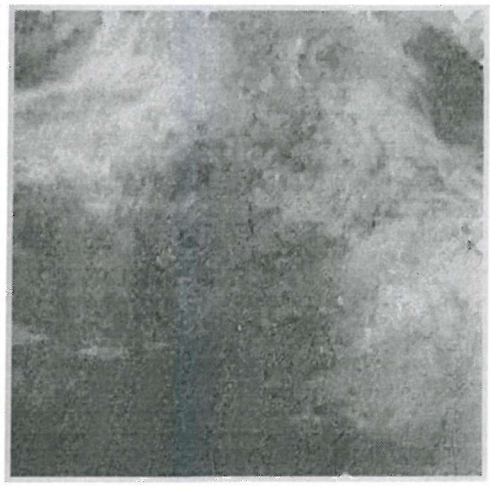

(c) Projected Data Post Smoothing

***Figure 5.3:*** *(a) Raw data with the region to be projected cut out in black, (b) Constant–distance projection, pre–smoothed and (c) post–smoothing. The image is METEOSAT D2 (infra–red) from 0500 GMT, July 16th 1998. The projected data are from Latitudes 45-60N, Longitudes 16W-5E with a scaling of 1 pixel to 4km*

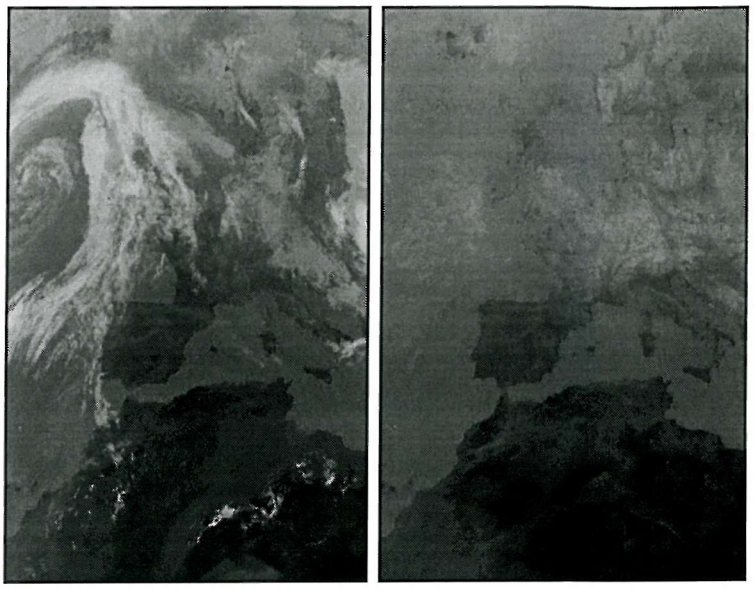

(a) Image with unsuppressed background

(b) Background template

(c) Image with background suppressed

***Figure 5.4:*** *(a) Constant–distance projection of METEOSAT D2 (infra–red) image from 1000 GMT on June 19th 1998, (b) its corresponding background template generated from the preceding six days' 1000 GMT images and (c) the data after suppression of the background. Some noise remains in the background template over the Atlantic from long–term cloud persistence in the region, which may add noise to the cloud data in the region.*

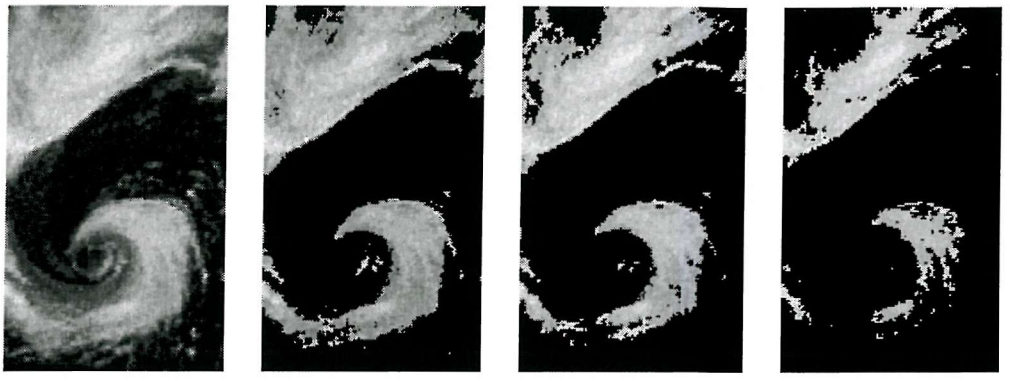

(a) Raw (b) Raw, T=128 (c) Raw, T=150 (d) Raw, T=180

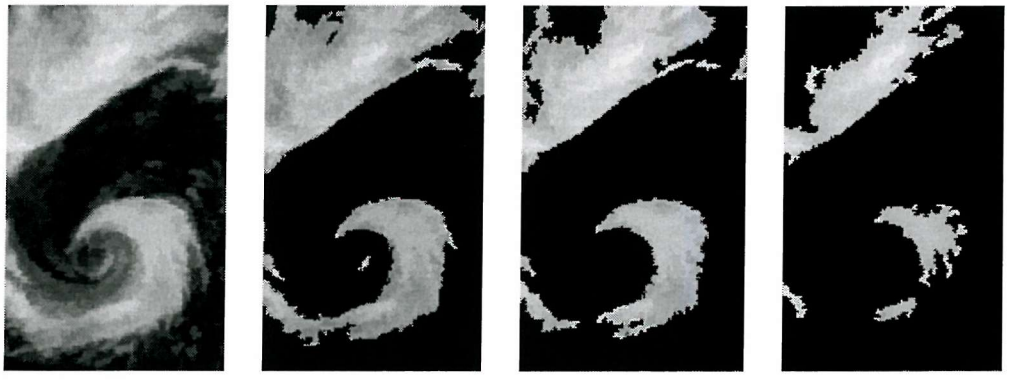

(e) Smoothed (f) Smooth, T=128 (g) Smooth, T=150 (h) Smooth, T=180

***Figure 5.5:*** *A comparison between non–coherent and coherent cloud objects. (a)Raw imagery, cloud enhanced, and thresholded at a greyscale T of (b)128, (c)150 and (d)180. (e)Filtered data (filtered using the morphological approach described in Section 5.2.2) thresholded at a greyscale of (f)128, (g)150 and (h)180. The data shown are from the 1830 METEOSAT D2 image taken on the 10th May 1998. The multiple thresholds show a greater degree of attachment between pixels for the smoothed data, whilst maintaining the general content of the raw data.*

### 5.2.1 Median Filtering

A median filter replaces the pixel under analysis with the median value of the pixels in the filtering window surrounding that pixel. The size and shape of median filter window changes its performance. A circular window has been applied in this study, although potentially other shapes may give smoother results. Some of the issues concerning circular filtering in digital spaces are discussed further in Section 5.2.2. The choice of filter shape, whilst having an influence on the final smoothness of the surface, should not unduly affect the degree of edge smoothing. Seven sizes of median filter were tested, varying in radius from 1 to 10 pixels. Figure 5.6 shows the results of applying each filter to a geocorrected image.

Coherence and edge gradient performance are shown in Figures 5.7 and 5.8 respectively. As can be seen, the median filter smoothes edges significantly. Whilst a coherent structure results from a fairly small median filter (3 or 4 pixel radius), the edge gradient decays significantly too, even at a radius of three pixels. In practice, the degree of edge smoothing is dependent on the ratio of feature width to filter size. It may however be appropriate to use data smoothed using a small median filter for generating skeletons, as the coherence of the resulting structures is high, and maintaining the original edge gradient is not a critical factor for skeleton algorithms[6].

[6] Unless a skeleton*profile* is being constructed. For more information on skeleton profiles, see Section 6.1.3

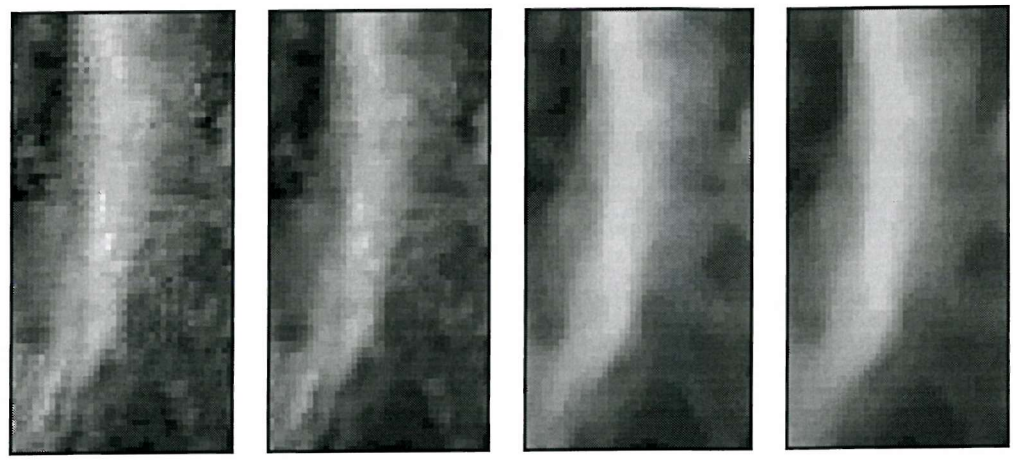

(a) Raw (b) R1 (c) R2 (d) R3

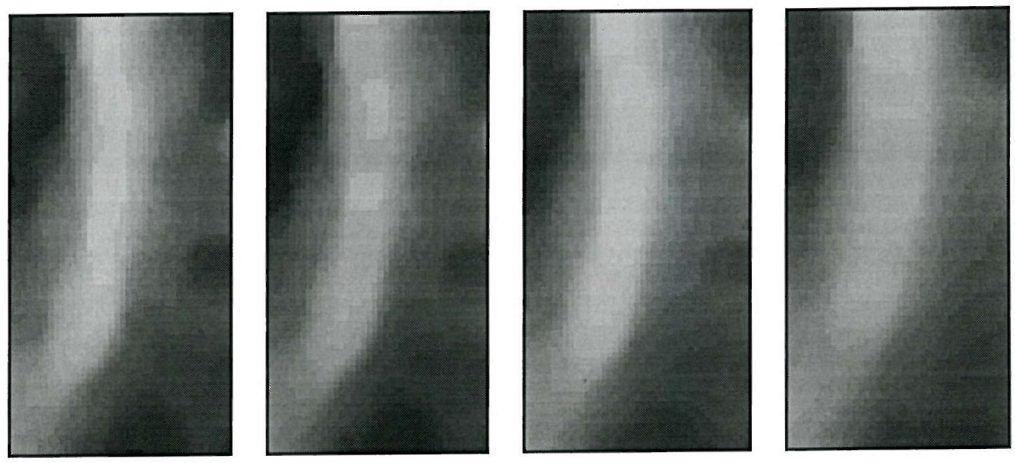

(e) R4 (f) R5 (g) R6 (h) R10

***Figure 5.6:*** *(a) Raw imagery smoothed using a median filter of radius R equal to (b) 1, (c) 2, (d) 3, (e) 4, (f) 5, (g) 6 and (h) 10 pixels. Data are METEOSAT D2 images from 2200GMT on the 23rd of April 1998.*

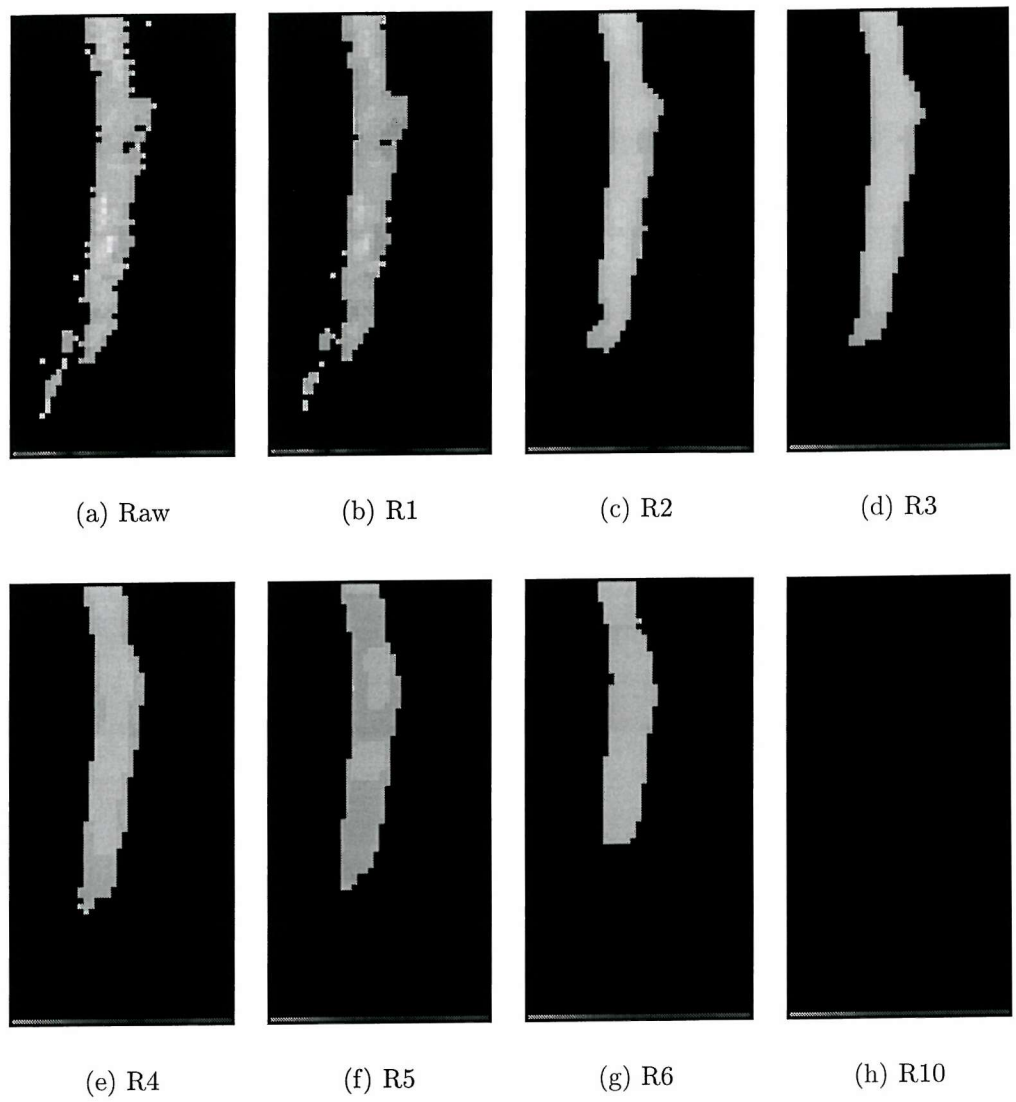

(a) Raw (b) R1 (c) R2 (d) R3

(e) R4 (f) R5 (g) R6 (h) R10

***Figure 5.7:*** *Imagery thresholded at a greyscale of 170, showing the variation in cloud object coherence: (a) Raw imagery smoothed using a median filter of radius (b) 1, (c) 2, (d) 3, (e) 4, (f) 5, (g) 6 and (h) 10 pixels. Data are METEOSAT D2 images from 2200GMT on the 23rd of April 1998.*

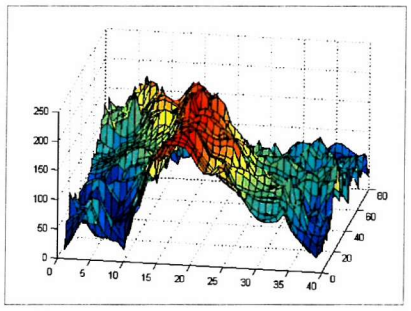

(a) Raw Edge Plot

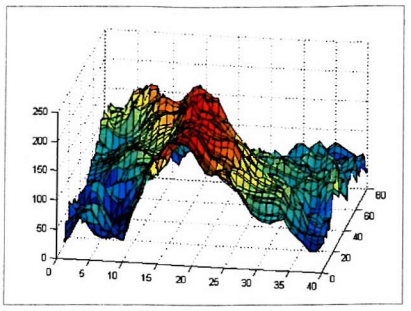

(b) Median Radius 1

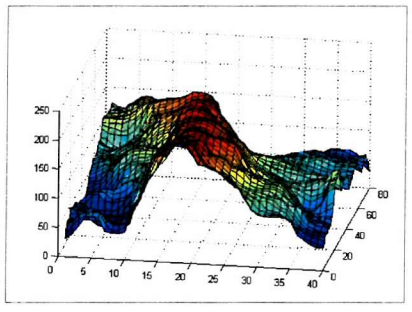

(c) Median Radius 2

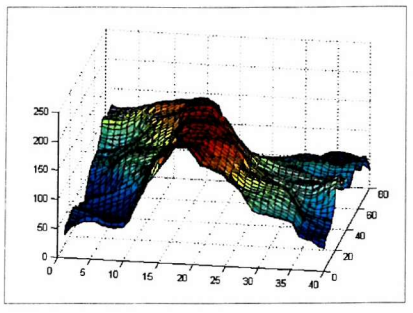

(d) Median Radius 3

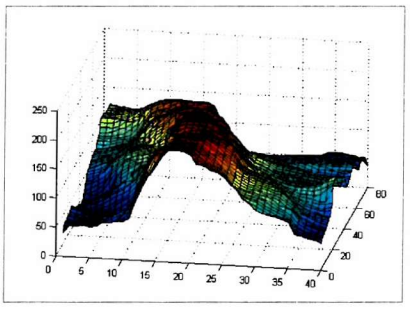

(e) Median Radius 4

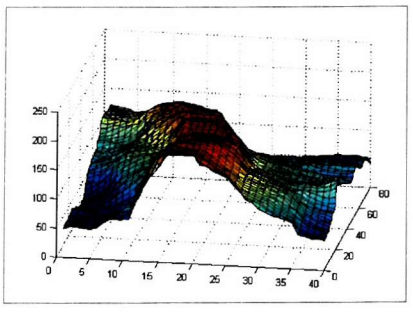

(f) Median Radius 5

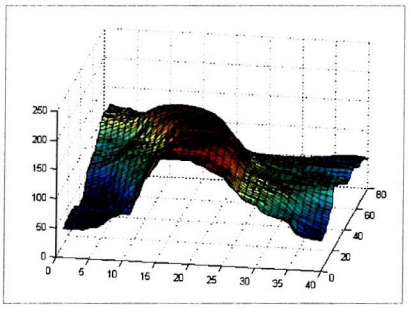

(g) Median Radius 6

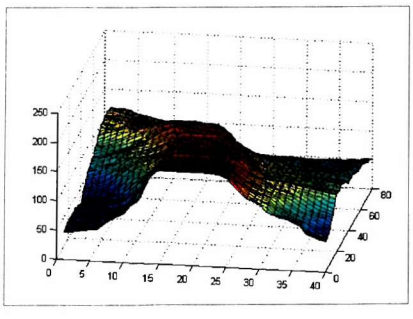

(h) Median Radius 10

***Figure 5.8:*** *Edge degradation with varying sizes of median filter: (a) Raw imagery smoothed using a median filter of radius (b) 1, (c) 2, (d) 3, (e) 4, (f) 5, (g) 6 and (h) 10 pixels. Data are METEOSAT D2 images from 2200 GMT on the 23rs of April 1998. The vertical axis is greyscale.*

### 5.2.2 Fuzzy Morphological Filtering

To capture cloud shape information at the scale of whole objects, it is necessary to reduce the small–scale variation of cloud structure that is not relevant to the larger shape analysis, effectively reducing the precision of the representation of the *contents* of a cloud shape. A morphological filter has been developed that preserves the nature and gradient of the cloud edges, whilst smoothing the cloud tops. This is achieved using a variant of the *rolling ball* algorithm[7]. In its simplest form, this consists of rolling a ball[8] of fixed radius alternately above and below the surface under analysis for a number of iterations, and remapping the surface to the locus of the lowest / highest point on the ball, respectively (Figure 5.9). An iteration of this filter consists of rolling the ball both above *and* below the surface. Whilst some difference may result from rolling the ball firstly above, or firstly below the surface, this difference is typically negligible over a few iterations of the filter. Nagao and Matsuyama [72] describe an alternative to the morphological filter developed here based on filtering in the direction of minimum data variance.

In order to smooth the centres of the cloud more than the edges, however, a variable–sized structuring element must be used. Care must be taken, however, with implementing a variable structuring element filter, as can be shown by considering a simple variable–size adaptation of the standard rolling ball filter. This consists of fitting the largest ball possible between the surface and a lower or upper plane. It is important to note that the selection of a *spherical* structuring element *itself* must be made with care, since the variation in the data *vertically* may be significantly different to the horizontal variation. Indeed with cloud data, there is a significant difference between these two, and it is important to ensure that the correct degree of smoothing occurs due to the variation in horizontal and vertical components. In practice, the data are suitably preprocessed and stretched so that the largest sphere considered corresponds both to the largest sensible horizontal and vertical structuring element. By preprocessing the cloud

[7] See for example Hashim et al [47].
[8] Or so–called *structuring element*

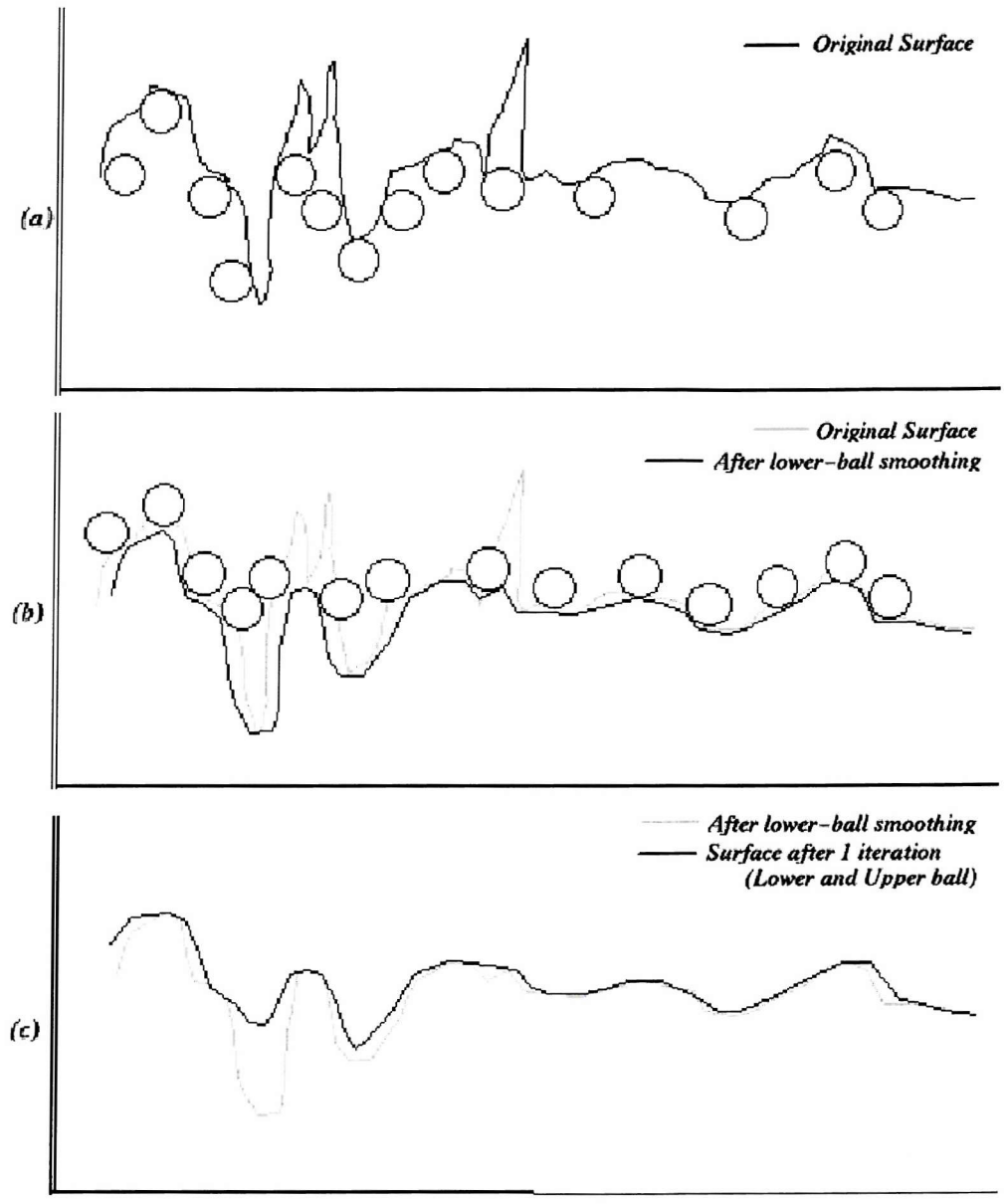


***Figure 5.9:*** *A standard rolling ball algorithm: a ball of fixed radius is rolled alternately below (a) and above (b) the surface to be smoothed. The surface is replaced by the locus of the top / bottom of the ball. One iteration of this filter consists of rolling the ball both above and below the surface.*

data to cover the greyscale range of $0 - 255$, a lower plane of greyscale 0 and an upper plane of greyscale 255 can be used.

As illustrated in Figure 5.10, large spheres fit under the middle of a cloud, and smaller ones at the edges (and vice–versa for spheres above the cloud). The use of a variable sized ball on its own presents problems, however, and does not result in the desired greater smoothing in the middle of the cloud than at its edges and

greater edge detail preservation.

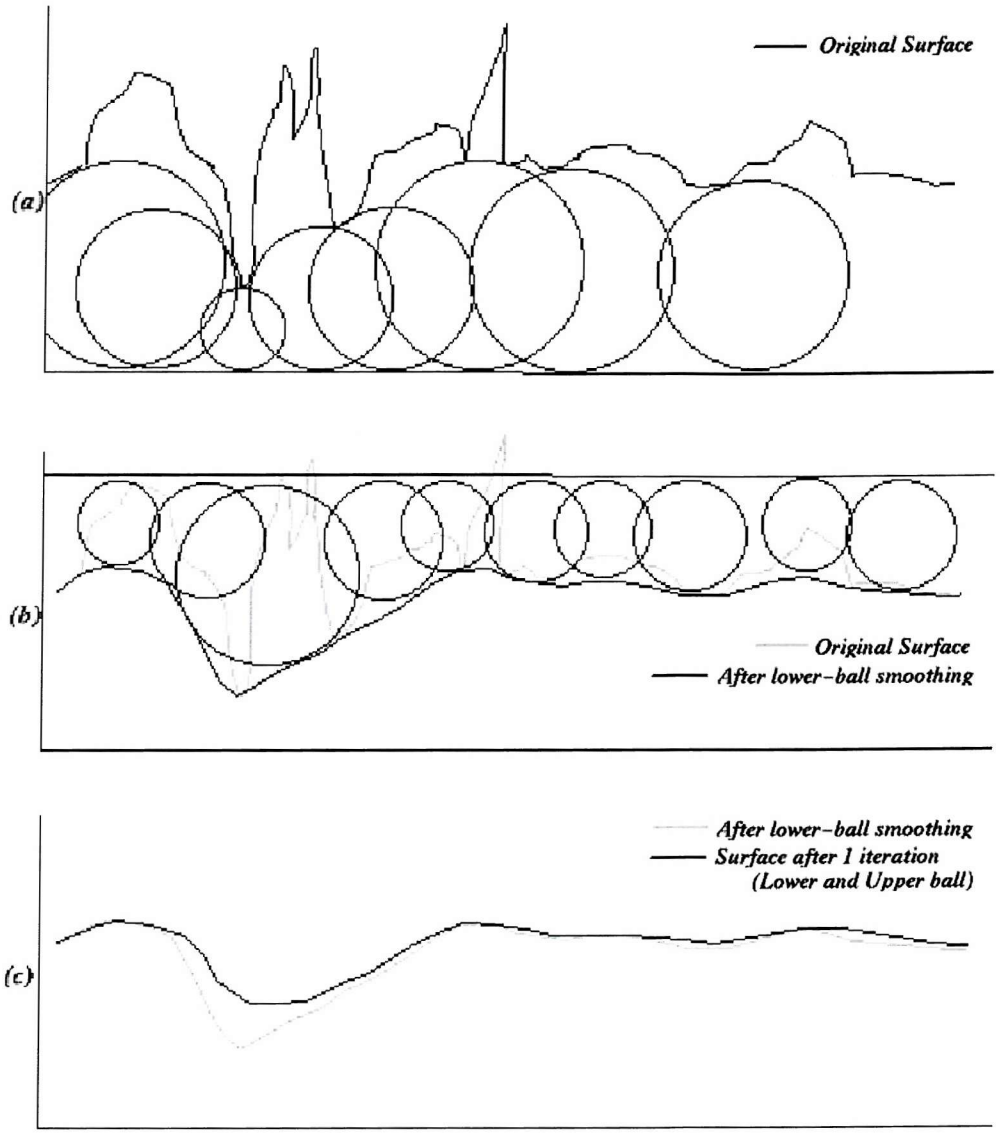


***Figure 5.10:*** *A variable–size rolling ball algorithm. The largest ball to fit between a baseline and the surface, and a sensible upper line*[10] *and the surface, respectively. As per the standard rolling ball algorithm, the surface is replaced by the locus of the top / bottom of the ball. Large spheres fit under the middle of a cloud where most smoothing is desired, whereas smaller spheres fit under the edges resulting in better preservation of the edge information.*

Implementing the variable ball size smoothing technique on discrete imagery is difficult in light of the nature of digital representations of circles and spheres. If sphere edges are caught on noisy low pixels near crisp discrete image data edges then the resulting maximum sphere height can be altered considerably. This is not just a problem for pixels near to edges either, since flat areas in the middle of clouds may fit large spheres underneath them that are large enough to get caught

by noisy low edge pixels (Figure 5.11). Also, whilst rolling variable–sized spheres *below* the cloud surface results in more smoothing in the middle of the cloud and subsequently rolling the spheres *above* the surface smoothes the non–cloud regions, both stages also erode the gradients in the transition phase between cloud and non–cloud, the very edge gradients the filter must preserve.

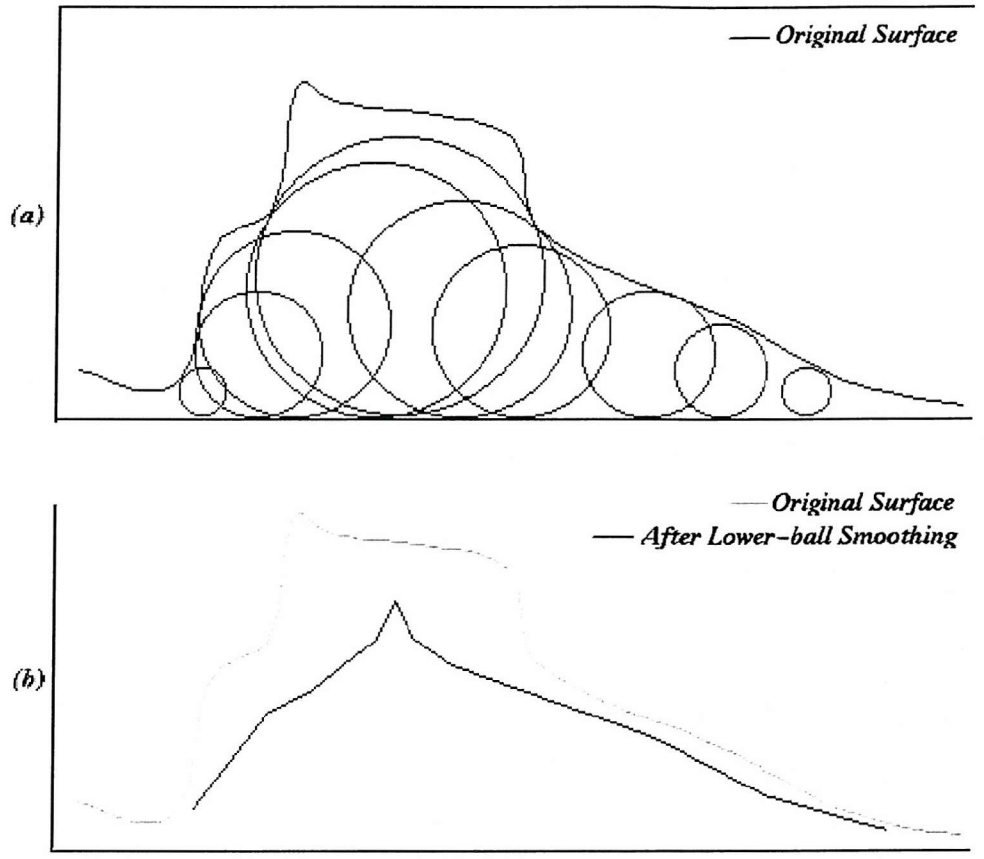


***Figure 5.11:*** *Some of the ways in which the variable size rolling ball filter can be compromised: crisp edges are smoothed too strongly and multiple layers of cloud result in the uppermost layer being smoothed out.*

In order to overcome some of these problems, a new approach has been used, whereby only a vertically sliced segment of the ball has to fit above / below the surface. A two–dimensional representation of the approach is given in Figure 5.12. The largest sphere *segment* that will fit under / over any image data region is used, allowing crisp edges to be dealt with by fitting the segment under the cloud pointing *away* from the cloud edge. This removes spikes in the data without removing ridges or crisp transitions: there has to be some local coherence in the data in at least *one* direction, over a horizontal distance equivalent to the segment radius. The formula for the new filter is given in Equation 5.5.

At each surface pixel location, the pixel is given an offset proportional to the difference between the surface height relative to the lower (upper)[11] plane and the tallest sphere segment that fits between the pixel and the lower (upper) plane. The sphere segment is a vertical segment of a sphere, and for the segment to class as having *fit*, all points within the segment must be below (above) the cloud surface, i.e. the neighbourhood of the pixel is also checked, in the direction of the segment, to ensure the region of segment under (above) the neighbours fits beneath (above) them. No sphere larger than 25 pixels' radius is used[12], and the amount of smoothing can be controlled over iterations of the filter using a *learning rate* to adjust the proportion of the difference between surface height and segment height that is used to adapt the data on each iteration. Because the base (upper) plane has been taken as planar, and normal to the vertical, the lower (upper) half of the sphere segments can be ignored in each iteration by effectively moving the base (upper) plane closer to the surface by an offset equal to the sphere radius.

[11] Lower or upper, depending on whether the filter iteration is a lower or upper surface smoothing step.

[12] No smoothing is applied if a segment of a sphere of diameter 50 pixels fits under (over) the surface, as this is taken as already sufficiently smooth.

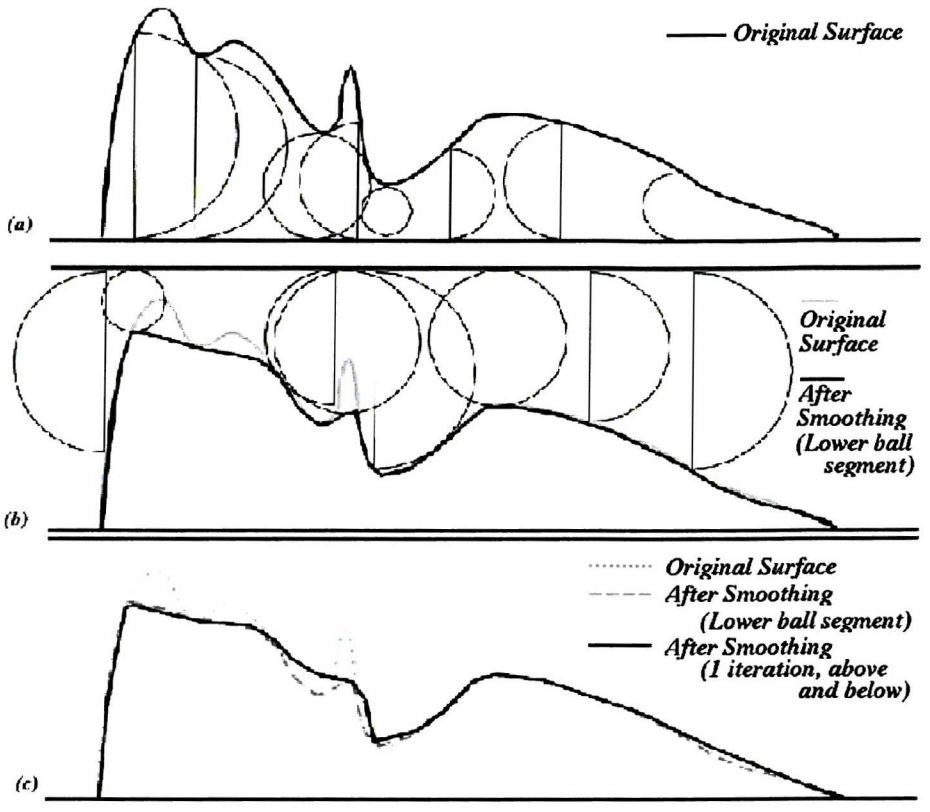


***Figure 5.12:*** *A 2–D representation of the new rolling ball algorithm using ball segments rather than complete balls.*

$$I(x,y) = I(x,y) + \lambda(\kappa(x,y) - I(x,y)) \tag{5.5}$$

where

$I(x,y)$ = raw image data surface

$\Phi I(x,y)$ = filtered image surface

$\lambda$ = learning rate = 1 by default

$$\kappa(x,y) = \text{vertical offset} = \begin{cases} \Delta(r_{max}), & 0 \leq r_{max} \leq 25 \\ I(x,y), & r_{max} > 25 \end{cases}$$

$r_{max}$ = maximum sphere radius that fits under image data

$\Delta(r_{max})$ = sphere offset

$$= \begin{cases} 2 * r_{max} + \underset{\theta=0}{\overset{2\pi}{max}}(\underset{r=0}{\overset{r_{max}}{min}}(\overline{I}(r,\theta) - S(r,\theta))) & \exists\theta \text{s.t.} \\ & (\underset{r=0}{\overset{r_{max}}{min}}(\overline{I}(r,\theta) - S(r,\theta)) > 0) \\ 0 & \text{otherwise} \end{cases}$$

$r$ = sphere radius

$\theta$ = radial sphere check position

A discussion of how the approach determines the size and direction of the sphere segment that fits is now given by considering the filter applied to a data point at the end of the tail of a comma cloud (Figure 5.13). The greyscale data around the point will fall off quite sharply in all directions except for the direction further into the comma cloud towards its centre. A sphere segment will fit under the greyscale data in the direction of the comma centre however, therefore the comma cloud's tail will not be smoothed away. This is illustrated in Figure 5.13(a) by the two cloud cross–sections. In cross–section A (taken as indicative of all cross–sections not directed *into* the comma), a sphere section is unable to fit exactly under the cloud surface as the vertical variation in the data in this direction is much greater than the horizontal. If this cross–section were considered in isolation, the resulting smoothing would be significant, as illustrated by the heavy black line in the cross–section data. In cross–section B, however, the horizontal and vertical variations in the data are of a similar magnitude, and a sphere section fits under the cloud easily, resulting in little smoothing. Figure 5.13(b) illustrates how the horizontal variation in the cloud affects the directions in which a sphere segment can fit. As the sphere radius is grown, the radial directions in which a sphere segment may fit under the comma cloud's surface, illustrated in black, change. Figure (b) considers the horizontal extent of the cloud *only*, however. By analysing cloud cross–sections similar to those in (a) in the angular directions shaded in black, for a sphere segment of the given radius, the directions in which the segment fits both horizontally and vertically can be determined. The sphere radius is grown as per Figure (b) until a segment no longer fits in *any* direction under the cloud surface.

In order to address the issue of assessing whether continuous sphere segments fit under digitised surfaces, the sphere segment data are checked to ensure they fit under (over) the satellite data surface at set points on the circumference of circles at step radii of one pixel away from the pixel under test, and at angular separations so that the horizontal separation of neighbouring test locations for the largest radius sphere segment (of 25 pixels) is approximately one pixel (Figure 5.14). The surface pixel values surrounding the pixel under test are interpolated to the sphere check locations, as per Equation 5.6 and Figure 5.15.

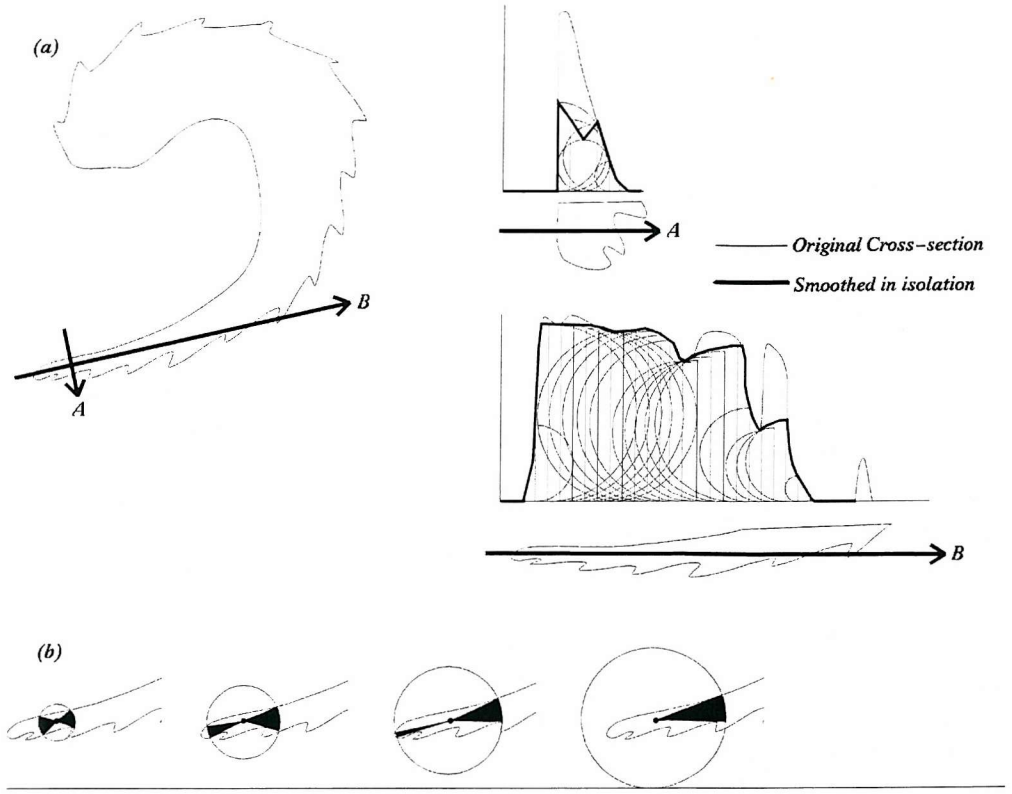


***Figure 5.13:*** *Directional variation in a cloud surface. Figure (a) shows a comma cloud. Two cross-sections of the cloud have been taken (lines A and B) to show the effect of smoothing at their crossing point. Figure (b) shows the possible directions in which a segment of a sphere may fit under the cloud surface, with increasing sphere radius, considering the horizontal variation of the cloud only.*

$$Greyscale = \frac{\sum_{i=1}^{4} x_i g_i}{\sum_{i=1}^{4} x_i} \tag{5.6}$$

*where*

$$x_i = \begin{cases} 1 - A_i, & 1 - A_i > 0 \\ 0, & \text{otherwise} \end{cases}$$

$g_i$ = greyscale of $i^{th}$ pixel being interpolated

($A_i$ is the distance between the centre of the $i^{th}$ pixel and the circle test point

Figure 5.16 shows the effect of the filter on the same dataset as earlier analysed using the median filter. As can be seen, significantly less of the original data is lost. The edge plot (Figure 5.18) confirms that the edge gradients do not decay

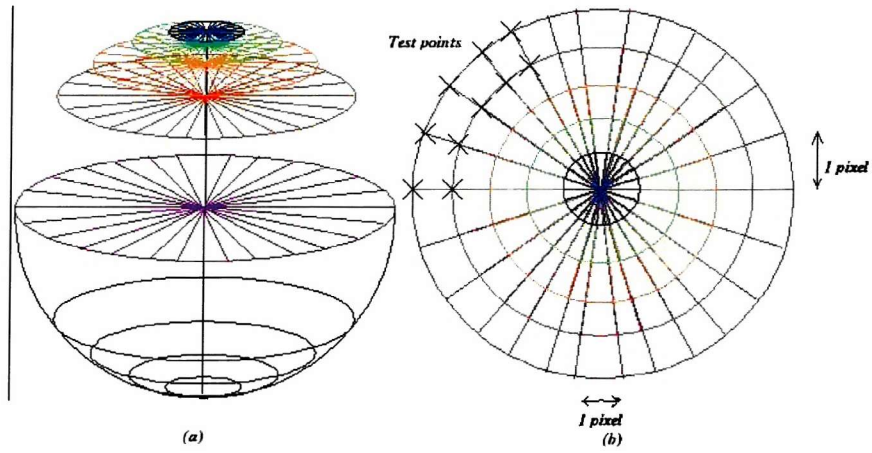


***Figure 5.14:*** *Definition of a discrete sphere for use in the adapted rolling ball filtering algorithm. (a) Vertical profile of discrete sphere representation. (b) Image data are tested at the ends of each radius of each sphere, the image data having been interpolated as indicated in Figure 5.15.*

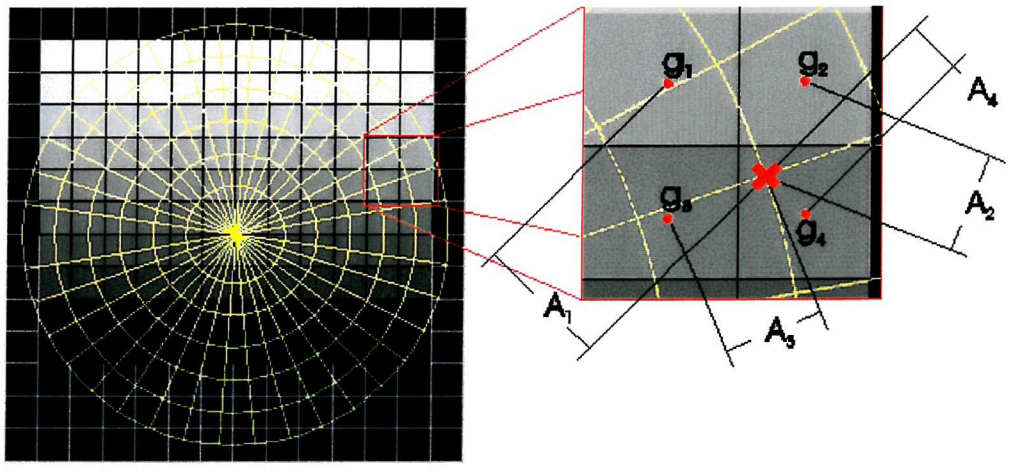


***Figure 5.15:*** *Pixel interpolation for correct assessment of the greyscale under a sphere. See also Equation 5.6.*

with further iterations of the filter, but the coherence of the cloud ridge increases as desired, as illustrated in the coherence plots (Figure 5.17).

This has demonstrated the effectiveness of the filter for maintaining the structure of a ridge, improving its coherence and keeping its edge gradients. Applying the filter to *other* types of cloud shows its effectiveness for cloud data smoothing: Figure 5.5 was used to illustrate the nature of a coherent cloud structure by analysing a vortex. The coherent image data have been filtered using this morphological filter. Figure 5.19 contains a storm cell, which has sharp edges

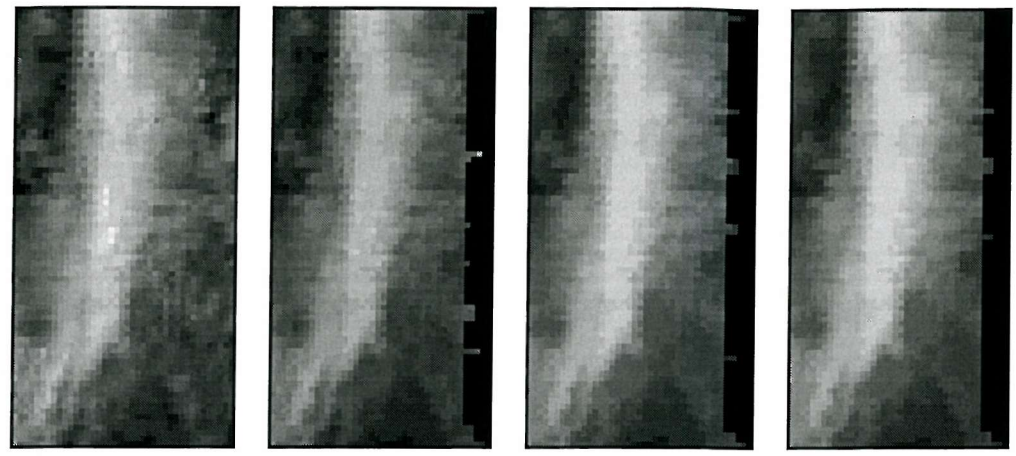

(a) Raw (b) 1 iteration (c) 2 iterations (d) 3 iterations

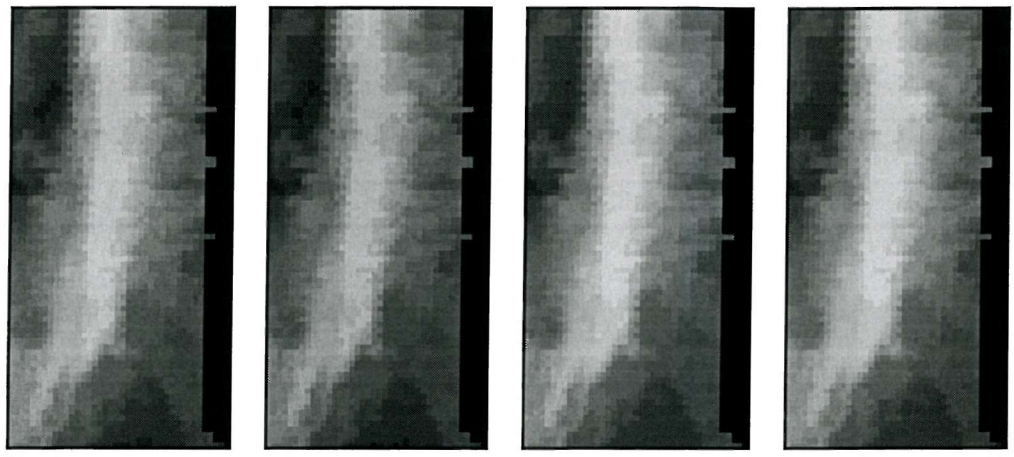

(e) 4 iterations (f) 5 iterations (g) 6 iterations (h) 10 iterations

***Figure 5.16:*** *A raw image (a) and the result of applying a morphological filter for (b) 1, (c) 2, (d) 3, (e) 4, (f) 5, (g) 6 and (h) 10 iterations. The image data is METEOSAT D2 infrared imagery from 2200 GMT on 23rd April 1998.*

which again have been preserved, whilst reducing the internal noise which are irrelevant to the analysis at the scale of the whole cell. Finally, Figure 5.20 shows the performance of the filter on fine texture, as contained in an open–and closed–cell cumulus field. This qualitative discussion of the filter's characteristics has shown it to provide a suitable type and degree of filtering for subsequent object and edge analyses. It is broadly true that having defined the desired characteristics of an image filter, there are many ways to construct such a filter. Whilst this particular morphological filter may not be computationally the most effi-

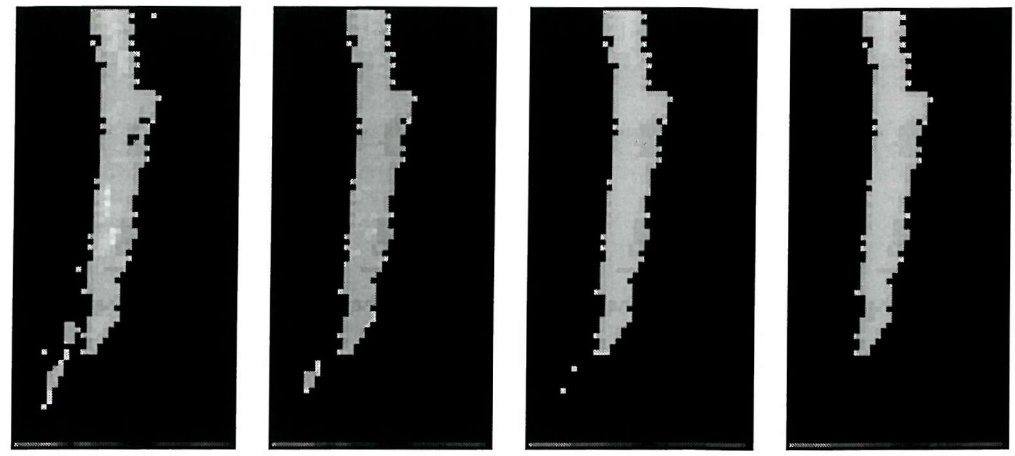

(a) Raw Coherence Plot (b) 1 iteration (c) 2 iterations (d) 3 iterations

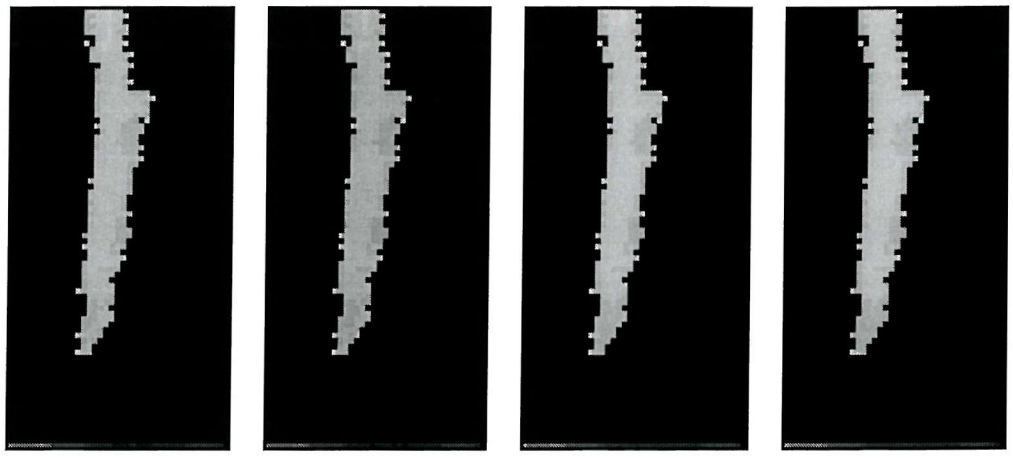

(e) 4 iterations (f) 5 iterations (g) 6 iterations (h) 10 iterations

***Figure 5.17:*** *The change in cloud coherence, based on a high–pass threshold at a greyscale of 170, with morphological filtering: (a) Raw Data, (b) 1, (c) 2, (d) 3, (e) 4, (f) 5, (g) 6, (h) 7, (i) 8, (j) 9 and (k) 10 iterations.*

cient method for producing the desired smoothing characteristics, it has achieved those characteristics nonetheless. The computational cost of this filter was not excessive, however: the algorithm was implemented in C++, and took approximately twenty seconds per iteration (once below *and* above the cloud surface) on a computer with a 150MHz processor and 120Mb of RAM, running Windows NT 4.0. Approximately six iterations of the filter were typically necessary to obtain sufficient smoothing for coherent cloud structures.

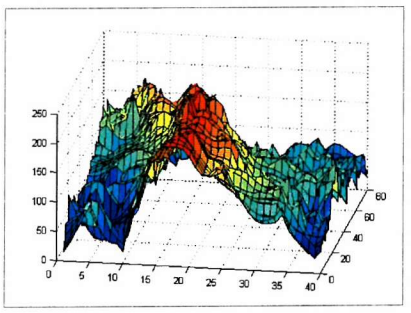

(a) Raw Edge Plot

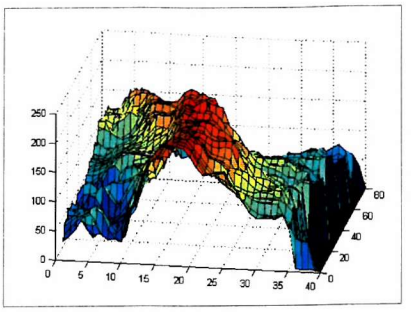

(b) 1 iteration

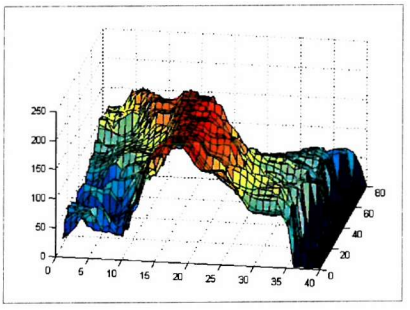

(c) 2 iterations

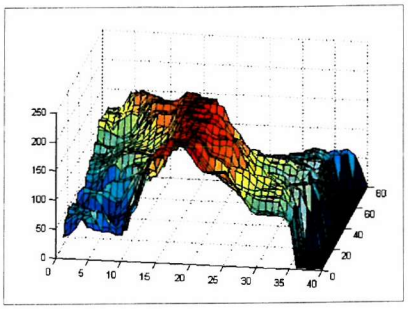

(d) 3 iterations

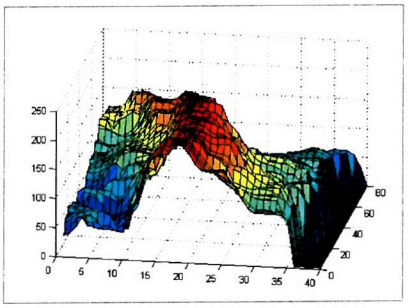

(e) 4 iterations

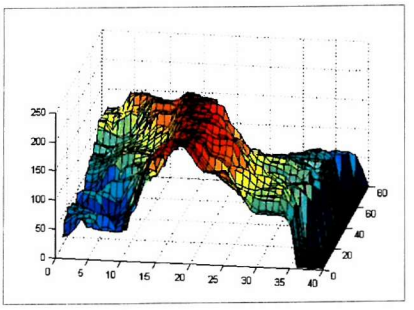

(f) 5 iterations

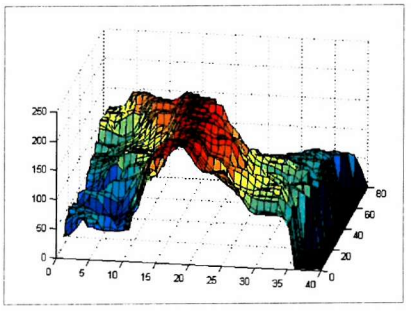

(g) 6 iterations

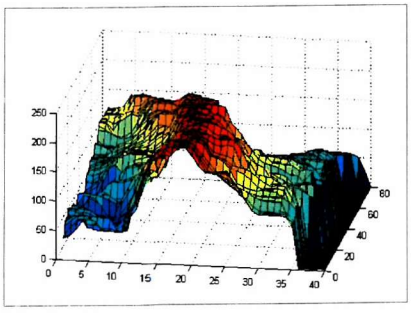

(h) 10 iterations

***Figure 5.18:*** *The change in edge structure with morphological filtering: (a) Raw Data, (b) 1, (c) 2, (d) 3, (e) 4, (f) 5, (g) 6, (h) 7, (i) 8, (j) 9 and (k) 10 iterations.*

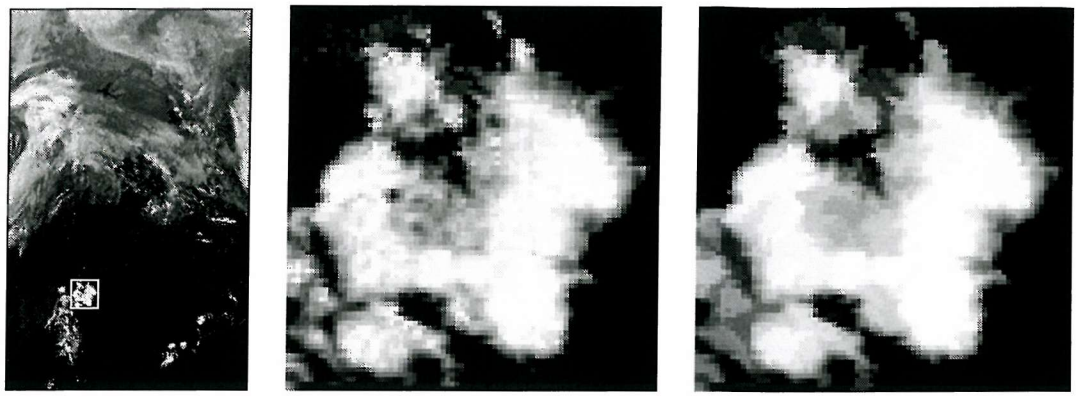

(a) Raw Image (b) Section (c) Smoothed section

***Figure 5.19:*** *(a) Raw image: 1500 GMT METEOSAT D2 image from 18th June 1998, (b) Storm cell from image and (c) Storm cell smoothed after 7 iterations. Note that the crispness of the edge information in the image has been preserved.*

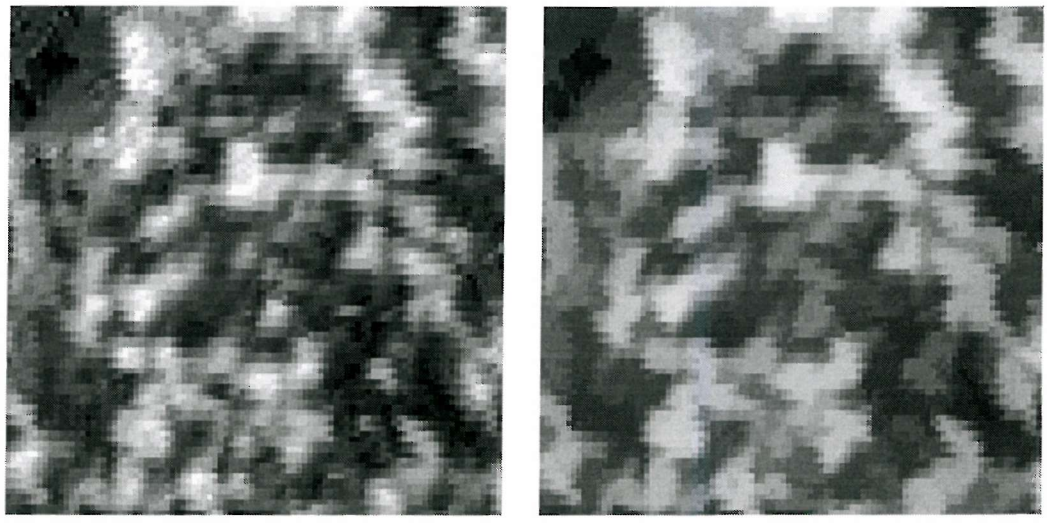

(a) Raw Data (b) Smoothed

***Figure 5.20:*** *(a) A section of cumulus cloud from METEOSAT D2 image from 15th June 1998 1600GMT, (b) smoothed after 7 iterations of the morphological filter. Note the filter has preserved the cloud shapes despite the high degree of texture in the image.*

## 5.3 Cloud Object Extraction

Having prepared and smoothed the cloud, two techniques are applied to extract the cloud from the prepared images. These are the starting point for extended feature extraction as discussed in the next chapter, but also provide objects that can themselves be analysed and tracked.

### 5.3.1 Multi–level thresholding

To analyse cloud vertical structure to some degree, the smoothed data is sliced at all greyscales from the maximum present in the data, the top of the cloud, to a minimum value for the cloud content in the imagery[13]. At each slice, independent objects are extracted and their area and centroid calculated. Each independent object is also assigned a unique colour. Objects in each subsequent slice are matched with those in the slice above based on which higher objects are subsets of the current object. Where a single higher object matches with one in the present slice, the present object is assigned the same colour as the higher one. Where, however, there are multiple unique objects in the slice above that are contained within the boundaries of the current object, the current object is assigned a *new* colour. In this way, a peak–unique contour map is built up, showing where the tops of each coherent structure split. This is illustrated in Figure 5.21: the cloud image projected on the base of the scene has been sliced vertically, and the objects shown in any frame are colour coded according to the objects they match with in slices above / below the current one. The black dots represent the centroids of the objects at all slices.

This is similar to an approach applied by Peak and Tag [80] for cloud segmentation prior to classification: discrete cloud objects in consecutive greyscale slices are extracted, although in Peak and Tag's approach, the slices are taken with *increasing* rather than decreasing cloud height. Where objects split into two or

[13] Note this is not the cloud *base*, due to the fact that the cloud is only viewed from above, but is effectively the largest cloud *footprint*.

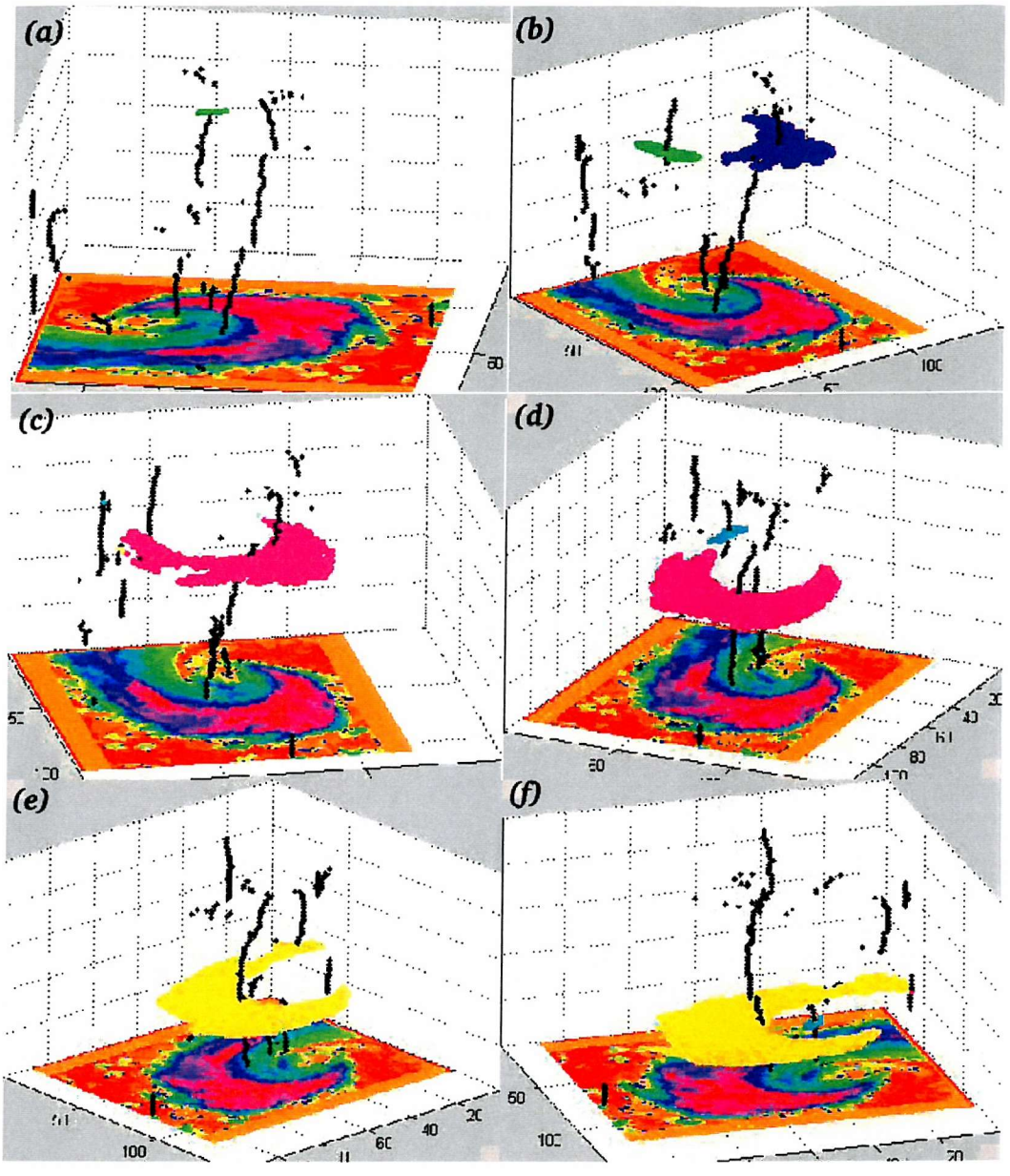


***Figure 5.21:*** *Objects extracted using a multi–layer thresholding technique (Perspective view). The centroids of each vertical slice are indicated by the black dots. The respective frames show different slices through the cloud, from top to bottom, from different viewing angles.*

more sub–objects over a greyscale interval, an object hierarchy develops. By taking the lowest greyscale for any subsequently non–splitting object path, cloud objects of a particular nature can be extracted.

From the knowledge of which cloud slices are attached to which others and knowledge of the centroid location of each slice, it is possible to produce a type of *vertical skeleton* of the structure. The dynamics of this skeleton show where any

convective processes may be occurring within the cloud. Similarly, associating the area of a slice with its centroid provides information regarding which levels of cloud are growing over time.

### 5.3.2 *Fuzzy Growth Approach*

The second approach consists of identifying *core* regions of cloud content and growing these to include areas that have some *association* with the cloud core, capturing this *degree* of association by using a fuzzy measure of cloud membership. Udupa and Samarasekera [103] discuss fuzzy connectedness in the context of object generation.

The satellite imagery is initially differenced from background templates as has been described previously (without the resulting stretch of greyscales), to provide a first pass at identifying the cloud content. This is then high–pass thresholded to leave pixels whose brightness is sufficient to ensure they only depict cloud. Pixel clusters of less than fifty pixels are then removed. In the remaining bright pixel clusters, cracks are propagated to obtain distinct core objects, as described in Table 5.2.

Having obtained the cores, a fuzzy system is used to assign the pixels immediately neighbouring the core a *membership* or *degree of association* to their core. The pixels neighbouring *these* neighbours are also then analysed, provided the degree of association of the previously assessed pixels is sufficiently high. This iterative growth process continues until no more pixels have sufficient associativity to the cloud core to warrant any further growth. This is similar to an approach by Feher and Zabusky [36] for determining the associativity of flow regions to vortex structures in vorticity fields in computational fluid dynamics.

The inputs to the fuzzy system used for growing these cloud regions are the pixels' absolute radiance (a global thresholding component), the relative difference between their radiance and the nearest core pixel radiance (a local thresholding component) and the gradient of radiance from the core to the pixel under analysis.

1. The mean greyscale $\mu$ of each cluster is determined and pixels darker than the mean are taken as possible starting points for cracks to propagate from, forming a subset $A$ from all the pixels in the cluster, $\xi$.

2. A subset $B(x_A)$ of $A$ is created for a member $x_A$ of $A$, such that the greyscale of all pixels in $B$ is equal to or darker than the greyscale of $x_A$ and all pixels in $B$ touch $x_A$ or a pixel already in $B$. This is an iterative process whereby $x_A$ itself is first added to the subset $B$, then the immediate neighbours of $x_A$ are initially examined and added to $B$ if equal to or darker than $x_A$. The neighbours of each new member of $B$ are themselves examined in turn, and added to $B$ if they are darker than the member of $B$ under analysis, until no more pixels can be added to $B$.

3. As long as the subset $B \subset A$ includes a pixel at the *edge* of the initial pixel cluster (neighbouring $\xi'$) *and* one neighbouring a pixel *equal to or lighter than* the mean (i.e. $\xi \cap (A')$), the pixels in $B$ are changed to background pixels and removed from $A$.

4. This is repeated for all members of $A$ and all clusters $\xi$.

5. Any resulting pixel clusters $\xi$ with fewer than fifty pixels are removed.

***Table 5.2:*** *Algorithm for propagating cracks in cloud shapes, to leave homogeneous cloud cores.*

This is illustrated in Figure 5.22. The fuzzy rule base used in this system is given in Appendix A. The membership function transitions and rule confidences were determined empirically by testing a number of different values. The membership functions and rule confidences selected gave good performance for a number of different cloud types. The transitions and rule confidences could be optimised further by application of an adaptive learning technique applied to the fuzzy system (such as the neurofuzzy methods described by Brown and Harris [13], for example), but care would be required in selection of the training cases for such a system to ensure good generalised performance.

Figure 5.23 gives an example of the cloud cores extracted from METEOSAT infrared imagery and the effect of the fuzzy growth algorithm for adding edge pixels. It can be seen clearly from this example that the algorithm has added few edge pixels in the case of a crisp transition from a cloudy to a non–cloudy region, and has added many more pixels in the case of a dispersed cloud edge (See also Figure 6.9). Comparing this approach with the results shown in Figure 3.3, it can

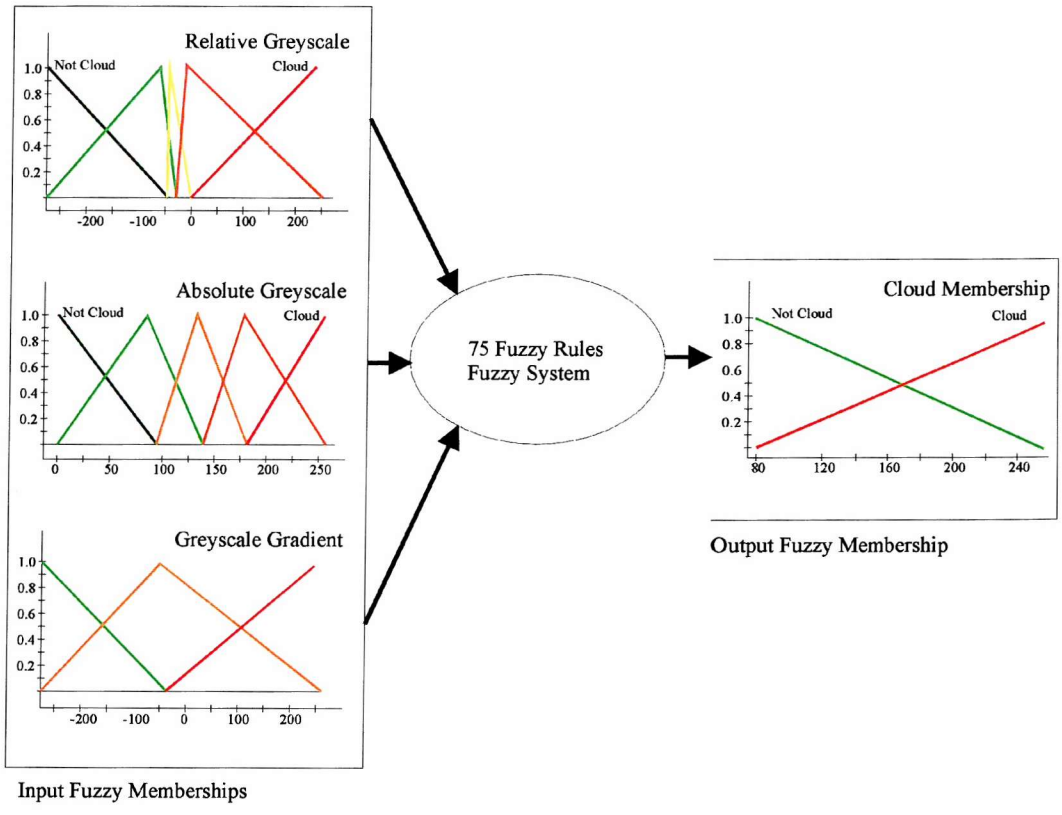


***Figure 5.22:*** *Fuzzy System for cloud edge growth. Relative and Absolute greyscale and greyscale gradient measurements are passed to the fuzzy system, which provides a cloud membership as an output.*

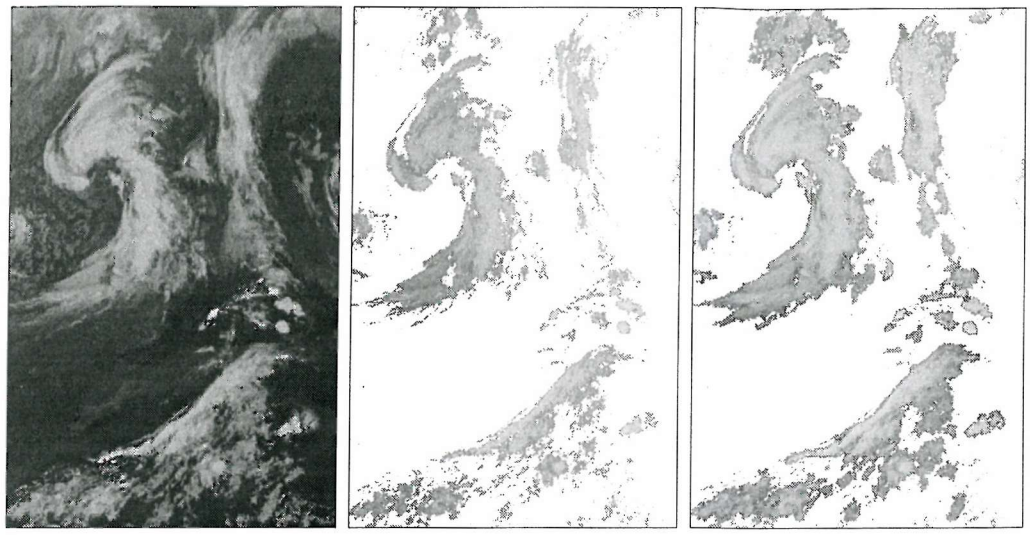

(a) (b) (c)

***Figure 5.23:*** *Cloud Extraction and Enhancement. (a)Constant distance projection of METEOSAT D2 image from August 27, 1997. (b)Cloud cores extracted using the background template differencing and crack propagation technique. (c) Cloud grown to include the edge regions using a fuzzy system.*

be seen that it also offers much better performance than single–level thresholds for cloud identification, capturing more of the cloud lower in the image than the high threshold in Figure 3.3(a) without capturing too much of the background as in Figure 3.3(b), i.e. effectively providing some degree of local thresholding.

The fuzzy system used in this section was developed from NeuFrame's Neufuzzy template[14] integrated into some C++ code, and had negligible[15] computational cost when applied to $800 * 800$ METEOSAT D2 images running on a computer with a 150MHz processor and 128Mb of RAM under Windows NT 4.0.

This work was presented at the First AMS conference on Artificial Intelligence, as detailed in Newland et al[76].

[14] Jointly developed by the Department of Electronics and Computer Science, University of Southampton and Neural Computer Sciences: http://www.ncs.co.uk

[15] i.e. less than ten seconds

### 5.3.3 Discussion of Cloud Object Extraction Techniques

Clearly the applications of the two cloud object shape analysis techniques discussed here are very different, with the first approach concentrating on a mechanism for the vertical (and by implication also the temporal) variation in cloud shape, as can be described by matching whole slices of smoothed cloud data. The second approach produces whole cloud objects and captures the essence of the cloud edge in doing so.

No further discussion of the first approach is given in this thesis, although the resulting cloud slices could certainly be used as valid parameters to be matched, much like the skeletons and edges discussed in the next chapter. There is also the possibility of determining the vertical motion of the cloud structures by matching cloud objects from *different* greyscale slices over time, not only with objects from the same slice. This would require some constraint to ensure that the resulting matches were also vertically consistent.

The fuzzy object growth approach for cloud object identification shows some significant noise, whilst still achieving the main goal of providing differentiated growth between crisp and dispersed cloud edges. The algorithm has been applied to cloud data in Figure 5.23 that has not been subjected to any prior smoothing. Applying the core and growth algorithm to smoothed data should produce cleaner transitions from cloud cores to non–cloud regions in the case of dispersed cloud edges.

# 6. CLOUD OBJECT PARAMETERISATION

Three new parameterisations of clouds have been generated in this thesis that capture new information about the cloud content, namely *skeletons*, *fuzzy edges* and *whole cloud objects*. Skeletons capture the major axis of the cloud shape, fuzzy edge information describes the nature of dynamic processes across and in the vicinity of the cloud edge and the whole cloud shape provides an indication of the size and growth of the weather system. In addition, the motion of these parameters has been used to describe the evolution of cloud at different scales, and different components of the evolution. Whole objects have been discussed in the previous chapter. A discussion of skeletons and edges follows.

## *6.1 Cloud Skeletons*

The skeleton or medial axis transform of a 2–D shape is its mid–line or axis of symmetry. It is defined using one of two root analogies in most literature (e.g. Serra [90]), namely that of wave propagation, where the skeleton is defined as the meeting points of a wavefront propagating inwards / outwards from an object's edge, or the set of centres of *maximal disks* whose entirety is contained within / outside the object edge, but whose circumference lies on the object boundary at two or more different places (Figure 6.1).

Similarly, there are typically two types of algorithm used for skeleton generation, namely thinning and skeletonization, the former being an iterative edge erosion approach leaving a skeletal structure on completion, and the latter generating the skeleton more directly. In practice, there are many ways to implement both

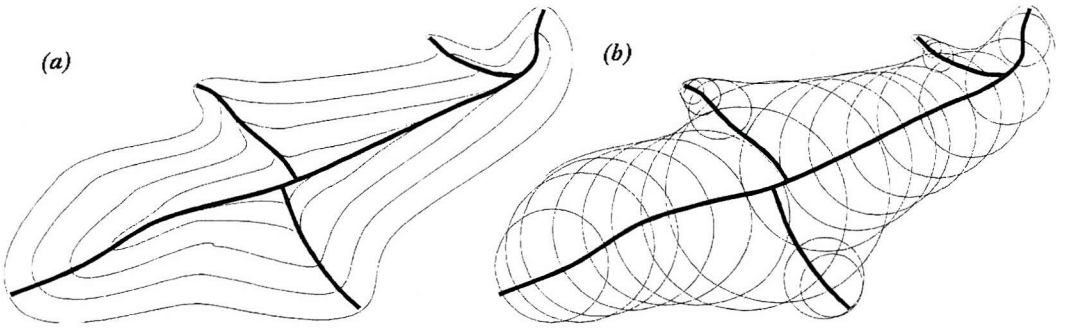


***Figure 6.1:*** *Wavefront propagation (a) and Maximal disk (b) analogies for generating skeletons of shapes.*

processes and the distinction between iterative and direct analysis is a little less clear. It is sufficient to say that the desired outcome of any of the techniques is the axis of symmetry, of single-pixel width, that is *homotopic* or without any breaks for any given cloud object.

Generating skeletons for clouds is a novel application of medial axis transforms. The results presented here have been generated using a maximal sphere approach applied to thresholded binary representations of the smoothed cloud objects. Other techniques for applying skeletons to the cloud data are also suitable, however. In particular a veinerization approach to skeleton generation is described which offers the potential for much smoother and more coherent skeletons. A greyscale–sliced vertical skeleton profile of cloud is also introduced and discussed in this thesis, that provides a richer description of the cloud's vertical structure. This is achieved by applying the skeleton analysis to slices of cloud at many different heights or similarly at different degrees of cloud dissipation, and indicates the variations in directions of cloud spread with height.

### 6.1.1 Maximal Disks

The approach used for generating skeletons in this thesis is not guaranteed to be homotopic in digital space, but has a conceptually simple implementation whilst still showing the benefits of the skeletal analysis for cloud data. A digital representation of a circular disk is passed over each pixel of a binary thresholded cloud object and the disk radius is increased until one or more points on the disk

edge coincides with a cloud edge pixel. If two or more disparate sets of points on the disk edge touch the cloud edge then the centre of the circle is a skeleton point. The analysis of the next pixel in the cloud object then starts with a disk of radius one–less than the current pixel's maximum radius. This is illustrated in Figure 6.2. The algorithm applied is given in Equation 6.1.

$$\Psi = C(X_{max}) \forall X_{max} \in \Phi^{+} \tag{6.1}$$

*where*

$\Psi$ = set of skeleton points

$X_{max}$ = maximal disk

$= X_r, \forall X_r \in \Phi^{+}$ s.t $X_r \cap \Phi^{+} = X_r$

and $X_r \cap (X_r \cap \Phi)'$ is disjointed

$X_r$ = digital representation of a circle of radius $r$

$C(X_{max})$ = centre of maximal disk

$\Phi^{+}$ = cloud object including border

$\Phi$ = cloud object excluding border

Using this algorithm in digital space has a number of problems related to the representation of circles in digital space and the sensitivity of the approach to any noise in the object representation[1] when determining whether two or more sets of points touch the object's edge. As a result, the homotopy of the skeleton is broken, as discontinuities in the skeleton result from any variation or abberation on the cloud edge. Despite these problems, the approach produces stable skeletons when the image data are initially smoothed, or at least any noisy holes in the binary representation of the cloud object are removed (this is the requirement of skeletal analyses for coherent objects). Examples of this skeleton type are given in Figure 6.3. Note that the results shown have not been generated using cloud data pre–smoothed using the coherence–enhancing filter discussed in the last section.

[1] Either in terms of holes in the object or in individual pixel changes on the edges

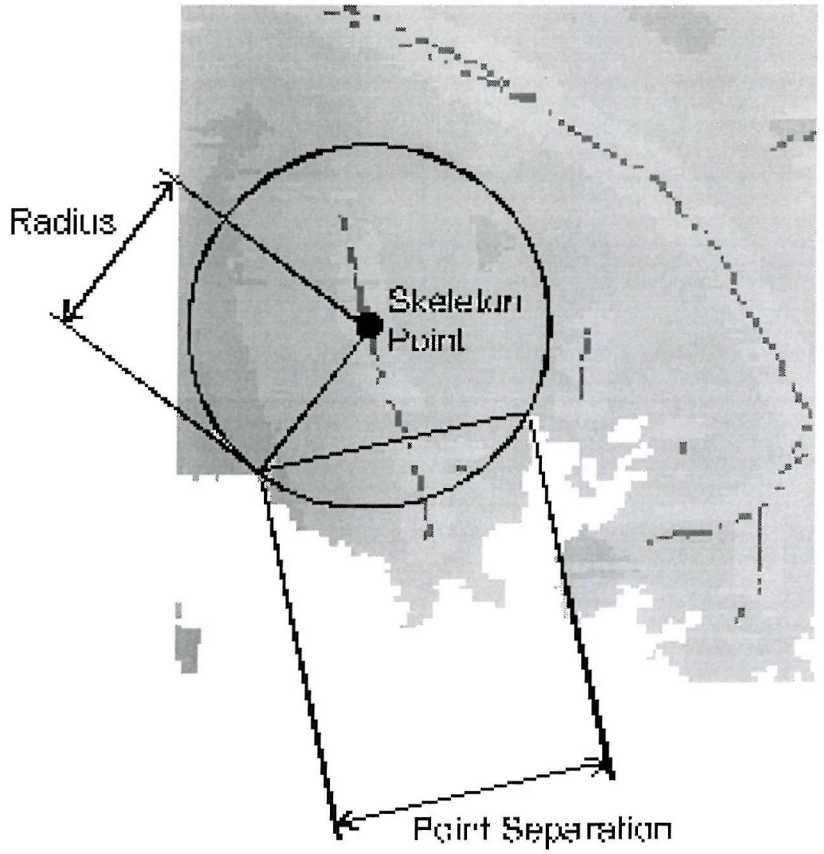


***Figure 6.2:*** *Maximal disk approach for skeleton generation. The circle shown touches two different parts of the cloud edge, the necessary condition for its centre to be lying on the skeleton.*

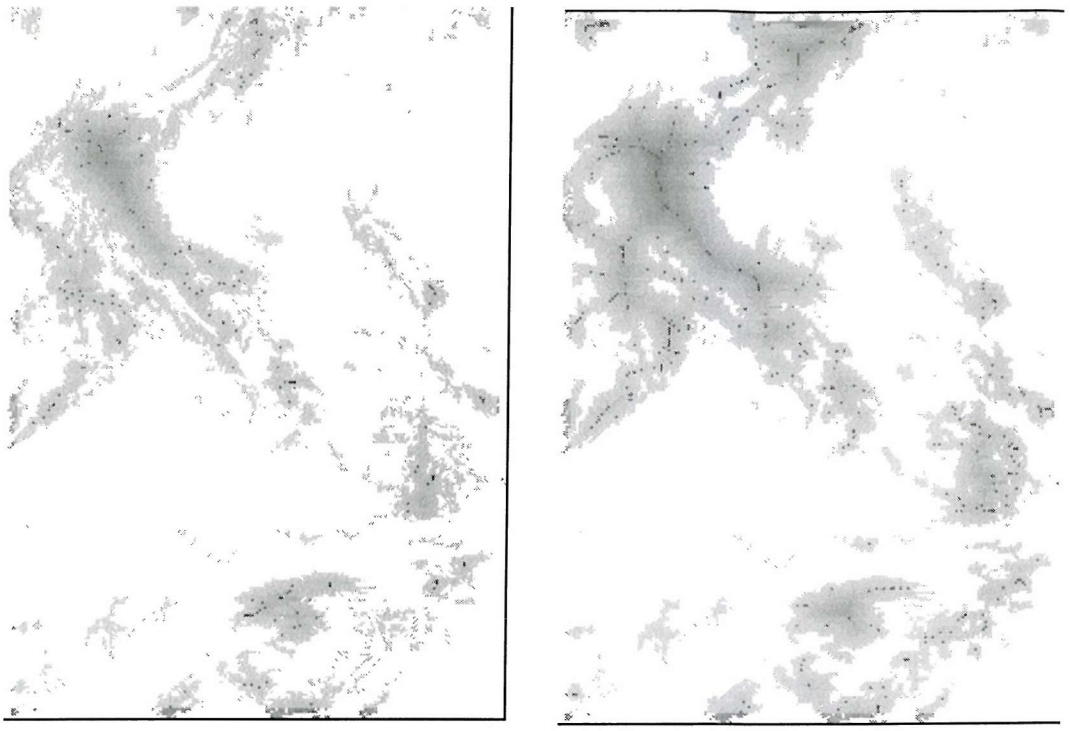

***Figure 6.3:*** *Examples of maximal circle approach for skeleton generation. (a)For a non–coherent cloud core and (b)for the same cloud once grown using a fuzzy growth algorithm (this data has not been pre–filtered using the coherence enhancing tool). The noise in the skeleton from non–coherent data is clearly evident in (a). The data is taken from METEOSAT D2 imagery from 19 August 1997.*

Such pre–smoothing would further improve the skeleton stability, however.

### 6.1.2 Skeletal Matching

Having generated skeletons for whole clouds in each frame of a satellite data sequence, the skeletons can be matched using any line matching technique. In this work, a simple nearest–neighbour approach has been used to match skeletal points in one frame with their nearest skeletal point in the next frame. This works acceptably for sparse skeleton sets, but has a number of problems that can be addressed by suitable adaptations of the analysis. A major problem even for sparse data is that of the so–called *aperture* problem, where a point on a line or arc could potentially match to a number of points on that line / arc in the next timestep if it lies at the centre of curvature of the matching line or the line has many bends locally. This is illustrated more fully in Figure 6.4. For less sparse

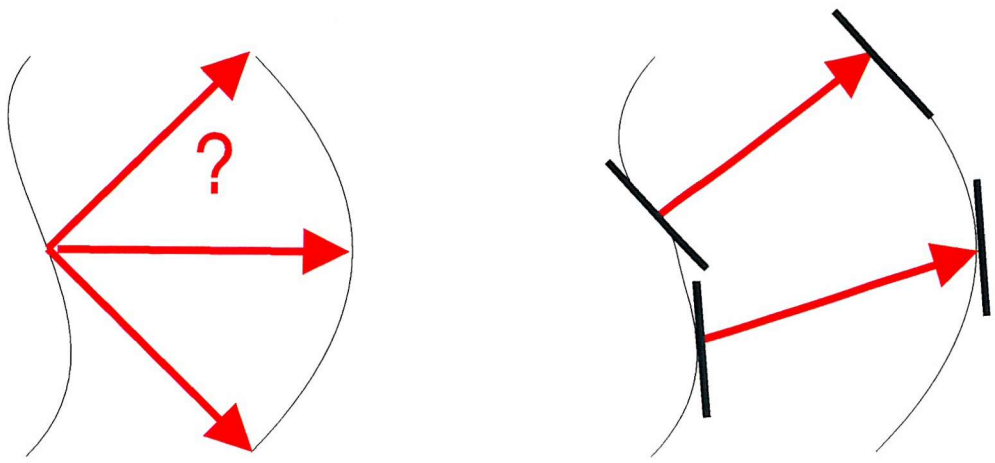


***Figure 6.4:*** *Aperture Problem. The first figure shows the ambiguity of a nearest neighbour match. In this instance, the point on the first arc is on the centre of curvature of the second arc, resulting in an indeterminate number of possible matches. In the typical case there may be at least multiple possible matching points. The second figure shows one approach to minimise this problem, where matches are made between points that have the same local gradient.*

data, a conceptually similar problem is often one of picking the correct match from a number of nearest neighbours on different lines / arcs. A discussion of workarounds to these problems is given later in this chapter.

The algorithms for generating and matching skeletons were coded in C++ and were validated using simple shapes whose skeletons and motion were known. Figure 6.5 provides an example of this validation, where a simple shape has been rotated in the first instance, and grown in the second. The skeletons matched in this data were generated using the maximal sphere approach. Note that the centre of rotation is clearly visible in the first set of skeleton vectors and the growth has been captured in the second.

Figures 6.6 and 6.7 show the application of the skeleton tracking to sequences of cloud data, using two different visualisation techniques. The first image shows the cloud component of the first and last frames of the seven–frame sequence analysed, with the skeletons overlaid, next to the skeleton vector tracks: the vectors for frames 1–6 are shown in red, with the vectors for the last frame pair shown in black. The second image shows the first frame of a sequence in the lower diagonal of the image and the last frame in the upper diagonal, with the

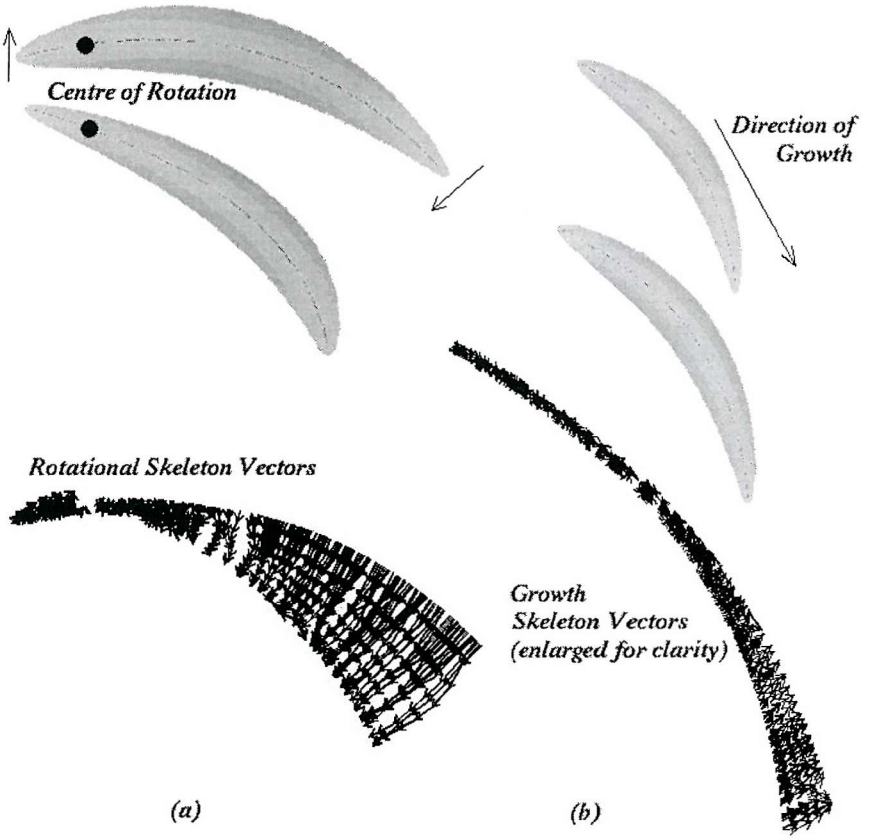


**Figure 6.5:** *Skeleton tracking on a simple shape. The left–hand image triplet (a) shows the first and last frames of a sequence of a rotating simulated cloud shape. The skeleton vectors are shown between the two, clearly indicating the nature and centre of rotation. The right–hand image triplet (b) shows the first and last frames of the simulated shape under growth, again with the resulting skeletal vectors shown between the two frames.*

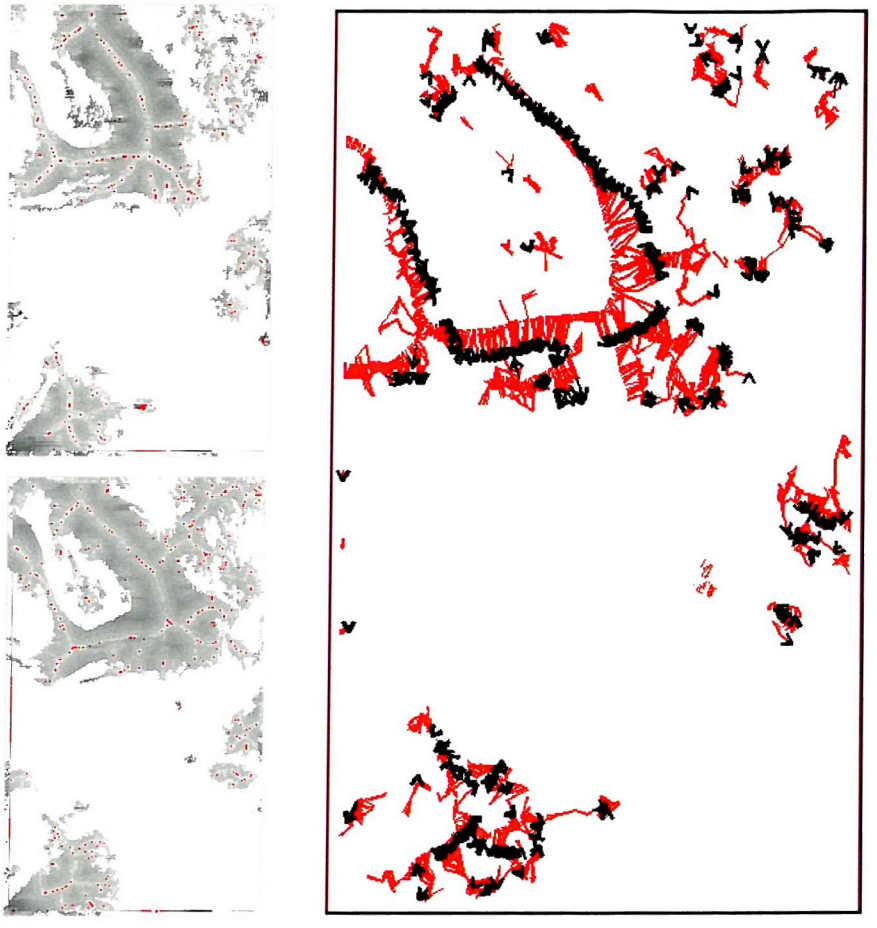

***Figure 6.6:*** *Example of skeleton matches: 1. This figure shows the first and last frames of the extracted cloud objects with skeletons highlighted. The skeletal vectors are shown next to the frames, with the track of vectors across the first six timesteps shown in red and the skeletal track for the last timestep shown in black. The data are from METEOSAT D2 images from 18 February 1996.*

vectors for the whole sequence overlaid on both halves of the image.

The approach has clearly shown its ability to track the different limbs of the weather system and highlight the parts of the weather system that have not moved significantly over the time sequence. It also identifies the rotation points for the limbs, and the relative progression of the different branches on the leading edge of the system can be seen.

There are also a number of places for improvement in both the skeleton generation and matching that can be seen from the images: The lack of homogeneity of the skeleton can be seen clearly, for example, in the black vector heads in the first image in Figure 6.6, and a number of instances of *many–to–one* vector matches

**Figure 6.7:** *Example of skeleton matches: 2. This figure shows an alternative method for displaying the information: the lower diagonal of the image shows the first frame of cloud data and the upper diagonal shows the last frame. The skeleton vector tracks are overlaid across both halves of the image. The data are from METEOSAT D2 images from 18 February 1996.*

can be seen in both images. Despite these problems, the technique has shown the potential for skeletal analysis to describe cloud motion in a new and rich way. A discussion of methods to reduce the errors seen in these results is now provided, however, along with further enhancements of the technique appropriate to cloud analysis.

### 6.1.3 *Alternative algorithms and applications for skeletons in cloud analysis*

A much more robust and stable algorithm for generating skeletons than the maximal disk approach has been suggested by Deseilligny et al [27] using a *veinerisation* approach. There are five stages to this approach, namely:

- Perform an edge–distance transform on a binary representation of the object under analysis (Figure 6.8). In practice this can be achieved by a similar approach to the maximal spheres technique previously described, using the radius of the largest sphere touching an edge as the distance transform.
- Compute the veinerization graph of the distance transform. The details of this are provided by Deseilligny et al., but in principal it provides an indication of the primary directions of slope in the distance transform data. Within this graph is the desired skeleton, plus a number of branches off the skeleton which are not of interest. There are particular problems with digital edge–distance transforms that cause difficulties in generating the veinerization graph. These have been addressed by Deseilligny et al., by careful selection of some arbitrary rules with which to choose the optimal connectivity for ambiguous cases.
- Generate a homotopic extinction function from the graph. This is a measure of the importance of any point on the skeleton, related to points *downstream* of it (its so–called *Zone of Influence*). The simplest analogy is that of a river flowing down the ridges on the veinerization graph: if any point on that river is dammed, the homotopic extinction function for that point is

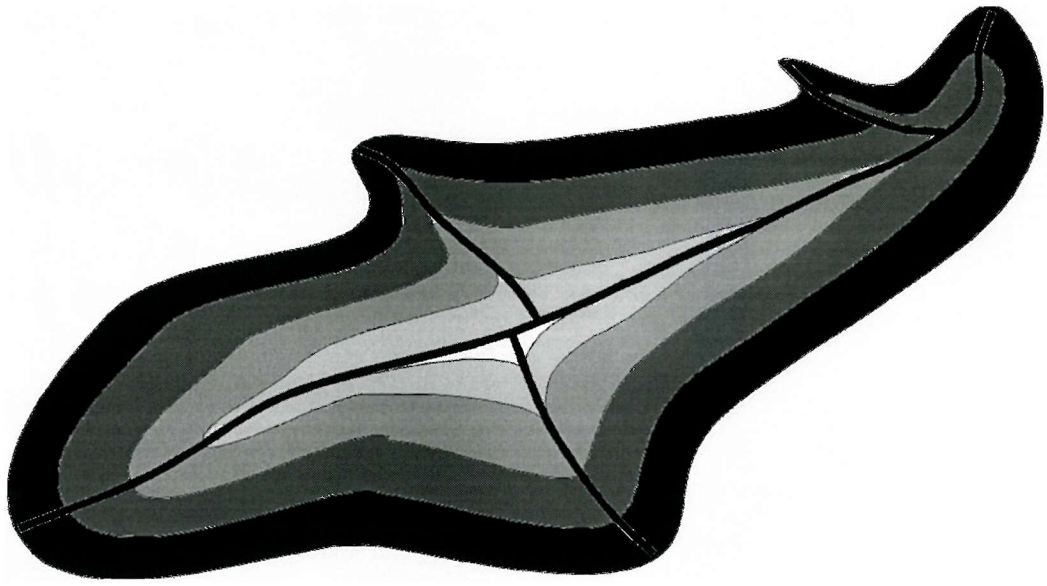

***Figure 6.8:*** *A sketch of an edge–distance transform for an arbitrary shape, with its skeleton overlaid. The greyscale indicates the distance from the edge, with brighter greyscales indicating greater distance. In practice, the greyscale change would be much smoother than the step changes shown: this illustration shows the central protion of the shape lying five distance–units from the edge of the shape, whereas most shapes would be much larger.*

the number of pixels on the veinerization graph *downstream* of the dam point that would also be cut off.

- Select some anchor points for the veinerized graph from the extinction function or based on a combination of criteria, e.g. the local angular variation in veinerization graph. These become in effect the dam points, and their selection dictates the *detail* in the resulting skeleton.

- Prune the veins to include only anchor-point extremities.

(As per Deseilleigny et al [27])

This ensures homotopy in the skeleton, addresses the issues of representation of continuous functions in digital space and is quite adaptable, both in selection of *distance–to–edge* criteria and anchor point selection. An extension of this approach for clouds is to perform a veinerized skeleton analysis on binary slices through every layer of the smoothed greyscale representation of a cloud to build a 3–D skeleton *profile*. Clearly this is computationally expensive, but provides a

rich representation of the spread of the cloud through its height.

To improve on *matching* the generated skeletons over time, a simple mechanism to overcome the aperture problem and many of the non–sparse match ambiguity problems is to match points based *both* on distance and the *gradient of the skeletal arc* through the points to be matched, so that a matching pair of points are close over the timestep but also have the same local arc gradient relative to some global direction, as this rarely changes significantly in any neighbourhood (Figure 6.4). Guichard [45] uses the spatial gradient[2] as a constraint for matching points along a contour or edge. Another mechanism for handling non–sparse data is to look at the topology of the skeletons over time. Where the local topology of a region of skeleton does not change significantly, the nodes of the skeleton can be matched easily and points on the intermediate branches can then be matched proportionally between nodes. Topology changes in the cloud skeleton may themselves be of interest, and worth further investigation. Baroni et al [9] match *curvature* points along edges, giving an example of an alternative type of point of interest that can be matched along edge data. It is important to stress that any such topological / curvature point analysis is critically dependent on the homogeneity and stability of the skeleton generation technique, and would therefore require an approach like that of Deseilligny et al., rather than the maximal disk technique shown earlier.

Finally, it is worth reiterating that the skeleton results shown in this chapter are for data that have not been pre–smoothed using the coherence–enhancing filter discussed in the previous section. This would improve the stability of all the skeletons and skeletal matches shown.

## 6.2 Cloud Edges

Edges of clouds cannot be defined precisely within satellite images. To handle this imprecision, edge *regions* are used to capture both the possible extent within which any binary edge representation could be drawn, and to capture the degree

[2] the gradient of the motion vector relative to the local contour direction

of imprecision of the cloud edge around the cloud. This has been achieved in practice using the output of the cloud core and edge growth object extraction technique described in Section 5.3.2.

The pixels around the cores are associated with the core regions based on the gradient of greyscale tangential to the core edge through the pixel under analysis and the absolute value of the background–normalised greyscale. Having generated a first pass at core associations, an adjustment is made to give local agreement on core association. The adjustment is made by comparing neighbouring pixel characteristics and their degrees of association. Where a neighbourhood has a low core association, a pixel in the neighbourhood with a high core association is suppressed if its greyscale characteristics are not significantly different from the neighbours, and vice versa.

Figure 6.9 shows a cloud core, the core after the edge regions have been grown using the fuzzy growth system and the resulting extracted edges. The edge data clearly show the differences between a *crisp* transition from a cloudy to a non–cloudy region, as is typical of cloud where the wind is blowing parallel to the cloud edge, and a *dispersed* transition where typically there is a wind component crossing the edge of the cloud causing the dispersion.

There is still a significant amount of noise in the edge map, as can be seen from Figure 6.9, but the image data shown have not been subject to any prior smoothing, and the fundamental difference between the *crisp* and *dispersed* edges in the cloud content can clearly be seen: the crisp transitions are identifiable by edges of single–pixel thickness, and the dispersed edges or more correctly edge *regions* extend over a few pixels. Using the edge–preserving coherence–enhancing filter described in Section 5.2.2 would result in less noise in the cloud data, generating less noisy edge maps that would be easier to interpret.

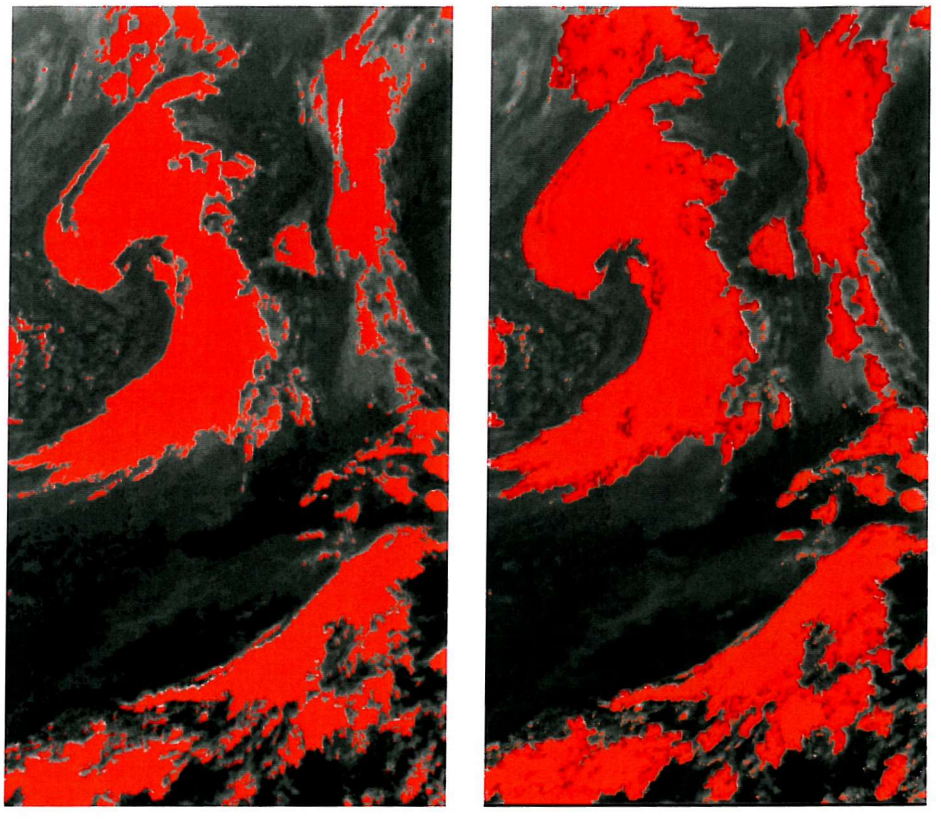

(a) Cloud Core (b) Grown Cloud Region

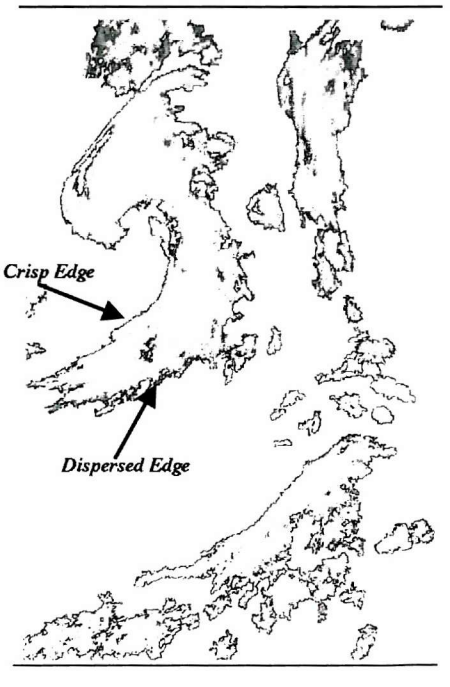


(c) Edges

**Figure 6.9:** *(a) Cloud Core, (b) Grown Edges added and (c) The edge regions with the cores removed. The edge data were grown out of the core regions using a fuzzy system assigning each grown pixel a degree of association with the cloud core. The data shown are from METEOSAT D2 imagery from 27 August 1997.*

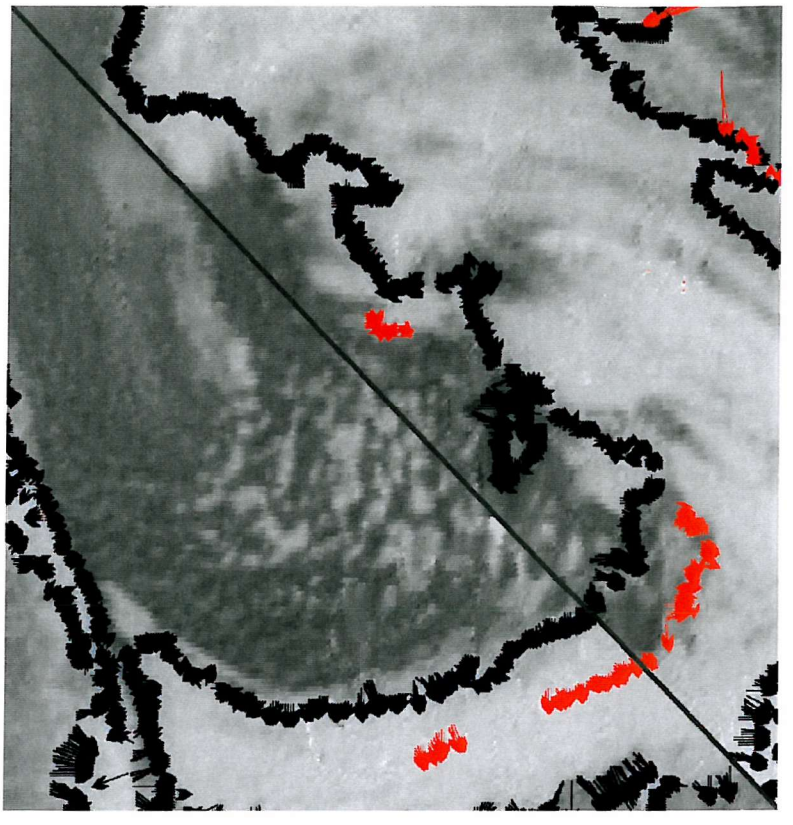

***Figure 6.10:*** *Edge Vector Matches. The lower half of the image shows the first frame of a sequence of METEOSAT D2 imagery from 18 February 1996, and the upper diagonal the seventh frame (three hours later). The black vectors are the cloud edge matches from frames 1–2 and the red vectors from frames 6–7.*

### 6.2.1 Edge Matching

Edges, similarly to skeletons, can be matched using any line matching technique. In this work, the nearest–neighbour approach used for skeletons was adapted slightly to cope with the *regional* nature of the edges analysed (as compared to the single–pixel thickness of the corresponding skeletons). Again, this works acceptably for sparse sets of edges (indeed, edges are typically easier to handle than skeletons due to the lower number of branches requiring matching). The ability of the approach to capture cloud motion has been demonstrated in Figure 6.10. The same caveats for matching performance are applicable to these results as were described earlier for the skeletal data. Again the ability to produce *cleaner* edge data using presmoothed clouds, as discussed at the end of the last chapter, would clearly also impact the quality of edge matches.

The results from this chapter were presented at the First AMS conference on Artificial Intelligence, as detailed in Newland et al[76], and in Lewis et al[4].

# Part III

# COMMENT AND CONCLUSIONS

# 7. DISCUSSION

The initial study in this thesis used a fuzzy system to segment spatial regions in an image sequence based on the suitability of different motion analysis tools. This proved the possibility for such segmentation. The ideas surrounding the work identified the relevance of applying different motion analyses to the same data to analyse different aspects of the motion therein. The fuzzy system was applied to segment the data into regions suitable for three fundamentally different types of motion analysis, namely textural analyses, frontal or extended moving body analyses and small object matching. Simplifying assumptions were made for determining suitability criteria for each analysis. This provided an understanding of the nature of cloud motion in satellite images however, and significantly highlighted two problem areas:

- An analysis of cloud motion at the finest scale possible does not scale up to provide knowledge of the motion at larger scales.
- External causes of cloud motion at different scales, whilst currently attributed to the imprecise concept of *wind* relate to very different types of phenomena across the scales so that *wind* at synoptic scale is totally unrelated to some wind eddy at a local scale.

The new parameters developed for this research for capturing the structure of cloud at the scale of a whole cloud object have been shown to provide significantly different types of information to the current textural analyses. This has led to a new way of treating motion in satellite data, from which a better understanding of the dynamics and their relationship to scale can be identified.

## 7.1 Combining Motion Analyses

Another benefit from the new motion analyses generated comes from comparing the vectors from matching each different parameter. Analysing the vectors together provides a very different picture to that of any one of the vector sets on its own. Figure 7.1 gives an example of more than one motion analysis applied to a frontal weather system. The front was moving to the south–east. The local wind effect in the frontal region, passing over the cloud, passed *along* the front, to the north–east. A texture–based analysis alone gives a confusing picture of the dynamics. The cross–correlation vectors shown in Figure 7.1 mostly cover the core of the cloudy region, although some of the vectors near the edge of the cloud illustrate the confusion in dynamics from using this parameter alone, where they track the motion of the cloud edge. The edges of the cloud are easy to track due to the strong greyscale gradient at the edge, but the motion of the edges is very different to the motion of the cloud peaks within the front, which are blown along with the local wind component. By overlaying the skeleton–derived vectors, the two causes of cloud motion are much clearer, and the two different components of the dynamic can be recognised as different. As a result of this, analyses requiring knowledge of local–scale wind effects can be directed towards the texture vectors within the cloud boundaries. Similarly, motion analyses concentrating on synoptic scale phenomena, or interested in the development of the weather system as a whole, would be passed the skeleton and any edge vectors.

The difference between the motion captured by the skeleton and edge vectors is similarly significant. Whilst they are at a different scale to the current cross-correlation approaches, they are themselves in orthogonal spaces, so the motion captured by analysing the evolution of a cloud skeleton differs from the motion of the same cloud's edges.

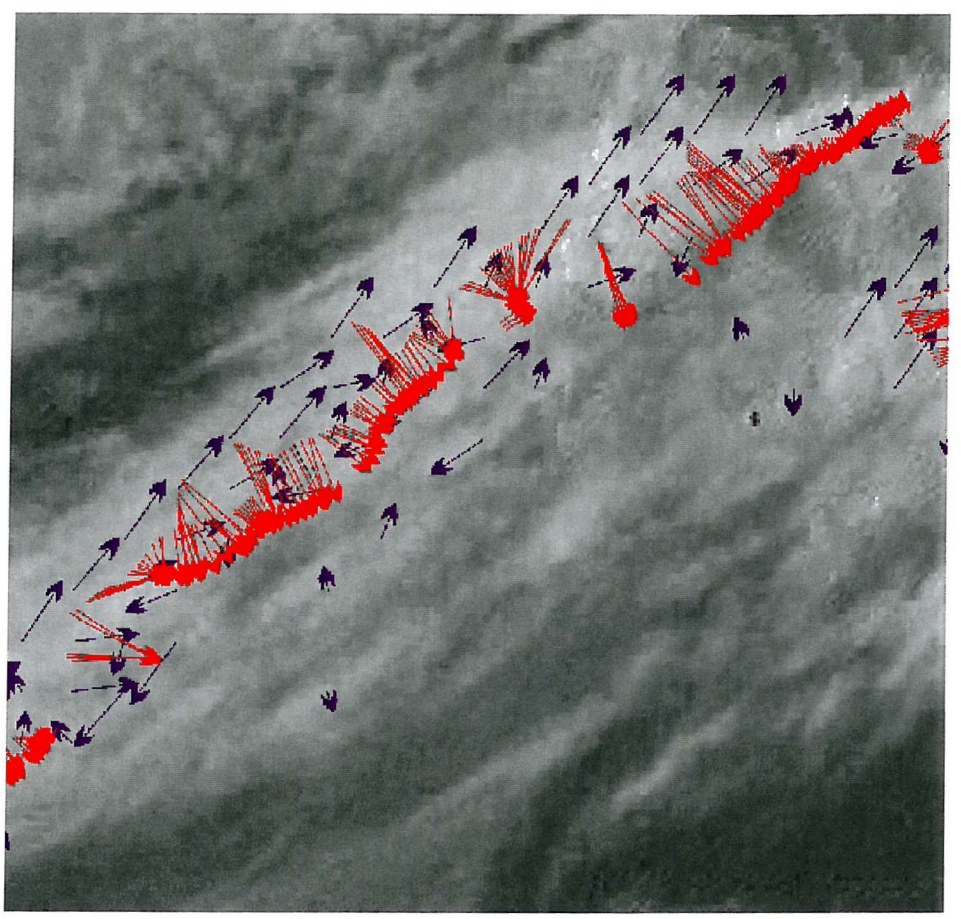

**Figure 7.1:** *Two vector types overlaid. The red vectors represent skeletal motion and indicate the transition of the front in the image in a south–easterly direction. The blue vectors represent texture region motion and indicate the south–westerly wind.*

## 7.2 Future Work

Operational trials of the analyses applied in this thesis would provide quantitative measures of their possible impact to forecasting and modelling. A necessary first step for this would be to address the robustness of the algorithms. In particular, the algorithms applied would require greater degrees of error and validity checking and some optimisation to reduce computational overhead for such an implementation, and a rigorous comparison between a suitable cross–section of algorithms that provide the types of parameter used or identified in this thesis would be recommended. Applying the techniques to data prior to having national borders and markers added and not subject to any compression techniques is similarly linked to a larger scale test of the approach. The computational cost of the algorithms applied in this thesis has been small enough however to prove the feasibility of their operational application: whilst some of the results took more than a potential half–hourly operational cycle to produce, code optimisations and hardware enhancements[1] would be able to reduce the results cycle to within the necessary range.

There would also be much potential in a more detailed study comparing and contrasting the different types of motion vector found, and automating the comparison of different data. Other types of parameter and further different scales of motion could similarly be studied (e.g. the preliminary work into the use of slices of greyscale data for providing another level of shape matching, matching weather systems etc., and identifying smaller scale features to match). It is worth noting that by identifying and subtracting any weather system motion from all the vectors, internal cloud dynamics processes are likely to become clearer, since internal cloud dynamics are driven by flow–relative atmospheric motion.

Multispectral analyses and incorporating more data into the analyses (e.g. height information) would again provide more meteorological context for cloud extraction, smoothing and parameterisation, as well as aiding in parameter tracking

[1] The most powerful processing used during the course of this thesis was a 150MHz computer with 128Mb of RAM, running Windows NT.

and vector interpretation. Currently, visible, infrared and water vapour motion vectors are all used as indicative of the windfield. Analysing each using the rich descriptions described in this thesis will again provide more detailed characteristics of the motion observed in each channel of data. It is recognised that water vapour motion is significantly different to visible and infrared cloud motion, both due to the fact that the motion represents a deep layer mean and that the structures being followed are less coherent. A comparison of the large–scale motion of water–vapour structures could therefore reasonably be expected to differ slightly from weather system dynamics as captured from cloud structure motion. Any such differences may provide insights into weather system lifecycles, where the difference between motions captures new information. CLOUDSAT data should also soon be available, providing richer descriptions of cloud cross–sections and verification data for cloud structure descriptions captured in current and future cloud shape parameters. Tieing in radar data to identify where the rainfall is in a cloud body may again correlate with cloud shape changes.

Determining the scale–dependence of each vector, i.e. over what range of scales the vector is indicative of some motion, would have many applications, for example for assessing whether point wind data at a given location within a cloud are valid for analysing the synoptic scale motion at that point (which would be true under *very* steady atmospheric conditions *only.*). An automatic scheme for assessing this *vagueness* for vectors, and also for all other current wind data and validation sources (e.g. radiosondes, wind radar etc) would allow models to use the vagueness measures when accepting wind data sources, as well as greatly assisting human operators in interpreting atmospheric motion data at different scales.

Having obtained a much richer set of motion types with which to analyse cloud motion, it would be useful to revisit the initial work looking at segmenting imagery based on the applicability of different motion techniques. Having a better understanding of how atmospheric motion acts at different scales may allow the approach to provide an indication of where in the imagery is suitable for any particular scale of analysis. If there are no features suitable for analysis of local

scale motion in a region, some measure of this should be possible.

Similarly, skeletal analyses could be enhanced by making use of the *skeletal radii*[2] at each point along a skeleton as well as the skeleton itself. The variation in cloud width along the skeleton and the change in this variation should give a much richer description again of where a cloud system is developing. Similarly, skeleton–relative motion analyses and skeleton–relative edge type analyses would both be interesting to study further.

Further development of the analysis could provide novel validation techniques for the modelling community. For example, the new motion vectors could be used for checking predicted radiance images from 3– or 4–D variational assimilation techniques, weather system motion information, local scale wind information and cloud lifecycle knowledge.

The use of fuzzy systems in this work has shown the potential of the approach for prototyping image segmentation algorithms. To apply these techniques to large sets of data, it would be most sensible to allow the rules to adapt themselves based on feedback on past performance. This would require suitable performance measures to be identified. In the case of fuzzy segmentation based on motion analysis applicability, initial feedback could be provided by using a dense set of vectors of all types from which an expert could identify where each vector set has provided some valid analysis.

The analyses would also be suitable for other non–rigid motion problems where the motion can be described at multiple scales, e.g. analysis of ocean features or Computational Fluid Dynamics data. In addition, the coherence–enhancing smoothing technique introduced could be used for data preprocessing for video data compression.

[2] The radii of the maximal disks, or the distance to the nearest edge, for each point on the skeleton.

# 8. CONCLUSIONS

The need for global wind information is widely recognised as critical for most domains of meteorology, from modelling and climatology to forecasting. Whilst cloud motion in satellite image sequences has been used as an indicator of wind motion since the start of the geostationary meteorological satellite programs, the limitations of current operational approaches have become increasingly apparent in light of improvements in the user communities. In particular the assumption that cloud acts as a passive tracer for the wind, and the generic use of the term *wind* for atmospheric motion at a very broad range of scales has caused problems for satellite–based analyses. The lack of any meteorological context in the current cross–correlation based motion analyses, and the difficulties of validating identified cloud motion using validation data of a different scale[1] has hindered the development of solutions to overcome these problems.

A novel approach for analysing cloud motion from a *cloud object* perspective has been introduced in this thesis, providing a new starting point from which to determine global wind data. The approach itself differs from the traditional *texture-based* analyses by focussing on the cloud content in the imagery, and applying *multiple* motion analyses to provide a much richer description of the motion. This has allowed the standard assumption of cloud passivity as a wind tracer to be removed, and other components of cloud dynamics, other than the underlying windfield, have been identified in the results presented. By changing the perspective of the analysis of satellite image sequences from one purely of determining global wind data to one of providing a rich representation of the

[1] Weather balloon measurements collected over tens of metres used for validating satellite–derived winds collected over hundreds of kilometers

dynamics of the cloud in the imagery *from which* any wind component can be identified, this thesis creates a new area for the community to research to identify a number of new or better meteorological satellite products.

In order to apply multiple motion analyses to the cloud content of the satellite image sequences, new parameterisations of cloud have been developed. An adaptation of the rolling-ball algorithm has been developed to provide a coherence-enhancing, edge-preserving image filter, to improve parameter extraction from the raw cloud data. A novel use of morphological skeleton algorithms has been generated for analysing the *shape* of the cloud content and its development over time. Similarly, a fuzzy system has been applied to analyse the nature of the edges of the cloud, to provide better identification of *crisp* and *fuzzy* edges than edge gradient alone. The results have shown the ability of these parameters to capture the larger–scale motion displayed by cloud systems, and an indication of where clouds are being dissipated by the wind flow and where the wind is parallel with the cloud edge (which is indicative of jet flow regions, for example).

This mixture of tracking methods has provided a much richer description of the cloud dynamics. By comparing and contrasting the different vectors, it has been shown that the cause of the cloud motion captured by a given motion vector can be identified. The motion analysis algorithms described in this thesis provide the framework within which such a measure of motion causality could be developed and also show the types of motion necessary for making such discrimination. The methods introduced have been applied to a number of different sets of satellite data as illustrated by the examples shown, and have been shown to provide stable results in each of the meteorological conditions captured. The approaches are therefore suitable for larger–scale studies.

The five key areas where improvements to the approach could be focussed are:

1. Large–scale testing on a much larger cross–section of meteorological situations.

2. Wider comparison of motion analysis outputs to identify the underlying

meteorological characteristics of each type of motion analysis.

3. Applying the techniques to other channels of data and comparing the analyses across different spectra.

4. Providing learning or feedback to the fuzzy systems used.

5. Addressing the initial problem of fuzzy segmentation based on motion type in light of the subsequent analyses.

The work has principally demonstrated benefit to the meteorological community in three regards: the new parameters used for describing the dynamics of cloud at a synoptic scale, which capture motion unassociated with the underlying wind-field, have application both for weather system tracking and analysis and cloud lifecycle analysis. In particular, the use of skeletons may provide a much richer analysis of vorticity than is currently available. The use of multiple motion analyses provides better identification of the suitability of cloud motion vectors for describing the wind or any other motion type captured, and the use of a multi–scale analysis has shown the breadth of phenomena currently described under the umbrella term of *wind*, as well as providing a possible approach for breaking down the definition, and comparing motion types across this breadth of scale. Finally, a new method for identifying possible jet flow locations based on the nature of the cloud edge has resulted from the edge analysis of cloud structures: jet flow regions are unreliably reported at present.

Future development of the approach could provide novel validation techniques for the modelling community. For example, checking predicted radiance images from 3– or 4–D variational assimilation techniques, weather system motion information, local scale wind information and cloud lifecycle knowledge are all possible validation outputs of the approach. Similarly, the approach offers a means to determine the degree to which any motion at one scale can be generalised across other scales. The work would also be suitable for other non–rigid motion analysis problems where the motion can be described at multiple scales, e.g. analysis of ocean features or Computational Fluid Dynamics data. In addition,

the coherence–enhancing smoothing technique introduced could be used for data preprocessing for video data compression.

This thesis has therefore provided a description of a new object–based approach for analysing cloud dynamics in sequences of satellite imagery, which has been shown to provide a much richer representation of motion than is available using current approaches to satellite image analysis. New parametric representations of cloud have been developed within this approach to show how cloud motion can be captured in a number of different ways and at different scales. The parameters in themselves would provide operational benefits over current analyses, however the approach introduces the notion of multiple motion analyses for cloud analysis providing many different types of motion information, which allows the possibility for other motion capture techniques to be developed and contrasted with those presented here. The work therefore advances the field of cloud motion and wind analysis from satellite data and provides a new perspective on satellite motion analysis for many other fields of meteorology.

# A. OBJECT GROWTH FUZZY RULES

Table A.1: Fuzzy Rule Base for Cloud Growth

ENTIRE SYSTEM FUZZY RULES REPORT

INTERNAL NETWORK 1 WITH 1 SUBNETWORK

SubNetwork1 with 3 Input Variables and the 75 following Fuzzy Rules

| IF Relative Greyscale is | AND Absolute Greyscale is | AND Greyscale Gradient is | THEN Cloud Degree is | (Confidence) |
|---|---|---|---|---|
| Not Cloud | Not Cloud | Cloud Edge | Not Cloud | (1.00) |
| Close to cloud edge | Not Cloud | Cloud Edge | Not Cloud | (1.00) |
| Cloud Fringe | Not Cloud | Cloud Edge | Not Cloud | (1.00) |
| Cloud | Not Cloud | Cloud Edge | Not Cloud | (1.00) |
| Definite Cloud | Not Cloud | Cloud Edge | Not Cloud | (1.00) |
| Not Cloud | Lower Cloud | Cloud Edge | Not Cloud | (1.00) |
| Close to cloud edge | Lower Cloud | Cloud Edge | Not Cloud | (1.00) |
| Cloud Fringe | Lower Cloud | Cloud Edge | Not Cloud | (0.80) |
| Cloud | Lower Cloud | Cloud Edge | Not Cloud | (0.30) |
| Definite Cloud | Lower Cloud | Cloud Edge | Not Cloud | (0.20) |
| Not Cloud | Cloud | Cloud Edge | Not Cloud | (1.00) |
| Close to cloud edge | Cloud | Cloud Edge | Not Cloud | (0.62) |
| Cloud Fringe | Cloud | Cloud Edge | Not Cloud | (0.58) |
| Cloud | Cloud | Cloud Edge | Not Cloud | (0.25) |
| Definite Cloud | Cloud | Cloud Edge | Not Cloud | (0.18) |
| Not Cloud | Upper Cloud | Cloud Edge | Not Cloud | (0.60) |
| Close to cloud edge | Upper Cloud | Cloud Edge | Not Cloud | (0.14) |
| Cloud Fringe | Upper Cloud | Cloud Edge | Not Cloud | (0.14) |

*continued on next page*

*continued from previous page*

| IF Relative Greyscale is | AND Absolute Greyscale is | AND Greyscale Gradient is | THEN Cloud Membership is | (Confidence) |
|---|---|---|---|---|
| Cloud | Upper Cloud | Cloud Edge | Not Cloud | (0.14) |
| Definite Cloud | Upper Cloud | Cloud Edge | Cloud | (1.00) |
| Not Cloud | Definite Cloud | Cloud Edge | Cloud | (1.00) |
| Close to cloud edge | Definite Cloud | Cloud Edge | Cloud | (1.00) |
| Cloud Fringe | Definite Cloud | Cloud Edge | Cloud | (1.00) |
| Cloud | Definite Cloud | Cloud Edge | Cloud | (1.00) |
| Definite Cloud | Definite Cloud | Cloud Edge | Cloud | (1.00) |
| Not Cloud | Not Cloud | Acceptable Gradient | Not Cloud | (1.00) |
| Close to cloud edge | Not Cloud | Acceptable Gradient | Not Cloud | (1.00) |
| Cloud Fringe | Not Cloud | Acceptable Gradient | Not Cloud | (1.00) |
| Cloud | Not Cloud | Acceptable Gradient | Not Cloud | (1.00) |
| Definite Cloud | Not Cloud | Acceptable Gradient | Not Cloud | (1.00) |
| Not Cloud | Lower Cloud | Acceptable Gradient | Not Cloud | (1.00) |
| Close to cloud edge | Lower Cloud | Acceptable Gradient | Not Cloud | (0.80) |
| Cloud Fringe | Lower Cloud | Acceptable Gradient | Not Cloud | (0.70) |
| Cloud | Lower Cloud | Acceptable Gradient | Not Cloud | (0.20) |
| Definite Cloud | Lower Cloud | Acceptable Gradient | Not Cloud | (0.10) |
| Not Cloud | Cloud | Acceptable Gradient | Not Cloud | (1.00) |
| Close to cloud edge | Cloud | Acceptable Gradient | Not Cloud | (0.50) |
| Cloud Fringe | Cloud | Acceptable Gradient | Not Cloud | (0.48) |
| Cloud | Cloud | Acceptable Gradient | Not Cloud | (0.15) |
| Definite Cloud | Cloud | Acceptable Gradient | Not Cloud | (0.10) |
| Not Cloud | Upper Cloud | Acceptable Gradient | Not Cloud | (0.50) |
| Close to cloud edge | Upper Cloud | Acceptable Gradient | Not Cloud | (0.08) |
| Cloud Fringe | Upper Cloud | Acceptable Gradient | Not Cloud | (0.04) |
| Cloud | Upper Cloud | Acceptable Gradient | Not Cloud | (0.02) |
| Definite Cloud | Upper Cloud | Acceptable Gradient | Not Cloud | (0.02) |
| Not Cloud | Definite Cloud | Acceptable Gradient | Cloud | (1.00) |

*continued on next page*

*continued from previous page*

| IF Relative Greyscale is | AND Absolute Greyscale is | AND Greyscale Gradient is | THEN Cloud Membership is | (Confidence) |
|---|---|---|---|---|
| Close to cloud edge | Definite Cloud | Acceptable Gradient | Cloud | (1.00) |
| Cloud Fringe | Definite Cloud | Acceptable Gradient | Cloud | (1.00) |
| Cloud | Definite Cloud | Acceptable Gradient | Cloud | (1.00) |
| Definite Cloud | Definite Cloud | Acceptable Gradient | Cloud | (1.00) |
| Not Cloud | Not Cloud | Cloud | Not Cloud | (1.00) |
| Close to cloud edge | Not Cloud | Cloud | Not Cloud | (1.00) |
| Cloud Fringe | Not Cloud | Cloud | Not Cloud | (1.00) |
| Cloud | NotCloud | Cloud | Not Cloud | (1.00) |
| Definite Cloud | Not Cloud | Cloud | Not Cloud | (1.00) |
| Not Cloud | Lower Cloud | Cloud | Not Cloud | (1.00) |
| Close to cloud edge | Lower Cloud | Cloud | Not Cloud | (0.70) |
| Cloud Fringe | Lower Cloud | Cloud | Not Cloud | (0.60) |
| Cloud | Lower Cloud | Cloud | Not Cloud | (0.10) |
| Definite Cloud | Lower Cloud | Cloud | Not Cloud | (0.05) |
| Not Cloud | Cloud | Cloud | Not Cloud | (0.73) |
| Close to cloud edge | Cloud | Cloud | Not Cloud | (0.45) |
| Cloud Fringe | Cloud | Cloud | Not Cloud | (0.44) |
| Cloud | Cloud | Cloud | Not Cloud | (0.05) |
| Definite Cloud | Cloud | Cloud | Not Cloud | (0.03) |
| Not Cloud | Upper Cloud | Cloud | Not Cloud | (0.40) |
| Close to cloud edge | Upper Cloud | Cloud | Not Cloud | (0.06) |
| Cloud Fringe | Upper Cloud | Cloud | Not Cloud | (0.05) |
| Cloud | Upper Cloud | Cloud | Not Cloud | (0.04) |
| Definite Cloud | Upper Cloud | Cloud | Cloud | (1.00) |
| Not Cloud | Definite Cloud | Cloud | Cloud | (1.00) |
| Close to cloud edge | Definite Cloud | Cloud | Cloud | (1.00) |
| Cloud Fringe | Definite Cloud | Cloud | Cloud | (1.00) |
| Cloud | Definite Cloud | Cloud | Cloud | (1.00) |

*continued on next page*

| *continued from previous page* | | | | |
|---|---|---|---|---|
| IF Relative Greyscale is | AND Absolute Greyscale is | AND Greyscale Gradient is | THEN Cloud Membership is | (Confidence) |
| Definite Cloud | Definite Cloud | Cloud | Cloud | (1.00) |

# B. IMAGE FORMATS AND COMPRESSION ARTEFACTS

Figure B.1(a) shows an example of the publicly disseminated WEFAX data that has been preprocessed in Darmstadt to correct the radiance values and add coastline and lat–lon check marks. The image looks significantly different to the preprocessed image shown in Figure B.1(b), which has not been subjected to the radiance correction. Whilst the radiance correction is necessary, the difference in image quality is of equal concern when analysing the imagery. Figure B.2 compares the shape of the surface for a small window of the data, and clearly shows some artefacts in the publicly disseminated data that are not present in the raw imagery. These are most probably due to the storage mechanism for the publicly available images. Figure B.3 compares the format for the latest image available at Nottingham's METEOSAT archive site, stored in GIF format with the archived data in JPEG format. The difference is again most noticeable in 3–D projection, as shown in Figure B.4. Clearly the use of radiance–corrected data prior to national border addition and not subject to any data compression techniques is the ideal source of data for meteorological satellite image analysis. Practical constraints often result in the necessitated use of the degraded images shown, however.

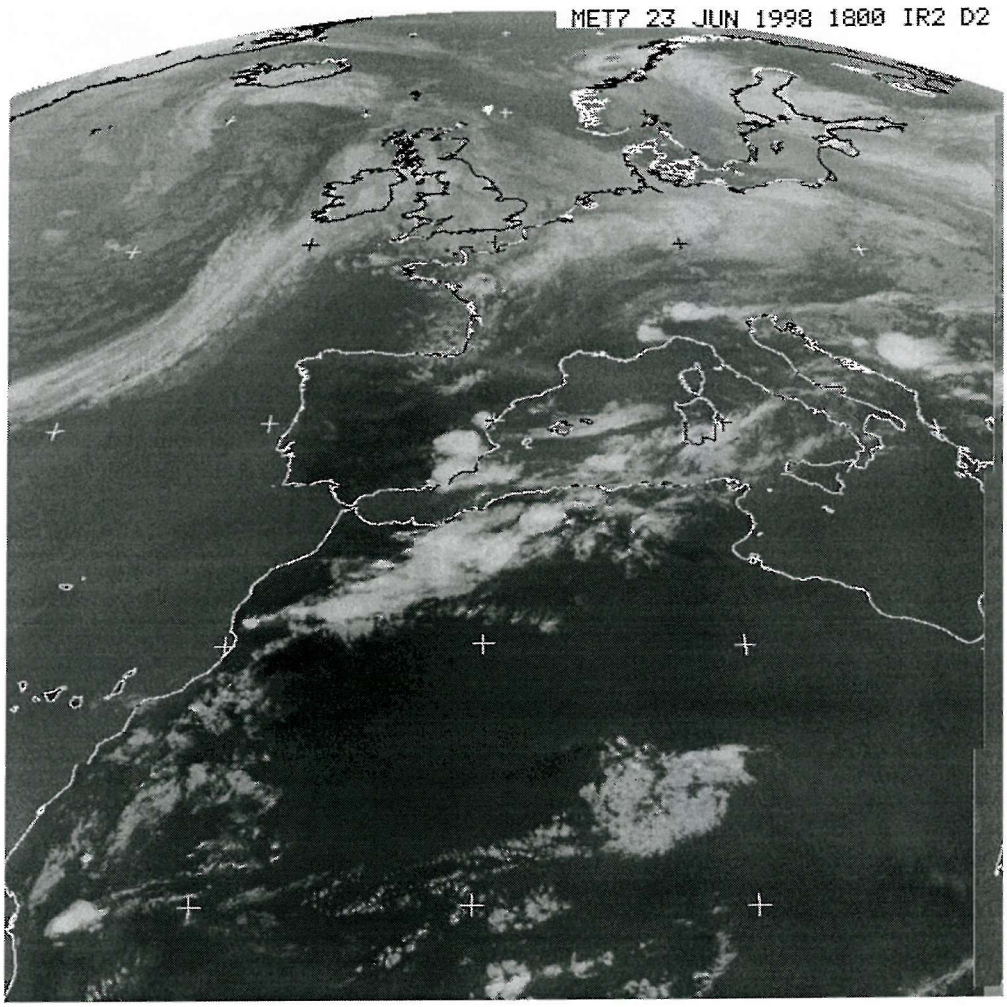


(a) WEFAX data publicly available, transmitted from EUMETSAT

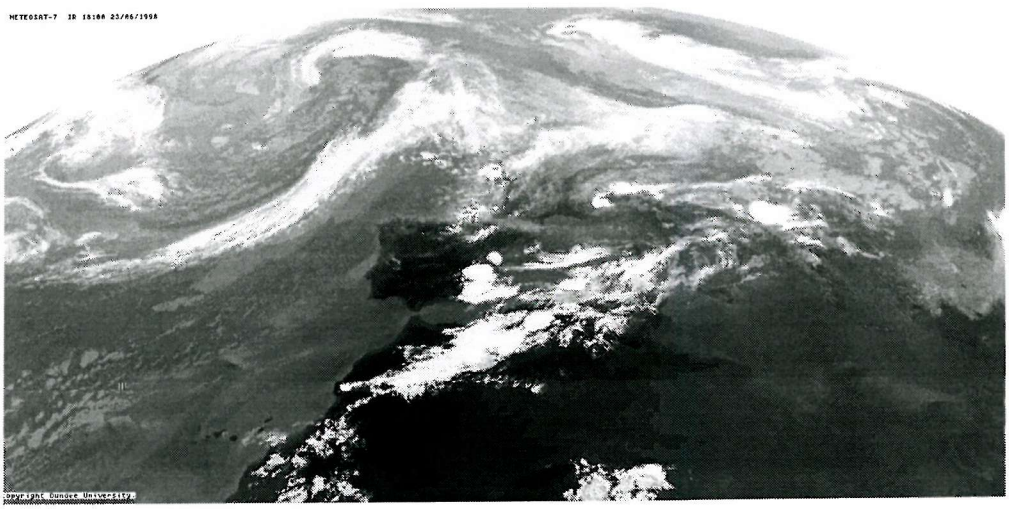

(b) RAW data downloaded at EUMETSAT prior to public dissemination

***Figure B.1:*** *Comparison of raw and retransmitted METEOSAT D2 data from 1800 on 23 June 1998*

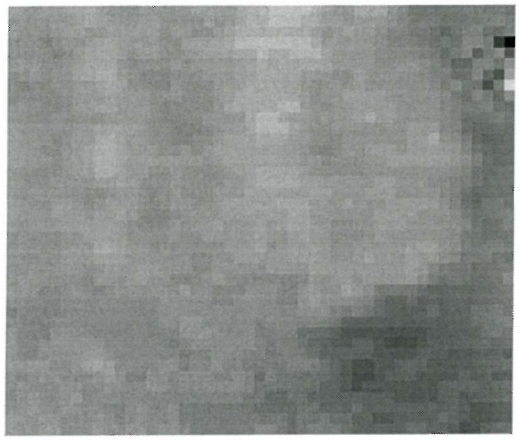

(a) WEFAX data: projected region

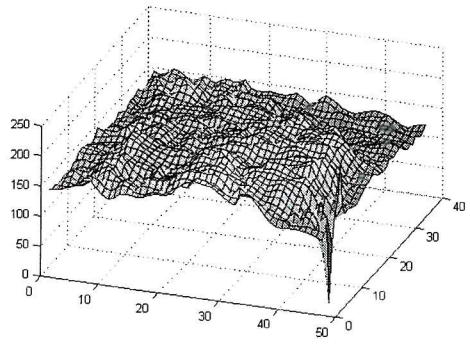


(b) WEFAX data: projection

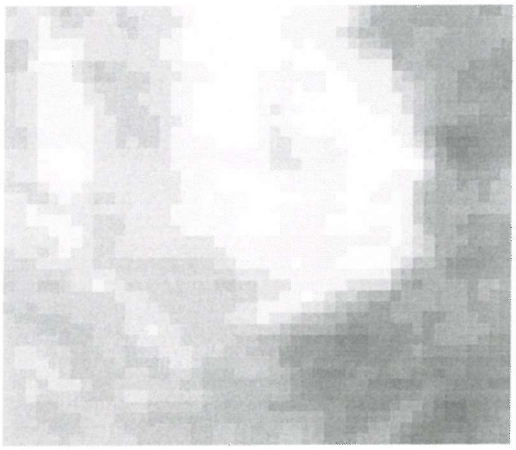

(c) RAW data: projected region

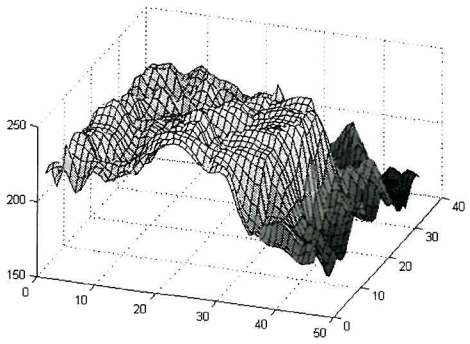


(d) RAW data: projection

***Figure B.2:*** *Comparison of projected raw and retransmitted data*

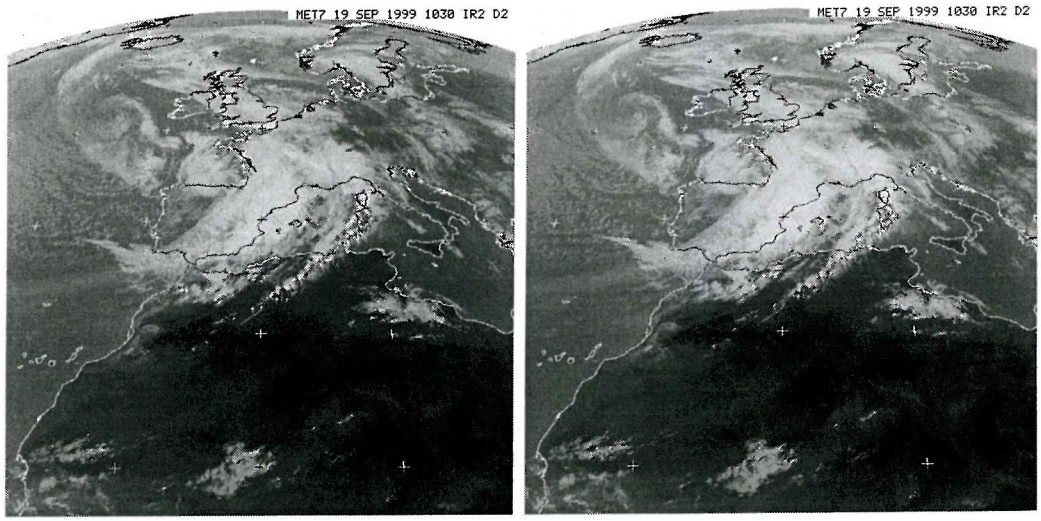


(a) Image in GIF format (b) Image in JPEG format

***Figure B.3:*** *Comparison of GIF and JPEG storage formats. Data are METEOSAT D2 imagery from September 19 1999 at 1030GMT.*

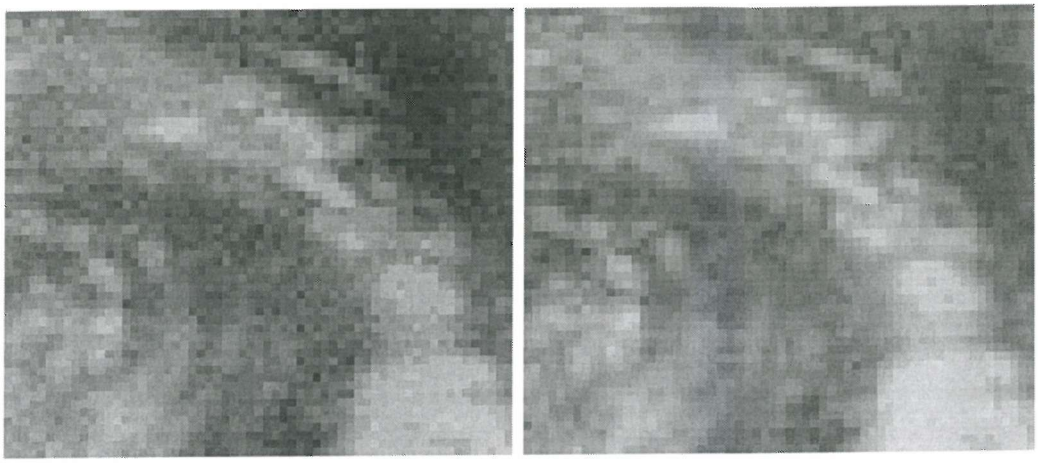

(a) GIF: projected region

(b) JPEG: projected region

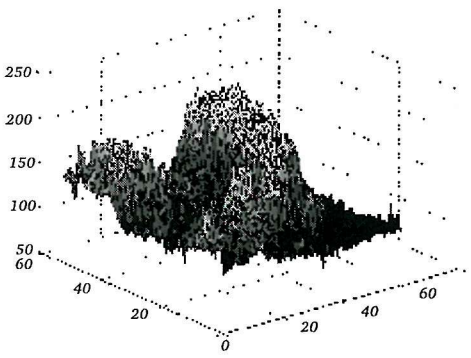


(c) GIF: projection

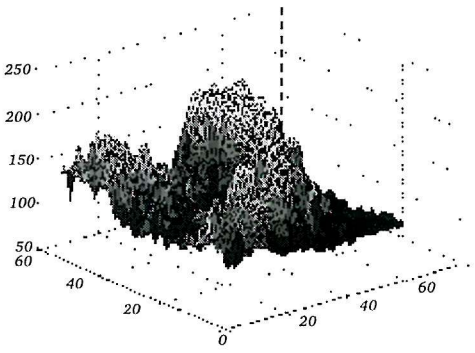


(d) JPEG: projection

***Figure B.4:*** *Comparison of projected GIF and JPEG data*

# C. MORPHOLOGICAL IMAGE PROCESSING

For cloud object analysis to be quantitative, it must follow certain constraints. The first manifests itself due to the fact that the cloud is digitised, and therefore its location is not certain, and must be independent of a one–pixel translation in any direction. The second relates to the fact that different cloud structures of different sizes should be smoothed in the same way as the vagueness in the cloud shape is arguably scale–invariant. The third relates to local knowledge. We only know about the cloud developments within our field of view from which we may wish to make some comment about the meteorology beyond our field of view. The fourth relates to partitioning of space into two or more known regions and a boundary which always exists and is always unknown, e.g. between cloud / non–cloud / edge regions or cloud details that can be distinguished, those that cannot and those inbetween. There are four underlying principles of morphology which every morphological transformation $\Psi$ must satisfy (Table C.1) which map onto these quantitative analysis requirements.

1. Compatibility under translation.

$$\Psi^O(X_h) = [(\Psi^{-h}(X)]_{+h} \tag{C.1}$$

i.e. applying $\Psi^O$ to $X^h$ is equivalent to applying $\Psi^{-h}$ to X then shifting the result by vector h. $\Psi^O$ means apply $\Psi$ with respect to an origin O. NB *invariance*under translation means the origin is irrelevant to $\Psi$, i.e. $\Psi(X_h) = [\Psi(X)]_h$

2. Compatibility under change of scale.

$$\Psi_\lambda(X) = \lambda\Psi\left(X\lambda\right) \tag{C.2}$$

We have a family of transformations, $\Psi_\lambda$. The actual form of the relationship is important to note, as any family of $\Psi_\lambda$ will not suffice. NB *independence*with respect to image magnification implies $\Psi(\lambda X) = \lambda\Psi(X), \lambda > 0$

3. Local Knowledge.

$$\forall boundedZ', \exists boundedZ s.t.[\Psi(X \cap Z)] \cap Z' = \Psi(X) \cap Z' \tag{C.3}$$

i.e. for a bounded set $Z'$ in which we want to know $\Psi(X)$, we can find a bounded set Z in which the knowledge of X is sufficient to locally (within $Z'$) perform the transformation

4. Semi-continuity.

***Table C.1:*** *Underlying principles of morphology (Taken from Serra [90]).*

# REFERENCES


[1] J Aggarwal and N Nandhakumar. On the consequences of motion from sequences of images–a review. *Proceedings of the IEEE*, 76(8):917–935, August 1988.

[2] P Andrews. The development of an operational variational data analysis scheme at the ukmo. NWP on-line Scientific Note 5, Meteorological Office, http://www.meto.govt.uk/sec5/NWP/NWP_ScienceNotes/No5/No5.html, 1997.

[3] C Arcelli and G Sanniti di Baja. A width-independent fast thinning algorithm. *IEEE Transactions on Pattern Analysis and Machine Intelligence*, PAMI-7(4):463–474, July 1985.

[4] P Atkinson and N Tate, editors. *Advances in Remote Sensing and GIS Analysis*, chapter 4: Cloud Motion Analysis, pages 39–59. John Wiley and Sons, 1999.

[5] M Bader, G Forbes, J Grant, R Lilley, and A Waters. *Images in Weather Forecasting: A Practical Guide for Interpreting Satellite and Radar Imagery.* Cambridge, 1995.

[6] W Baker. Utilization of satellite winds for climate and global change studies. *Palaeogeography, Palaeoclimatology, Palaeoecology (Global and Planetary Change Section)*, 90:157–163, 1991.

[7] S. Banks. *Signal Processing, Image Processing and Pattern recognition.* Prentice Hall International Series in Acoustics, Speech and Image Processing. Prentice Hall, 1990.

[8] S. Banks. *Signal Processing, Image Processing and Pattern recognition.* Prentice Hall International Series in Acoustics, Speech and Image Processing. Prentice Hall, 1990.

[9] M Baroni, G Barletta, A Fantini, A Toso, and F Fantini. Assessing lv wall motion by frame–to–frame curvature matching and optical flow estimation. *IEEE Proc. Computers in Cardiology*, pages 477–480, 1992.

[10] D Blostein and N Ahuja. A multiscale region detector. *Computer Vision, Graphics and Image Processing*, 45:22–41, 1989.

[11] P Boekaerts. Autoadaptive cloud identification in meteosat images. Technical Report ESA SP–1183, European Space Agency, 1995.

[12] L Brown. A survey of image registration techniques. *ACM Computing Surveys*, 24(4):325–376, December 1992.

[13] M Brown and C Harris. *Neurofuzzy Adaptive Modelling and Control.* Prentice Hall, 1994.

[14] K Browning. Mesoscale aspects of extratropical cyclones: an observational perspective. Technical Report Internal Report 44, Joint Centre for Mesoscale Meteorology, University of Reading, UK, January 1995.

[15] V Bruce, P Green, and M Georgeson, editors. *Visual Perception: Physiology, Psychology and Ecology.* Hove, 2 edition, 1992. ISBN is 0-86377-146-7.

[16] G Büche, H Karbstein, and H Fischer. Experience in the height attribution of pure water vapour structure displacement vectors. In *Third International Winds Workshop, Ascona, Switzerland*, volume EUM P 18, pages 231–240. EUMETSAT, 1996.

[17] P Burrough and A Frank, editors. *Geographic Objects with Indeterminate Boundaries*, chapter 1: Natural Objects with Indeterminate Boundaries, pages 3–28. Taylor and Francis, 1996.

[18] P Burrough and A Frank, editors. *Geographic Objects with Indeterminate Boundaries.* Taylor and Francis, 1996.

[19] P Butterworth. Investigations into satellite winds–i. production. NWP on-line Scientific Note 2, Meteorological Office, http://www.meto.govt.uk/sec5/NWP/NWP_ScienceNotes/No2/No2.html, 1997.

[20] E Carterette and M Friedman, editors. *Handbook of Perception*, volume 5: Seeing. Academic Press, 1975.

[21] Z Chi, H Yan, and T Pham. *Fuzzy Algorithms: With Applications to Image Processing and Pattern Recognition*, volume 10: Advances in Fuzzy Systems – Applications and Theory. World Scientific, 1996.

[22] R Chin, J Jau, and J Weinman. The application of time series models to cloud field morphology analysis. *Journal of Climate and Applied Meteorology*, 26:363–373, March 1987.

[23] J Chou, R Weger, J Ligtenberg, K.-S Kuo, and R Welch. Segmentation of polar scenes using multi–spectral texture measures and morphological filtering. *Int. J. Remote Sensing*, 15(5):1019–1036, 1994.

[24] S Côté. *Measurement of Sea–Surface Velocities from Satellite Sensor Images using the Hopfield Neural Network.* PhD thesis, Faculty of Engineering and Applied Science, University of Southampton, 1996.

[25] P Courtier. Introduction to numerical weather prediction data assimilation methods. In *Developments in the Use of Satellite Data in Numerical Weather Forecasting*, pages 189–207. ECMWF, 1993.

[26] P Delagnes, J Benois, and D Barba. Active contours approach to object tracking in image sequences with complex backgrounds. *Pattern Recognition Letters*, 16:171–178, February 1995.

[27] M Deseilligny, G Stamon, and S Suen. Veinerization: A new shape description for flexible skeletonization. *IEEE Transactions on Pattern Analysis and Machine Intelligence*, 20(5):505–521, May 1998.

[28] S Dewitte, E Nyssen, D Crommelynck, and J Cornelis. Multi stage analysis of meteosat images. In *European Symposium on Satellite Remote Sensing II*, volume 2579, pages 170–181. SPIE, 1995.

[29] G di Baja and E Thiel. Skeletonization algorithm running on path–based distance maps. *Image and Vision Computing*, 14:47–57, 1996.

[30] F Diekmann. An overview on applications and capabilities in the meteosat image processing system. *Int. J. Remote Sensing*, 15(11):2285–2298, 1994.

[31] N Dimitrova and F Golshani. Motion recovery for video content classification. *ACM Transactions on Information Systems*, 13(4):408–439, October 1995.

[32] N Eigenwillig and H Fischer. Determination of midtropospheric wind vectors by tracking pure water vapour structures in meteosat water vapour image sequences. *Bull. Amer. Meteor. Soc.*, 63:44–58, 1982.

[33] EUMETSAT. *Workshop on Wind Extraction from Operational Meteorological Satellite Data*, volume EUM P 10, Washington, D.C., September 1991.

[34] EUMETSAT. *Second International Wind Workshop*, volume EUM P 14, Tokyo, Japan, December 1993.

[35] EUMETSAT. *Third International Winds Workshop*, volume EUM P18, Ascona, Switzerland, June 1996.

[36] A Feher and N Zabusky. An interactive imaging environment for scientific visualization and quantification (visiometric). *International Imaging Systems Journal, Special Edition*, 7:121–130, 1996.

[37] T Fujita. Interpretation of cloud winds. In *Workshop on Wind Extraction from Operational Meteorological Satellite Data, Washington, D.C.*, volume EUM P 10, pages 99–104. EUMETSAT, 1991.

[38] N Gamage and W Blumen. Comparative analysis of low–level cold fronts: Wavelet, fourier and empirical orthogonal functional decompositions. *Monthly Weather Review*, 121:2867–2878, October 1993.

[39] V Gärtner. Towards automatic product generation from meteosat images. *ESA Bulletin*, 82:94–100, 1995.

[40] Y Ge and M Fitzpatrick. On the generation of skeletons from discrete euclidean distance maps. *IEEE Transactions on Pattern Analysis and Machine Intelligence*, 18(11):1055–1066, November 1996.

[41] A Ghosh. Use of fuzziness measures in layered networks for object extraction: a generalisation. *Fuzzy Sets and Systems*, 72:331–348, 1995.

[42] I Gordon. *Theories of Visual Perception.* Wiley, 2 edition, 1997.

[43] D Gray, J Daniels, S Nieman, S Lord, and G DiMego. Nesdis and nws assessment of goes–8/9 operational satellite motion winds. In *Third International Winds Workshop, Ascona, Switzerland*, volume EUM P 18, pages 175–183. EUMETSAT, 1996.

[44] R Gregory. *Eye and Brain: The Psychology of Seeing.* Oxford University Press, 5 edition, 1998.

[45] F Guichard. A morphological, affine and galilean invariant scale–space for movies. *IEEE Transactions on Image Processing*, 7(3):444–456, March 1998.

[46] Gupta. NESDIS and NWS assessment of GOES–8/9 operational satellite motion winds. In *Nonlinear Image Processing IV*, volume 1902, pages 210–223. SPIE, 1993.

[47] M Hashim, A Watson, and M Thomas. An approach for correcting inhomogeneous atmospheric effect in remote sensing images. In *RSS95: Remote Sensing in Action, University of Southampton*, pages 597–604. Remote Sensing Society, 1995.

[48] M Hashimoto, Y Sakai, and H Kinoshita. An object extraction method using sampled active contour model. *Systems and Computers in Japan*, 26(13):66–74, 1995.

[49] D Hinsman. Wmo satellite activities: Standardization of techniques for cloud track wind observations. *Adv. Space Res.*, 14(3):119–125, 1994.

[50] L Hubert and L Whitney, Jr. Wind estimation from geostationary–satellite pictures. *Monthly Weather Review*, 99(9):665–672, September 1971.

[51] R Hummel and S Zucker. On the foundations of relaxation labelling processes. *IEEE Trans. Pattern Analysis and Machine Intelligence*, PAMI–5(3):267–287, May 1983.

[52] M Kastner, H Fischer, and H Bolle. Wind determination from nimbus 5 observation in the 6.3$\mu$m water vapour band. *J. Appl. Meteor.*, 19:409–418, 1980.

[53] G Kelly. Satellite observations for global modelling. *Adv. Space Res.*, 12(7):263–275, 1992.

[54] G Kelly, M Tomassini, and M Matricardi. Meteosat cloud–cleared radiances for use in three / four dimensional variational data assimilation. In *Third International Winds Workshop, Ascona, Switzerland*, volume EUM P 18, pages 105–116. EUMETSAT, 1996.

[55] K Kelly. Separating clouds from ocean in infrared images. *Remote Sensing of Environment*, 17:67–83, 1985.

[56] B Kerr and G Darkow. Storm–relative winds and helicity in the tornadic thunderstorm environment. *Weather and Forecasting*, 11(4):489:505, December 1996.

[57] C Kishtawal, S Basu, and P Pandey. An algorithm for retrieving vertical wind profiles from satellite–observed winds over the indian ocean using complex eof analysis. *Journal of Applied Meteorology*, 35:532–540, 1996.

[58] S Kosslyn. *Image and Brain: The resolution of the imagery debate.* MIT Press, 1996.

[59] L Lam, S-W Lee, and C S. Thinning methodologies – a comprehensive survey. *IEEE Transactions on Pattern Analysis and Machine Intelligence*, 14(9):869–885, September 1992.

[60] H Laurent. Feasibility study on water vapour wind extraction techniques. Esa contract, Laboratoire de Météorologie Dynamique du CNRS, Ecole Polytechnique, 91128 Palaiseau, France, 1990.

[61] H Laurent. Wind extraction from meteosat water vapor channel image data. *Journal of Applied Meteorology*, 32:1124–1133, June 1993.

[62] J Leese, C Novak, and V Ray Taylor. The determination of cloud pattern motions from geosynchronous satellite image data. *Pattern Recognition*, 2:279–292, 1970.

[63] H Lewis, M Brown, and A Tatnall. A software framework and toolkit for fuzzy land cover estimation from remotely sensed imagery. In *GTCE-LUCC, Barcelona, Spain*, 1998.

[64] H Lewis, S Côté, and A Tatnall. Determination of spatial and temporal characteristics as an aid to neural network cloud classification. *Int. J. Remote Sensing*, 18(4):899–915, 1997.

[65] H Lewis, Brown M, and Tatnall A. Incorporating uncertainty in land cover classification from remote sensing imagery. In *COSPAR, Nagoya, Japan*, 1998.

[66] F Leymarie and M Levine. Tracking deformable objects in the plane using an active contour model. *Pattern Analysis and Machine Intelligence*, 15(6):617–632, June 1993.

[67] A Lorenc. Atmospheric data assimilation. Scientific Paper 34, Forecasting Research Division, UK Meteorological Office, London Road, Bracknell, Berkshire RG12 2SZ, UK, May 1995.

[68] L Mahrt and J Sun. Dependence of surface exchange coefficients on averaging scale and grid size. *Q. J. R. Meteorol. Soc.*, 121:1835–1852, 1995.

[69] W Menzel, C Hayden, S Nieman, C Velden, and S Wanzong. Improvements in the quality assessment of automated satellite–derived cloud and water vapour motion vectors. In *Third International Winds Workshop, Ascona, Switzerland*, volume EUM P 18, pages 197–205. EUMETSAT, 1996.

[70] F Meyer and S Beucher. Morphological segmentation. *Journal of Visual Communication and Image Representation*, 1(1):21–46, September 1990.

[71] L Morone. The observational error of automated wind reports from aircraft. *Bulletin American Meteorological Society*, 67(2):177–185, February 1986.

[72] M Nagao and T Matsuyama. Edge preserving smoothing. *Computer Graphics and Image Processing*, 9:394–407, 1979.

[73] K Nam, J-S Kim, R-H P, and Y S. A fast hierarchical motion vector estimation algorithm using mean pyramid. *IEEE Transactions on Circuits and Systems for Video Technology*, 5(4):344–351, August 1995.

[74] J Nese, L Grenci, T Owen, and D Mornhinweg. *A World of Weather: Fundamentals of Meteorology.* Kendall/Hunt Publishing Company, 1996.

[75] F Newland, A Tatnall, and M Brown. Neurofuzzy extraction of wind data from remotely sensed images. In *Third International Winds Workshop, Ascona, Switzerland*, volume EUM P 18, pages 257–264. EUMETSAT, 1996.

[76] F Newland, A Tatnall, and M Brown. Fuzzy object-based generation of cloud motion from sequences of meteosat satellite imagery. In *First AMS Conference on Artificial Intelligence, Phoenix, Arizona*, pages 91–95. American Meteorological Society, 1998.

[77] D Nichol and M Fiebig. Image segmentation and matching using the binary object forest. *Image and Vision Computing*, 9(3):139–149, June 1991.

[78] A Ottenbacher, M Tomassini, K Holmlund, and J Schmetz. Low–level cloud motion winds from meteosat high–resolution visible imagery. *Weather and Forecasting*, 12(1), March 1997.

[79] G Pankiewicz. Pattern recognition techniques for the identification of cloud and cloud systems. *Meteorol. Appl.*, 2:257–271, 1995.

[80] J Peak and P Tag. Segmentation of satellite imagery using hierarchical thresholding and neural networks. *Journal of Applied Meteorology*, 33:605–615, 1994.

[81] J Purdom. Detailed cloud motions from satellite imagery taken at thirty second one and three minute intervals. In *Third International Winds Workshop, Ascona, Switzerland*, volume EUM P18, pages 137–146. EUMETSAT, 1996.

[82] J Raffaelli and G Seze. A study of time persistence of cloud types as seen from meteosat. In *9th METEOSAT Scientific Users' Meeting Report*, pages 141–146, 1992.

[83] P Ray. *Mesoscale Meteorology and Forecasting.* American Meteorological Society, second printing edition, 1988.

[84] T Reed and J Hans du Buf. A review of recent texture segmentation and feature extraction techniques. *CVGIP: Image Understanding*, 57(3):359–372, 1993.

[85] J Schmetz. Further improvements of cloud motion wind extraction techniques. In *Workshop on Wind Extraction from Operational Meteorological Satellite Data, Washington, D.C.*, volume EUM P10, pages 15–20. EUMETSAT, 1991.

[86] J Schmetz. Report from the working group on methods. In *Third International Winds Workshop, Ascona, Switzerland*, volume EUM P18, pages 9–11. EUMETSAT, 1996.

[87] J Schmetz, K Holmlund, J Hoffman, B Strauss, B Mason, V Gaertner, A Koch, and L Van De Berg. Operational cloud-motion winds from meteosat infrared images. *Journal of Applied Meteorology*, 32(7):1206–1225, July 1993.

[88] J Schmetz and M Nuret. Automatic tracking of high-level clouds in meteosat infrared images with a radiance windowing technique. *ESA Journal*, 11:275–286, 1987.

[89] A Seddon and G Hunt. Segmentation of clouds using cluster analysis. *International Journal of Remote Sensing*, 6(5):717–731, 1985.

[90] J. Serra. *Image Analysis and Mathematical Morphology*, volume 1. Academic Press, London, 1982.

[91] J Serra, editor. *Image Analysis and Mathematical Morphology*, volume 2: Theoretical Advances, chapter 13: Skeletons in Digital Spaces, pages 257–296. Academic Press, 1998.

[92] D Sinha and E Dougherty. A general axiomatic theory of intrinsically fuzzy mathematical morphologies. *IEEE Trans on Fuzzy Systems*, 3(4):389–403, 1995.

[93] E Smith and D Phillips. Automated cloud tracking using precisely aligned digital ats pictures. *IEEE Transactions on Computers*, c-21(7):715–729, July 1972.

[94] M Sonka, V Hlavac, and R Boyle. *Image Processing, Analysis and Machine Vision*. Chapman and Hall, 1993.

[95] A Stohl, K Baumann, G Wotawa, M Langer, B Neininger, M Piringer, and H Formayer. Dignostic downscaling of large–scale wind fields to compute local–scale trajectories. *Journal of Applied Meteorology*, 36(7):931–942, July 1997.

[96] M Susko and L Herman. Comparison of satellite-derived wind measurements wth other wind measurement sensors. *Journal of Spacecraft and Rockets*, 32(3):564–567, May-June 1995.

[97] S Swadley. Error analysis of automated winds derived from goes multispectral imagery. In *3rd Conference on Sat. Met. and Oceanography, Anaheim, California*, pages 181–186, February 1988.

[98] A Szantaï and M Desbois. Construction of cloud trajectories to study the cloud lifecycle. *Adv. Space Res.*, 14(3):115–118, 1994.

[99] Hamill T and T Nehrkorn. A short–term cloud forecast scheme using cross correlations. *Weather and Forecasting*, 8(4):401–411, December 1993.

[100] J Thépault. Assimilation of satellite data by 4d–var at ecmwf. In *Developments in the Use of Satellite Data in Numerical Weather Forecasting*, pages 249–285. ECMWF, 1993.

[101] M Tokuno. Operational system for extracting cloud motion and water vapor motion winds from gms–5 image data. In *Third International Winds Workshop, Ascona, Switzerland*, volume EUM P 18, pages 21–30. EUMETSAT, 1996.

[102] P. H. S. Torr. Geometric motion segmentation and model selection. In J. Lasenby, A. Zisserman, R. Cipolla, and H. Longuet-Higgins, editors, *Philosophical Transactions of the Royal Society A*, pages 1321–1340. The Royal Society, 1998.

[103] J Udupa and S Samarasekera. Fuzzy connectedness and object definition: Theory, algorithms and applications in image segmentation. *Graphical Models and Image Processing*, 58(3):246–261, May 1996.

[104] J Vega-Riveros and K Jabbour. Review of motion analysis techniques. *IEE Proceedings*, 136 Pt. 1(6):397–404, December 1989.

[105] C Velden. The impact of satellite-derived winds on hurricane analysis and track forecasting. In *Workshop on Wind Extraction from Operational Meteorological Satellite Data, Washington, D.C.*, volume EUM P 10, pages 113–118. EUMETSAT, 1991.

[106] C Velden. Positive impact of satellite–derived winds during the 1995 hurricane season: Example of optimizing data application and processing strategy. In *Third International Winds Workshop, Ascona, Switzerland*, volume EUM P 18, pages 81–90. EUMETSAT, 1996.

[107] G Wade, K Lau, and N Wood. Clustering applied to cloud wind determination. *Int. J. Remote Sensing*, 13(16):3135–3155, 1992.

[108] D Wang. A multiscale gradient algorithm for image segmentation using watersheds. *Pattern Recognition*, 30(12):2043–2052, 1997.

[109] Z Wang, K Browning, and G Kelly. Verification of the tracking technique used in an experimental cloud motion wind inferring system.

[110] Y Weiss and E Adelson. Perceptually organised em: A framework for motion segmentation that combines information about form and motion. Perceptual Computing Section Technical Report 315, M.I.T. Media Laboratory, MIT E15-384, Cambridge, MA 02139, USA, 1994.

[111] Q Wu, S McNeill, and D Pairman. Correlation and relaxation labelling – an experimental investigation on fast algorithms. In *Third International Winds Workshop, Ascona, Switzerland*, volume EUM P 18, pages 265–272. EUMETSAT, 1996.

[112] Q Wu, S McNeill, and D Pairman. Correlation and relaxation labelling: an experimental investigation on fast algorithms. *Int. J. Remote Sensing*, 18(3):651–662, 1997.

[113] R Zhang and J-G Postaire. Convexity dependent morphological transforms for mode detection in cluster analysis. *Pattern Recognition*, 27(1):135–148, 1994.